THE UNIVERSITY OF CHICAGO

NOVEL α-BTN ANTIBODIES MODULATE Vγ9Vδ2 ACTIVATION AND REVEAL INSIGHTS INTO THE EXTRACELLULAR ARCHITECTURE OF THE PHOSPHO-ANTIGEN SIGNALING COMPLEX

A DISSERTATION SUBMITTED TO
THE FACULTY OF THE DIVISION OF THE BIOLOGICAL SCIENCES
AND THE PRITZKER SCHOOL OF MEDICINE
IN CANDIDACY FOR THE DEGREE OF
DOCTOR OF PHILOSOPHY

INTERDISCIPLINARY SCIENTIST TRAINING PROGRAM:
BIOCHEMISTRY AND MOLECULAR BIOPHYSICS

BY

AMRITA RAMESH

CHICAGO, ILLINOIS

MARCH 2024

To my Mommy, Daddy and Sister, I am whole because of you. To my friends for the laughter.

TABLE OF CONTENTS

LIST OF FIGURES

LIST OF TABLES

ACKNOWLEDGMENTS

I first want to thank the scientific laws that govern the universe for producing the rich systems of life that we are lucky to study. To do research is to pursue truth, and the inherent nobility in this venture has been a guiding light for me along this difficult journey. It is my belief that Life does not defy entropy, it is a product of it. Life is unfathomably complex, messy, sometimes illogical and redundant. Life is stunningly creative, resilient, harsh and altruistic. I love Life so very deeply and this love feeds the core of my being. Earning this degree has deepened and substantiated this love, for which I am grateful.

This work is my attempt to excavate a minuscule nugget of truth in our small corner of the infinite universe. This work has stripped away my ego in the face of the vast unknown and in countless moments left me lost, confused, inspired and humbled. The biggest knowledge I will have gained from this degree is not what I discovered but instead the discovery of what I still don't know. Indeed, learning to think scientifically and probe the unknown fundamentally changes a person and these changes make Scientists my favorite breed of human. I have found my community to be insatiably curious, excited, thoughtful, helpful and thorough. It is a community full of good people who care about the truth and wish to use their truths to better the state of the world. I am proud to officially belong to this community of Certified Nerds and I have many people to thank for making this dream a reality.

Endless thank yous to my mother, father and sister for being the bedrock of support throughout my life. You have taught me everything I know and continually guide me to the ever-evolving best version of myself. Mother Beast, you are creative, sharp, adventurous, giving and above all thoughtful. Your careful, untiring hand has shaped every aspect of my development. By emulating you I have become independent, curious, artistic and resilient. My JTF Boys, you are sweet, gentle, hilarious, and purposeful in your self-care. You have soothed me and given me confidence in every difficult situation I encounter and are the source of every joke I've ever made. My Brinda beastie, you are my other half. Your existence makes

everything in my life more shiny. You are good at everything you do, a people-person at your core, and my love for you is hard to put into words. I am constantly in awe of how lucky I am to have such a beautiful and tight-knit family. Mommy, Daddy, Brinda, I cherish you.

Thank you to my advisor Erin, you are an inspiring, thoughtful and dedicated leader. I have benefited greatly from developing under your wing and will miss your outlook on science, policy and the world at large. Thank you to my scientific mentors Sobhan, Kristof, and Caitlin. You have gifted me many skills, but most importantly you have gifted me independence by expanded my mind. Thank you to the B.M.B. and U.Chicago community, including Tomasz, Mel, Sumit and James. Your patience and expertise has dramatically broadened the scope of this project and my development as a scientist.

Thank you to my dear friends in graduate school Kierstin, Mayuri, Augusta, Annisa, Sierra, Matt, Sean, Tiffany, Sean, Jorden, and Adarsh. You all have been the best part of my experience at U.Chicago, and your friendship is the most important thing I will take with me. You have inspired me with your outlooks, hilariousness and love. Our conversations have made me a better, deeper and more thoughtful person. You all have made the hardest of times fun, and unconditionally supported and loved me in ways I never knew to ask for.

Thank you to my best friends from other walks of life Rylie, Patricia, Arya, Alena, Nicola, Laura, Reid, Kyle, Grace, Sarah and Darius. My adventure buddies, confidantes, sources of inspiration on being a good person and more, I love you all. Our friendships continue to evolve and deepen, and for this I am so grateful. I cannot wait to spend our lives enjoying, learning from and loving each other.

ABSTRACT

Infected and malignant target cells trigger $V\gamma9V\delta2$ T cell activation by signaling phosphoantigen metabolite intracellular accumulation through Butyrophilin (BTN)-3A1 and BTN2A1 proteins to the $V\gamma9V\delta2$ T cell receptor (TCR). An incomplete understanding of molecular dynamics in the pAg-signaling complex precludes $V\gamma9V\delta2$ T cell immunotherapeutic efficacy. Here, we develop a panel of $\alpha-$BTN3A1 and $\alpha-$BTN2A1 antibody (mAb) reagents to probe the roles of BTN3A1 and BTN2A1 in pAg signaling. By modifying agonist $\alpha-$BTN3A1 mAb 20.1 with increased inter-Fab distances, we establish that ordered multimerization of BTN3A1 is not necessary to stimulate $V\gamma9V\delta2$ T cell activation. By similarly antagonist $\alpha-$BTN3A1, we demonstrate that 103.2 does not antagonize $V\gamma9V\delta2$ T cell activation conformational constraint but likely through steric occlusion of a critical binding interaction between BTN3A1 and a yet unknown co-receptor. Finally, we developed a panel of novel $\alpha-$BTN2A1 mAb $V\gamma9V\delta2$ antagonists that utilize different biophysical mechanisms to compete with the $V\gamma9V\delta2$ TCR for BTN2A1 binding. Our 2.8Å structure of BTN2A1 ectodomain in complex with the Fab of potent antagonist, 2A1.9 provides molecular insights into BTN2A1 residues critical for pAg-signaling. 2A1.9 may be developed into an immunotherapy adjuvant to sensitize tumors in which high BTN2A1 expression is a poor prognostic marker to $\alpha\beta$ T cell immunotherapies.

CHAPTER 1

INTRODUCTION

1.1 $V\gamma 9V\delta 2$ T cell roles in immunity

$V\gamma 9V\delta 2$ T-cells ($V\gamma 9V\delta 2s$) are a unique, innate-like subset of the adaptive immune system with the potential to be developed into an off-the-shelf immunotherapy. $V\gamma 9V\delta 2s$ comprise 2-5% of lymphocytes circulating in the peripheral blood of healthy humans but can expand to represent up to 50% of circulating lymphocytes in conditions of cellular stress[1]. In a Major Histocompatibility Complex (MHC)-independent manner[2,3] $V\gamma 9V\delta 2s$ proliferate polyclonally[4–6], mount cytotoxic defenses and recruit other branches of the immune system to fight a variety of bacterial, parasitic, and viral infections by responding to phosphoantigen (pAg) metabolite byproducts of isoprenoid biosynthesis[1]. We now know that phosphoantigen signaling starts with an intracellular accumulation of pAg that drives pAg binding to the intracellular domain of the Butyrophilin (BTN)3A1 protein[7]. This binding event then drives structural changes in BTN3A dimers that propagate extracellularly[8–11] as well as the formation of an intracellular complex with the related BTN2A1 protein[12–15]. Through molecular mechanisms yet unknown these events recruit the $V\gamma 9V\delta 2$ TCR to bind BTN2A1 through germline encoded residues rather than hypervariable CDR loops[12,13,16]. Ultimately, these events trigger a $V\gamma 9V\delta 2$ response leading to target cell killing, apoptosis or the recruitment of other branches of the immune system[1]. Excitingly, $V\gamma 9V\delta 2s$ are also capable of recognizing cells undergoing malignant transformation[17] and are the subject of many early-stage clinical trials aimed at treating a range of solid and liquid tumors[18]. While $V\gamma 9V\delta 2$ immunotherapies have good safety profiles, an incomplete understanding of the molecular underpinnings of $V\gamma 9V\delta 2$ activation precludes the realization of their immunotherapeutic potential.

1.1.1 Infections

Expansion of $V\gamma 9V\delta 2s$ has been observed in response to a diverse array of microbes. $V\gamma 9V\delta 2s$ were first discovered to respond to tuberculosis[19] infection. Our knowledge of pathogenic bacteria capable of stimulating $V\gamma 9V\delta 2$ proliferation has expanded to include brucella, erlichia, legionella, leptospira, listeria, other mycobacteria, salmonella, and tularemia[1,20,21]. Though $V\gamma 9V\delta 2s$ are primarily thought to operate in the peripheral blood, bacterial infections are capable of stimulating $V\gamma 9V\delta 2$ expansion in diverse tissues including bronchoalveolar lavage fluid, cerebral spinal fluid, the spleen and the female reproductive tract[1]. Intriguingly, protozoan parasites including malaria, leishmania and toxoplasma are also capable of causing $V\gamma 9V\delta 2$ proliferation as well[1,20]. Viral infections seem to have more diverse effects on $V\gamma 9V\delta 2$ behavior. While Epstein-Barr infections cause peripheral $V\gamma 9V\delta 2s$ expansion, a decrease in the frequency of circulating $V\gamma 9V\delta 2s$ is observed in patients infected with hepatitis, coronavirus, and Human Immunodeficiency Virus (HIV). However, $V\gamma 9V\delta 2s$ mount a cytotoxic response when exposed to cells infected with these viruses in vitro[1,20].

1.1.2 Cancer

Though $V\gamma 9V\delta 2s$ canonically proliferate during infection, it has become apparent that they are capable of recognizing and selectively killing malignant and distressed cells. $V\gamma 9V\delta 2s$ are being explored as treatment targeting solid tumors including Renal Cell Carcinoma (RCC), Non-Small Cell Lung Carcinoma (NSCLC), Hepatocellular Carcinoma (HCC), Colorectal Carcinoma (CRC), Gastric and Pancreatic cancer[18,22]. $V\gamma 9V\delta 2$ treatment of hematological tumors such as Acute Myeloid Leukemia (AML) and Multiple Myeloma (MM) is also being tested in clinical trials[18,22]. Fascinatingly, the expression of proteins involved in triggering $V\gamma 9V\delta 2$ responses (discussed in following sections) is associated with either better or worse prognosis in different cancers in different patients[23]. This suggests that $V\gamma 9V\delta 2s$ play diverse roles in tumor immunity however, the natural roles of $V\gamma 9V\delta 2s$ in the tumor

microenvironment remain unclear as the majority of studies analyze the $\gamma\delta$ T cell compartment as a whole. It has been shown that $V\gamma9V\delta2s$ can educate Natural Killer (NK) cells in the tumor microenvironment to kill mature Dendritic Cells (DCs) that may otherwise promote inflammation and tumor growth. Additionally, $V\gamma9V\delta2s$ can present antigen to CD4+ and CD8+ T cells likely in the lymph nodes (LN) by upregulating MHC I and II molecules, costimulatory molecules and chemokine receptors like CCR7[22]. Studies profiling $V\gamma9V\delta2$ populations in tumors are necessary to better understand the contexts in which they are helpful and harmful to anti-tumor immunity.

1.1.3 Characteristics of $V\gamma9V\delta2$ T cell responses

$V\gamma9V\delta2s$ survey cells for stress associated signals and ligands using the TCR, Natural Killer group 2 member D receptor (NKG2D) and Toll-like receptors (TLRs)[1]. $V\gamma9V\delta2s$ generally mount a Type 1 cytotoxic response when activated and kill target cells through the release of lytic mediators perforin and granzyme as well as pro-inflammatory cytokines Interferon-γ (IFN-γ) and Tumor Necrosis Factor-α (TNF-α)[1]. CD16 expression in $V\gamma9V\delta2s$ can induce target cell apoptosis via antibody-dependent cell-mediated cytotoxicity (ADCC) and may also promote phagocytic activity[1]. Target cell apoptosis may also be induced through Fas/FasL as well as TNF-related apoptosis inducing ligand (TRAIL) and TNF-α[1].

1.1.4 Immunotherapeutic potential

$V\gamma9V\delta2s$ exhibit a unique combination of features that make them ideal candidates for immunotherapeutic development. Most importantly, $V\gamma9V\delta2s$ do not employ canonical T-cell antigen-recognition as target-cells do not stimulate $V\gamma9V\delta2s$ via MHC[2,3]. MHC-independent target cell recognition potentiates the development of an off-the-shelf, universalized $V\gamma9V\delta2$ immunotherapy that lacks the risk for graft vs host disease (GVHD) and is unaffected by MHC-downregulation in tumors[24]. Data also suggests that $V\gamma9V\delta2s$ may not

be as susceptible to PD-1 checkpoint receptor-mediated inhibition as other T cell therapies and produce low amounts of IL-17a, a cytokine implicated in tumor growth and metastasis[24]. Preparing sufficient quantities of $V\gamma 9V\delta 2s$ for allogeneic transplant generally involves first identifying a donor with a robust and desirable $V\gamma 9V\delta 2$ repertoire followed by specific expansion of $V\gamma 9V\delta 2s$ from donor peripheral blood induced with IL-2 and bisphosphonate drugs. Ongoing studies are testing sort strategies on expanded $V\gamma 9V\delta 2s$ to select for or eliminate populations expressing certain combinations of cellular markers, including PD-1 for example[24]. *In vivo* stimulation of $V\gamma 9V\delta 2s$ with IL-2 and bisphosphonate drugs is also being explored[22] as well as the benefits of local versus systemic administration of treatment. Though disease stabilization, partial and even complete remission have been achieved in select patients, clinical trials overall show favorable safety profiles but lack efficacy due to lack of a persistent $V\gamma 9V\delta 2$ population following transplant or stimulation[22]. Anergy or activation induced cell death (AICD) lead to reduced numbers of $V\gamma 9V\delta 2s$ over time[22].

1.2 $V\gamma 9V\delta 2$ T cell antigens

$V\gamma 9V\delta 2s$ are triggered by intracellular increases in the concentration of phosphoantigen metabolite (pAg) byproducts of isoprenoid biosynthesis[25] in target cells, a process that occurs via the HMG-CoA reductase / mevalonate (MVA) pathway in eukaryotes and the non-mevalonate pathway in bacteria and plants. The stimulation of $V\gamma 9V\delta 2s$ with fractionated *M. tuberculosis* lysate first led to the identification of intermediates in the 1-deoxy-D-xylulose 5-phosphate (DOXP) / methylerythritol 4-phosphate (MEP) metabolic pathway as antigenic[21]. We now know that metabolic pathways that produce pAgs exist in many species and pAgs vary in the potency with which they stimulate $V\gamma 9V\delta 2s$[21]. The potency of pAgs is immediately determined by intrinsic molecular features and chemical modifications including phosphorylation and conjugation with other small molecules like nucleotides[26]. Additionally, metabolic regulation of pAg concentrations by processes altering the activ-

ity of enzymes in isoprenoid biosynthetic pathways as well as the levels of upstream and downstream intermediates affect the potency with which specific pAgs stimulate $V\gamma 9V\delta 2s$.

1.2.1 Bacterial phosphoantigens

The most potent pAg identified to date is (E)-4-hydroxy-3-methyl-but-2-enyl diphosphate (HMBPP), an intermediate of the bacterial DOXP/MEP pathway. It is believed that target cells suffering infection by an intracellular pathogen experience subtle increases in the intracellular concentration of HMBPP and other bacterial pAgs, ultimately triggering $V\gamma 9V\delta 2$ activation.

1.2.2 Endogenous phosphoantigens

Humans generate pAgs through the MVA pathway during the biosynthesis of isoprenoid species including cholesterol, steroids and other non-sterol isoprenoids[21]. Isoprenoid biosynthesis can be dysregulated in contexts of cellular stress including infections caused by eukaryotic pathogens such as malaria and malignancies. Isopentenyl diphosphate (IPP) is the most antigenic eukaryotic pAg and stimulates $V\gamma 9V\delta 2$ activation 10,000X less potently than HMBPP[21]. The tolerance of healthy levels of IPP and other endogenous pAgs necessitates the lower potency of IPP. Bisphosphonate drugs increase intracellular levels of endogenous pAgs by inhibiting enzymes in the MVA pathway that metabolize IPP or downstream metabolites[21]. Pamidronate and zoledronate are two commonly used bisphosphonate drugs that target the enzyme farnesyl diphosphate synthase (FDPS) which uses IPP as a subtstrate[21]. These drugs are utilized extensively to expand $V\gamma 9V\delta 2s$ for allogeneic transplant, stimulate $V\gamma 9V\delta 2$ *in vivo* and conduct basic research on $V\gamma 9V\delta 2s$.

1.2.3 Molecular features determining pAg antigenicity

As mentioned, pAgs are a diverse class of metabolites with varying antigenicity. The core antigen unit of pAg metabolites consists of a 4 carbon chain with a terminal pyrophosphate moiety[26]. The addition of large chemical groups including another phosphate to the pyrophosphate moiety does not affect pAg antigenicity, however loss of a phosphate from the pyrophosphate moiety dramatically reduces the ability of a pAg to stimulate $V\gamma 9V\delta 2$ activation except in pAgs conjugated to nucleotide monophosphates[26]. At the other terminus of the molecule, the addition of longer prenyl chains does not affect the ability of a pAg to stimulate $V\gamma 9V\delta 2$ activation, however the addition of bulky headgroups abrogates antigenicity[26]. Chemists now aim to exploit our understanding of the molecular constraints on pAg antigenicity to develop the therapeutic potential of pAgs. It has been suggested that the highly charged pyrophosphate moiety prevents pAg diffusion into and out of cells. Thus, pAg prodrugs are being developed with charge-neutral and pyrophosphate-protecting, cleavable headgroups to enable cellular uptake of pAgs[21]. Ultimately, these may be used to sensitize tumors to $V\gamma 9V\delta 2$ immunotherapies.

1.3 Overview of the phosphoantigen signaling complex

The question of how target cells signaled pAg accumulation to $V\gamma 9V\delta 2s$ remained open for almost 20 years. In classical immune recognition paradigms, target cells directly present diverse peptides, lipids and metabolites extracellularly on MHC or MHC-like molecules. T Cells survey the body for MHC or MHC-like molecules loaded with antigenic peptides primarily, as well as lipids or metabolites using their T Cell Receptor (TCR) via the TCR Complementarity Determining Region Loops (CDRs). Recognition of abnormal antigens then triggers a cytotoxic response and the recruitment of other branches of the immune system. That the triggering of a $V\gamma 9V\delta 2$ response seemingly does not require MHC or MHC-like molecules, nor the recognition of peptide antigens[2,3] puzzled immunologists. The eventual

discovery that $V\gamma 9V\delta 2$ activation required pAg binding intracellularly to BTN3A1[7] marked the beginning of a decade-long effort to understand the identity and molecular dynamics of the unconventional proteins involved in pAg signaling.

1.3.1 Butyrophilin family of proteins

BTNs were first discovered in the mammary glands of cows to be involved in the stabilization of fat balls in cows milk[?] . Human BTNs are ubiquitously expressed B7-like proteins, common B7 and B7-like molecules being costimulatory or regulatory molecules of T cell activation like CD80, CD86 and PD-L1[?] . The extracellular portion of most BTNs including BTN3A1 consists of an IgV and IgC domain and is linked to an intracellular B30.2 domain via a single-pass transmembrane helix (TM) followed by a relatively flexible juxtamembrane region (JTM)[?] . Together, the JTM and B30.2 domains are referred to as the full intracellular domain (BFI). BTNs primarily exist endogenously as homodimers or isoform heterodimers with dimerization driven by disulfide bonds or hydrogen bond contacts between extracellular IgC domains. BTN3A1, for example, complexes with its isoforms BTN3A2 and BTN3A3 to form BTN3A dimers.

1.4 BTN3A1: the $V\gamma 9V\delta 2$ antigen sensor

1.4.1 Roles of BTN3A1 domains in pAg signaling

The signaling of pAg accumulation begins with pAg binding to the B30.2 domain of BTN3A1[7]. This binding event is propagated through the BTN3A1 molecule through its JTM affecting the overall structure of the BTN3A1 BFI[8]. The JTM is approximately 70 amino acids long and two critical regions within the JTM comprising residues 1-16 and 39-64 appear to be crucial for of pAg-signaling[8]. It is becoming increasingly evident that pAg binding information is then propagated in trans within the BTN3A homo or heterodimer from the JTM of the

pAg-bound BTN3A1 molecule to the JTM of its dimerization partner[10]. Though the exact molecular mechanism and structural consequence remains unclear, this signal then travels through the single-pass TM of either the trans member or both members of the dimer to the BTN3A extracellular IgV domain(s)[10]. Intriguingly, swapping the BTN3A1 TM for a single-pass TM from other BTN or unrelated proteins does not affect the ability of BTN3A1 to signal pAg accumulation[9]. The effects of pAg binding on the dynamics and conformation of the BTN3A extracellular domain remains unclear. We know that BTN3A dimers adopt a a V-shaped conformation on the cell surface[13,27,28] and that dimerization is driven by extensive hydrogen bond and electrostatic contacts between 2 BTN3A monomers[27] to form a highly stable interface. Fascinatingly, BTN3A dimers in which BTN3A1 lacks but its dimerization partner retains an IgV domain can still function to signal pAg, however at least one IgV domain in trans of the pAg sensing monomer is necessary for pAg signaling[10]. The specific effects of this pAg-driven molecular cascade on the cellular organization and extracellular conformation of BTN3A dimers remains a mystery.

1.4.2 Molecular features of pAg sensing by BTN3A1

Structural studies conducted by past members of the Adams Lab show that pAgs bind to a positively charged pocket in the BTN3A1 B30.2 domain formed by the H351, H378, K393, R412, R418 and R469 residues[7]. Extensive hydrogen bonding networks between these BTN3A1 residues and the pAg pyrophosphate moiety[7] explain the loss of potency when triggering $V\gamma 9V\delta 2$ activation with monohosphate compounds otherwise structurally similar to pAgs[26]. Though H351 does not form hydrogen bonds with the pAg, mutagenesis of this residue abrogates the ability of BTN3A1 to signal pAg accumulation to $V\gamma 9V\delta 2s$[7]. The binding of pAg to the BTN3A1 B30.2 domain ultimately causes allosteric changes to B30.2 residues both proximal and distal to the pAg-binding pocket[28], potentially driving signal propagation to the JTM. Residues in the BTN3A1 IgV domain have also been implicated in

pAg signaling[16]. K37, S40, K94, and K107 form a basic patch on the IgV CFG face and mutagenesis of these residues differentially abrogates $V\gamma 9V\delta 2$ activation in a T cells expressing different clones of the $V\gamma 9V\delta 2$ TCR. Interestingly residues E106 and K107 have been implicated in binding BTN2A1 by NMR[16], and mutagenesis of these residues modulates but does not abrogate $V\gamma 9V\delta 2$ activation[16]. Adding a disulfide bond to the BTN3A dimer interface at residue D124 in one monomer and S207 in the other did not affect BTN3A1 membrane diffusion but diminished $V\gamma 9V\delta 2$ activation[28]. $V\gamma 9V\delta 2$ activation might therefore be dependent on conformational flexibility within the BTN3A1 IgC domain or the exchange of BTN3A2 and BTN3A3 isoforms into and out of the BTN3A dimer.

1.4.3 Specialized roles of BTN3A isoforms

BTN3A1 has two isoforms, BTN3A2 and BTN3A3 with which it readily heterodimerizes. The existence of 3 BTN3A isoforms is believed to have been caused by gene duplication during the evolution of primates[10]. Extracellularly, BTN3A2 has an identical IgV domain to BTN3A1 while BTN3A3 harbors the single K36R mutation. BTN3A IgC domains are 90% homologous. Key differences between the isoforms involve the intracellular domains. The BTN3A1 JTM harbors a highly positively charged motif unlike that of BTN3A2 and 3A3. BTN3A2 lacks the B30.2 domain and a portion of the JTM while BTN3A3 substitutes an arginine in place of the histidine at position 351 in the BTN3A1 B30.2 pAg binding pocket[10]. Target cells expressing BTN3A1 alone can weakly stimulate $V\gamma 9V\delta 2$ activation however the expression of either BTN3A2 or BTN3A3 is required for full potency in pAg signaling[10]. Fascinatingly, alpaca are among the only non-primate species that retain a $V\gamma 9V\delta 2$ T cell population that is triggered by pAg and BTN3. Alpaca have only one BTN3 isoform suggesting the existence of an ancenstral super-BTN3A in humans. Indeed, the R351H mutation in BTN3A3 restores its ability to signal pAg accumulation to $V\gamma 9V\delta 2s$[7] and, unlike BTN3A1, strongly stimulates $V\gamma 9V\delta 2$ activation when expressed without its iso-

forms[9–11]. Differences in the JTM are believed to affect how BTN3A isoforms dimerize[10,11], traffic to the cell membrane[29] and propagate intracellular pAg-B30.2 binding information extracellularly[10] explaining the reliance of BTN3A1 on its isoforms for optimal functioning. Indeed it is posited that this diversification of functions between BTN3A isoforms provides modern humans with the ability to fine tune the expression levels of each molecule to control pAg signaling-strength in different cellular contexts.

1.5 BTN2A1: a $V\gamma9V\delta2$ T cell receptor binding partner

1.5.1 Roles of BTN2A1 domains in pAg signaling

Expression of BTN2A1 is necessary for pAg signaling and activation of $V\gamma9V\delta2s$[12,13,30] and more specifically, the B30.2 domain of BTN2A1 is neessary for pAg signaling[12]. Following pAg accumulation, pAg binding to BTN3A1 drives association between the B30.2 domains of BTN3A1 and BTN2A1[14,15]. The JTM of BTN2A1 has been implicated in pAg signaling, as mutagenesis of residues 290-301 abrogates $V\gamma9V\delta2$ activation and removal of the BTN2A1 JTM prevents the association of the BTN3A1 and BTN2A1 B30.2 domains in the presence of pAg[15] in vitro. Interestingly, cellular FRET assays probing the role of the BTN2A1 JTM in BTN2A1 and BTN3A1 association show an increase in association when the BTN2A1 JTM is mutagenized[15,30]. Therefore, the role of the BTN2A1 JTM and TM in pAg signaling is still unclear. The BTN2A1 ectodomain is better characterized. It is the only established binding partner for the $V\gamma9V\delta2$ TCR[12,13] and binds via the CFG face of its IgV domain to the germline-encoded HV4 loop on the TCR $\gamma9$ chain[13,16]. This binding interface does not involve the $\delta2$ chain but is necessary for pAg signaling[12,13]. Interestingly, the BTN2A1 ectodomain has also been implicated in coordinating cellular colocalization with BTN3A1 as removal of the ectodomain abrogates FRET between BTN2A1 and BTN3A1[30]

1.5.2 Molecular features of BTN2A1 involved in pAg signaling

Crystal structures of the BTN3A1 and BTN2A1 B30.2 domains in complex in the presence of HMBPP highlight multiple interfaces, whether both are physiologically relevant remains unclear as mutagenesis of key residues in the BTN2A1 B30.2 domain from both interfaces abrogates BTN2A1:BTN3A1 binding and pAg signaling. These residues include R449 and V483, and T482 which utilize hydrogen bonds to contact the Pα and Pβ of the HMBPP pAg as it sits in the basic pAg binding pocket of the BTN3A1 B30.2 domain, respectively[14] but come from different orientations of docking between BTN2A1 and BTN3A1. BTN2A1 residue E485 coordinates binding with BTN3A1 residues R413 and K393 adjacent to the pAg binding pocket[14]. Interestingly, BTN2A1 D427 and E429 form contacts with the BTN3A1 B30.2 domain outside of the pAg-binding pocket interface[14], the physiological relevance of which is unclear as it has been postulated that the inability of pAgs with bulky headgroups to stimulate $V\gamma9V\delta2$ is due to the disruption of binding between the B30.2 domains of BTN2A1 and BTN3A1[31]. In the BTN2A1 JTM, residues L290, W292 and L297 are necessary for pAg signaling while mutagenesis of adjacent residues is better tolerated but still mildly deleterious[15]. Extracellularly, BTN2A1 uses disulfide bonds at the C-terminus of the IgC domain to drive homodimerization[13]. BTN2A1 contacts the $V\gamma9V\delta2$ TCR through key residues in the IgV CFG face including R37, R96, Y98 and E107[13]. A published structure of the BTN2A1 ectodomain in complex with the $V\gamma9V\delta2$ TCR show electrostatic contacts between the aforementioned R96, Y98 and E107 residues as well as multiple additional residues in the IgV CFG face including Q42, F43, S44, Q100 and Y105 (PDB ID:8dfw)[32]. NMR experiments have implicated other residues in the BTN2A1 IgV CFG face in interacting with the extracellular domain of BTN3A1 including residues S44, A46, G53, and E55[16]. Mutagenesis of the BTN2A1 residues Y98 and Q100 abrogates the putative interaction with BTN3A1 by NMR shift[16] however the relevance and strength of an interaction between the BTN2A1 and BTN3A1 ectodomains remains unclear[16].

1.5.3 Interactions between BTN3A1 and BTN2A1

BTN3A1 and BTN2A1 were first found to colocalize at resting state on the cell membrane by confocal microscopy and co-immunoprecipitation experiments[12,13]. Data suggesting the existence of an extracellular complex between BTN2A1 and BTN3A1 includes NMR experiments in which the addition of BTN2A1 causes shifts in BTN3A1 residue E106[13,16], FRET between mAbs bound to BTN2A1 and BTN3A1 ectodomains[12] and mutagenesis of BTN2A1 residues computationally predicted to interact with BTN3A1 affecting pAg signaling[14]. While these data do not unequivocally support the existence of a stable extracellular interaction, the intracellular association between BTN3A1 and BTN2A1 is becoming increasingly clear in molecular detail[14,15]. The binding between the BTN2A1 B30.2 domain and the BTN3A1 B30.2 domain requires the pAg metabolite and the affinity of this interaction ranges from 600nM with the bacterial HMBPP pAg to 155uM with the IPP endogenous pAg[14]. The molecular mechanism by which BTN2A1 and BTN3A1 transition from a pre-associated state on the cell membrane to a pAg-signaling, complexed state is unclear. Additionally, uncovering how this intracellular event gets propagated extracellularly will provide invaluable insight into this rare signaling mechanism.

1.6 The $V\gamma9V\delta2$ T cell receptor

The following section includes content I wrote for a published review in Immunological Reviews titled: Diversity in Recognition and Function of $\gamma\delta$ T cells.[33]

Studying the $V\gamma9V\delta2$ TCR repertoire and how it evolves during the development of an individual may also aid in solving key gaps in our understanding of the mechanisms of pAg signaling on the target cell. While the $V\gamma9V\delta2$ population is occasionally referred to as invariant, V-D-J rearrangement provides some variability within the CDR3 loops of both chains. Both the fetal and adult $V\gamma9V\delta2$ $\gamma9$ repertoire are composed of ≈40% public

clonotypes on average[34] promoting an assumption of the $\gamma 9$ chain to be "semi-invariant". However, these sequences arise from diverse recombination events and are paired with highly diverse $\delta 2$ sequences[34].

1.6.1 Molecular and repertoire features of the $\gamma 9$ chain

The CDR3γ prefers 1-2 N-Nucleotide additions and is relatively short, with some analyses showing over 50% of $\gamma 9$ CDR3s to be 14 amino acids in length[35]. These data suggest a selective pressure/restriction on the $\gamma 9$ chain CDR3 sequence throughout development for particular molecular features that likely influence what the TCR recognizes when surveying for pAg-burdened cells. The "semi-invariant" moniker for $\gamma 9$ is thus particularly interesting considering the engagement of BTN2A1 through residues R20, E22, E70, and H85. However, these residues are germline-encoded[12], which does not explain the preference for the limited set of $\gamma 9$ CDR3 sequences unless particular flanking sequences are required for stabilizing the BTN2A1 binding epitope. Other $\gamma 9$ chain residues are important for pAg reactivity; these include CDR3 residues K108 which must be positively charged and K109 which must be positively charged or neutral[36,37]. Some residues including T29, Y54, and T57 are controversial; past studies have shown that mutating these residues abolishes pAg reactivity[37] but recent data suggest that these residues have a minimal role in pAg-induced T cell activation[12]. Overall, data currently point to a primary role of the $\gamma 9$ chain in $V\gamma 9V\delta 2$ T cells in recognizing BTN2A1, however the implication of additional residues in pAg reactivity that do not bind BTN2A1 may suggest additional yet unknown roles for the $\gamma 9$ chain in mediating recognition of and response to pAgs.

1.6.2 Molecular and repertoire features of the $\delta 2$ chain

The $\delta 2$ chain, on the other hand, exhibits considerable CDR3 sequence variability between and within individuals as public CDR3 sequences generally do not exceed 2% of total TRD2

sequences[4]. Interestingly, $\delta 2$ repertoires show a strong enrichment of hydrophobic amino acids at position 97 in the CDR3 loop[38] a residue generated through N-nucleotide addition. Mutation of this residue and E28 of CDR1δ diminishes pAg reactivity[37]. More strikingly, R51 and E52 of the $\delta 2$ CDR2 loop are necessary for pAg reactivity[12,37]. It is still unclear why $\delta 2$ has strict requirements for these residues, it could be that they are important for binding another molecule on the target cell. More broadly, the majority of the adult private $\delta 2$ repertoire uses the TRDJ1 joining segment instead of TRDJ3 commonly found in fetal $\delta 2$ CDR3 loops[38,39] suggesting that microbial exposure may prompt a preference for the particular CDR3 residues coded for by TRDJ1. The private adult $\delta 2$ repertoire also has more N-nucleotide additions than the public repertoire and the number of N-nucleotide additions in private $\delta 2$ sequences increases throughout development, on average[4]. Overall, the $\delta 2$ repertoire has a constrained CDR3 length that is shorter, on average, than $\delta 1$ CDR3s[35], which is particularly interesting considering the potential diversity of this chain based on its mechanism of V-D-J recombination. Functionally, the $\delta 2$ chain seems to modulate the strength with which particular clones activate in response to pAgs[40] suggesting that the $\delta 2$ chain could play an important role in engagement of ligand on target cells. The development of unique $\delta 2$ repertoires in each adult, even in homozygous twins[41] suggests that the $\delta 2$ chain recognizes disease-specific epitopes, similar to the classical model of $\alpha\beta$ T cells. While some individuals show "clonotypic focusing" in their adult $V\gamma 9V\delta 2$ repertoire[34] a recent study shows that Gambian children have no greater similarities in their $V\gamma 9V\delta 2$ TCR repertoires than age-matched German children[4] expected to have different microbial exposures, providing evidence against postpartum pathogen-specific driven expansion of specific $V\gamma 9V\delta 2$ clones. Uncovering what the $\delta 2$ chain contacts on the target cell, and how it is involved in activation is an exciting avenue for future research, and will fill in a crucial piece in the increasingly intricate mechanism of $V\gamma 9V\delta 2$ activation.

1.7 Summary

The mechanism by which infected and cancerous target cells communicate pAg accumulation to the $V\gamma 9V\delta 2$ is remarkably unique. Of particular interest is the inside-out signaling mechanism that occurs seemingly independently of the canonical TCR ligand, the MHCx. The details of this signaling mechanism are slowly become more clear with time. Immense progress has been made in our intracellular understanding the molecular interactions and sequence of events following pAg binding to the intracellular domain of BTN3A1. Less clear is how this binding information is translated through dimeric BTN3A1 and BTN2A1 to be communicated to the $V\gamma 9V\delta 2$ T cell to signal stress. The central question of this thesis is elucidating how pAg accumulation alters the extracellular architecture of the pAg signaling complex to trigger a $V\gamma 9V\delta 2$ response. Ultimately, a detailed understanding of this signaling mechanism can be leveraged to improve the efficacy of $V\gamma 9V\delta 2$ immunotherapies.

CHAPTER 2

DEVELOPING NOVEL $\alpha - BTN2A1$ ANTIBODIES TO MODULATE $V\gamma 9V\delta 2$ ACTIVATION

2.1 Introduction

The role of the BTN2A1 intracellular domain in pAg-signaling is structurally and biophysically validated to bind to BTN3A1 in a pAg-dependent manner.[14,15] Less clear is how pAg-dependent intracellular binding of BTN2A1 to BTN3A1 triggers an extracellular transition that signals distress to the $V\gamma 9V\delta 2$ T cell. The extracellular domain of BTN2A1 is known to contact the $V\gamma 9V\delta 2$ TCR and may contact BTN3A1.[12,13,16] However, how BTN2A1 explicitly coordinates these intracellular and extracellular interactions to propagate information about pAg accumulation from the target cell to the T cell is less clear.

2.2 Results

Table 2.1: a-BTN2A1 Fab properties

Binder	CDR-L3	CDR-H1	CDR-H2	CDR-H3	KD (M) * *	k_on (/M/s)* *	k_off (/s)* *
2A1.1	SSSSLI	LYSSSI	SIYSSSGYTY	VYYQRGYIYSGF	7.79E-09	2.08E+05	1.62E-03
2A1.2	ASDWPI	FSYSSI	SIYSYYGSTS	YYYARGYVYAF	9.28E-09	2.29E+05	2.13E-03
2A1.3	ARSPLI	IYSSSI	SIYSYSGYTY	YYYYWGGVGDAL	1.23E-08	2.47E+06	3.02E-02
2A1.4	SSSSLI	FSSSSI	SIYSSSGYTY	WQSYRGYPWPGF	6.91E-09	9.49E+04	6.56E-04
2A1.5	SSSSLI	FSSSSI	SISSSSGSTS	GHLYWEYVQWGF	1.75E-08	1.15E+04	2.01E-04
2A1.6	SSSSLI	FSSSSI	SISSSSGSTS	GHYYYWYYPGYGF	ND	ND	ND
2A1.7	SSSSLI	FSSSSI	YIYPSSGSTS	YYYYRGYIDAM	6.73E-10	7.97E+05	5.36E-04
2A1.8	SSSSLI	FSSSYI	SIYSYYGSTS	ETVYKGYVPAL	4.61E-10	1.61E+06	7.42E-04
2A1.9	SSSSLI	LYSSSI	YIYPSSGYTS	YYYTRGYPDGM	3.73E-10	1.03E+06	3.84E-04
2A1.10	SSSSLI	FSSSSI	SISSSSGSTS	WFYERGYVVWAM	5.77E-09	9.57E+04	5.52E-04
2A1.11	SSSSLI	FSSSSI	SISSSSGSTS	GHTYWMYYSGWGM	1.80E-09	2.29E+06	4.12E-03
2A1.12	SSSSLI	FSSSSI	SIYSSSGYTY	IEYGRGYWDAF	4.07E-09	5.50E+05	2.24E-03
2A1.13	SQGELI	FSSSSI	SISSSSGSTS	GHYYYYYYSGWGF	1.82E-09	1.52E+06	2.77E-03
2A1.14	SKYMLI	FSYSSI	SISPYSSSTS	GHVYYHYYPGYGM	6.21E-10	2.95E+06	1.83E-03
2A1.15	SSSSLI	FSSSSI	SISSSSGSTS	GHQYYYYYGGWGF	ND	ND	ND

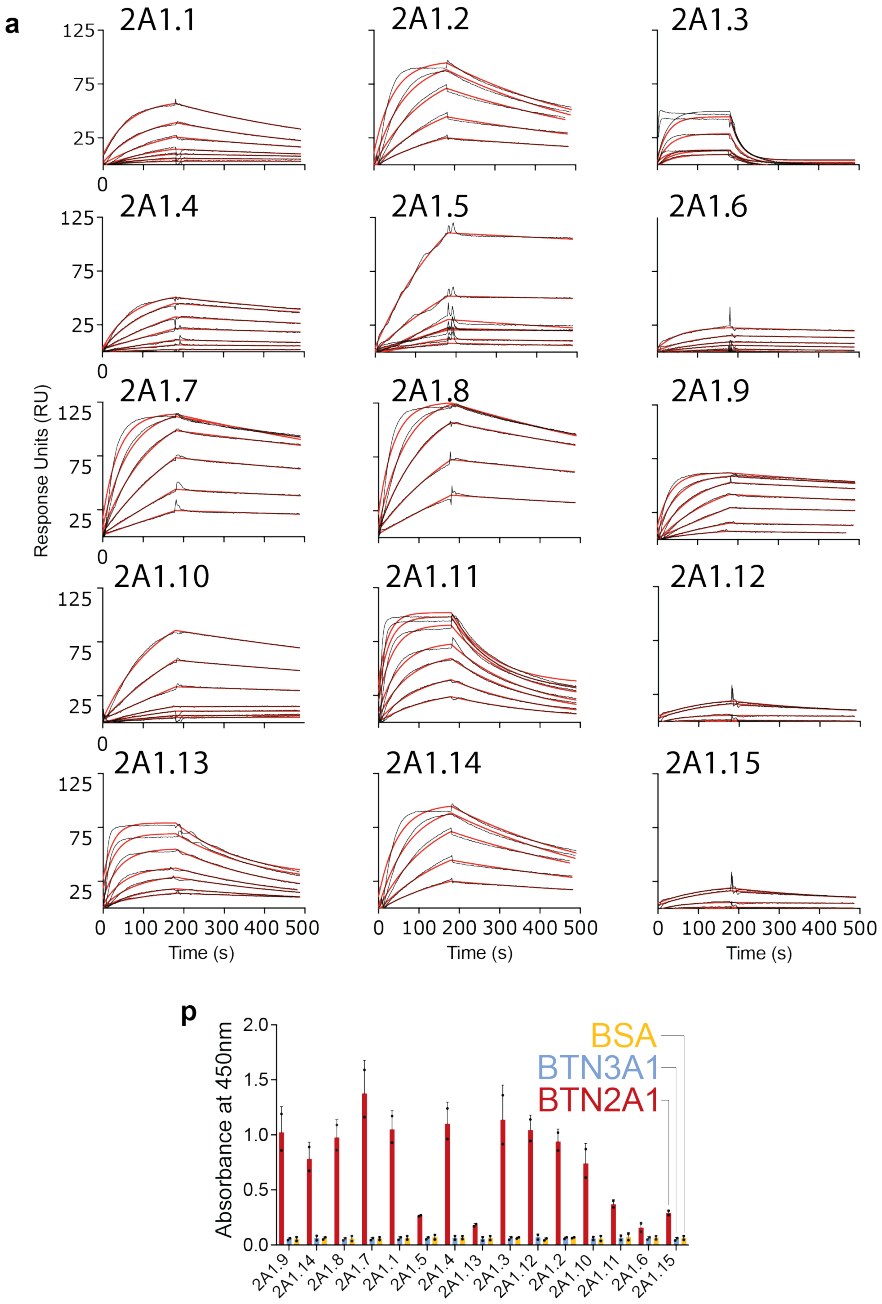

Figure 2.1: Biophysical affinity of $\alpha - BTN2A1$ Fabs

(A) Biophysical affinity of α-BTN2A1 Fabs binding to immobilized BTN2A1 ectodomain assessed by SPR in 2-fold dilutions (grey). Non-linear regression - association then dissociation calculated using GraphPad Prism (red). **(B)** α-BTN2A1 Fab specificity for BTN2A1 as assessed by ELISA. Fab expressed on bacteriophage was incubated with immobilized BTN2A1 ectodomain (red) or controls (BTN3A1 ectodomain (blue) or BSA (yellow)) as assessed by ELISA using Protein-L-HRP/TMB. Mean + SD (n=2). Reagents generated by me, SPR data collected by Dr. Tomasz Slezak.

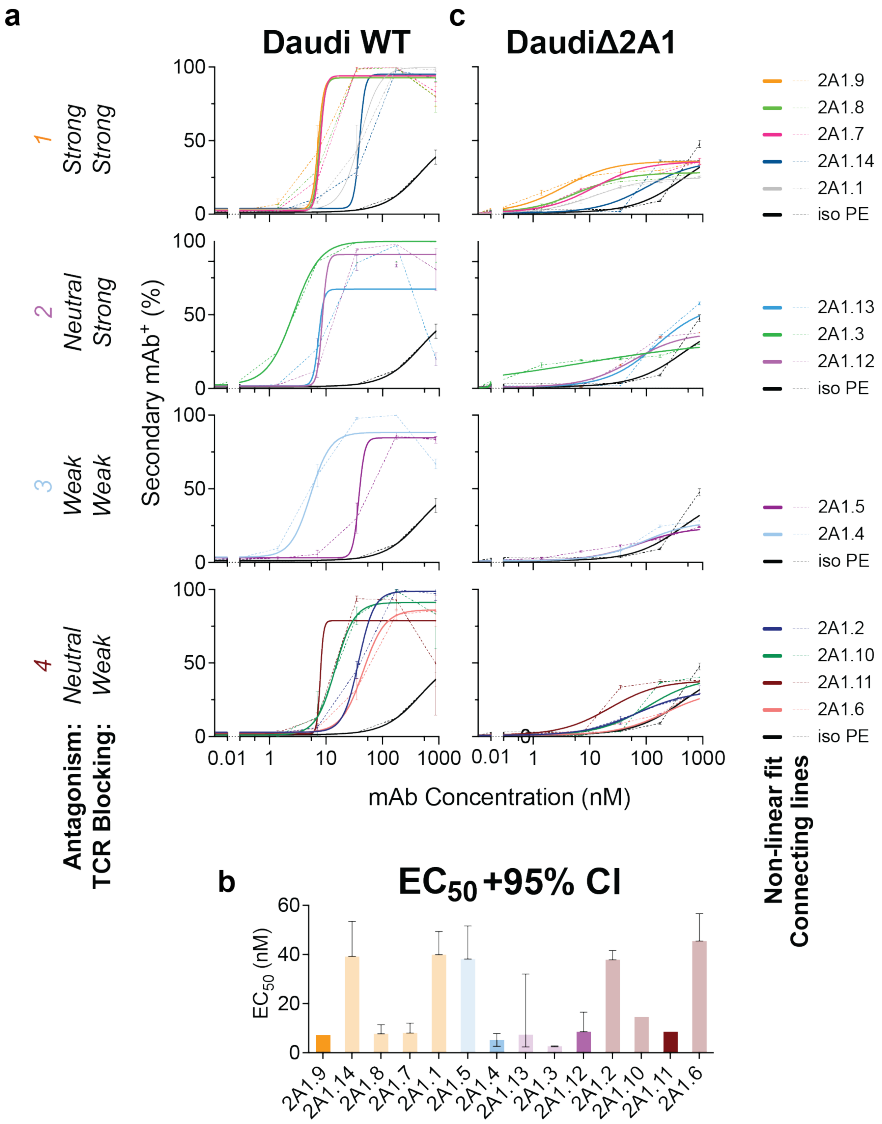

Figure 2.2: Cellular affinity of $\alpha - BTN2A1$ mAbs

(A,C) α-BTN2A1 mAb binding to (A) DaudiWT or (C) Daudi$\Delta 2A1$ cells at increasing concentrations, separated by mAb class. 1° mAb binding to BTN2A1 ectodomain visualized using α-mIgG1 2° antibody staining assessed by flow-cytometry (gated on no 1° mAb control). Mean + SD with connecting lines (dotted) (n=3), non-linear regression with variable slope - four parameters (solid). **(B)** EC50 of binding and 95% confidence intervals for α-BTN2A1 mAb binding to DaudiWT was calculated by non-linear regression with variable slope - four parameters (R2=0.9754, 0.9928, 0.9444, 0.9682, 0.9833, 0.9918, 0.8841, 0.5931, 1.000, 0.9603, 0.9947, 0.9254, 0.7812, 0.9779, 0.8660, 0.8196, 0.9995, respectively).

2.2.1 Development of high-affinity α-BTN2A1 mAbs without BTN3A cross-reactivity

To map immunogenic and inhibitory hotspots for $V\gamma9V\delta2$ activation on BTN2A1,I generated a panel of 14 α-BTN2A1 Fabs using phage display evolution mutagenesis[35,42] with BTN2A1 ectodomain as the target antigen 2.1. Negative selection was carried out using the BTN3A1 ectodomain as the target antigen and Fab selectivity was verified using phage-enzyme linked immunosorbent assay (ELISA) 2.1. α-BTN2A1 Fabs had a Herceptin human-IgG1 Fab scaffold and bound biotinylated, monomeric BTN2A1 ectodomain with varying biophysical affinities in the pico-nanomolar range as assessed by Surface-Plasmon Resonance (SPR) 2.1. Full-length mAb constructs were cloned by fusing the IgV domains of these Fabs to the murine-IgG1 Fab IgC-Hinge-Fc7.1. These mAbs also bound endogenous BTN2A1 on DaudiWT with a range of cellular affinities measured by EC50 of binding 2.2 and had negligible background staining on Daudi-Cas9 with KO of BTN2A1 (DaudiΔ2A1) cells 2.2.

2.2.2 α-BTN2A1 mAbs antagonize $V\gamma9V\delta2$ activation with varying potency

To test the effect of these α-BTN2A1 mAbs on $V\gamma9V\delta2$ activation, α-BTN2A1 mAbs were incubated with DaudiWT or DaudiΔ2A1 at a concentration of 6.8nM (1μg/mL) in the presence and absence of 5μg/mLM HMBPP. G115 Jurkats were then co-incubated with these mAb-pulsed target-cells overnight and assessed for CD69 expression via flow-cytometry 7.2. Both in the presence and absence of exogenous pAg, α-BTN2A1 mAbs antagonized $V\gamma9V\delta2$ activation with varying strength 2.3 2.4, whereas no mAb had agonist properties 2.32.4. DaudiΔ2A1 cells co-incubated with α-BTN2A1 mAbs did not stimulate Jurkat $V\gamma9V\delta2$ T cell activation 2.4. 2A1.9 was as strong an antagonist of $V\gamma9V\delta2$ activation as the α-BTN3A1 mAb 103.2 2.3 whereas other mAbs like 2A1.4 and 2A1.12 were weak antagonists,

and some including 2A1.11 had no effect on $V\gamma9V\delta2$ activation 2.3.

The potency of mAb antagonism was tested using primary $V\gamma9V\delta2$ T cells expanded from Peripheral Blood Mononuclear Cells (PBMCs) derived from healthy donors, 2.3 in activation assays similar to those previously described 7.2. 2A1.9 was the strongest antagonist of primary $V\gamma9V\delta2$ T cell activation, exceeding even 103.2, reducing CD107a, CD25 and CD69 expression below baseline expression levels 2.3. The weak antagonistic potency of 2A1.12 tracked with that seen in Jurkat activation assays 2.3. 2A1.12 also had greater variation in antagonism potency than other tested mAbs, suggestive of biochemical differences in its molecular interactions with BTN2A1. 2A1.11 had no effect on primary $V\gamma9V\delta2$ T cell activation 2.3, while still binding with appreciable affinity. DaudiΔ2A1 cells co-incubated with α-BTN2A1 mAbs did not stimulate primary $V\gamma9V\delta2$ T cell activation 2.4. I did not discover a mAb capable of stimulating $V\gamma9V\delta2$ activation 2.4.

2.2.3 Strong $\alpha - BTN2A1$ mAb antagonists block $V\gamma9V\delta2$ TCR engagement with BTN2A1 ectodomain

Linking $\alpha - BTN2A1$ Fab epitopes on the BTN2A1 ectodomain to Fab effects on $V\gamma9V\delta2$ activation provides potential insights into the molecular architecture of the mature pAg-signaling complex. BTN2A1 is a binding partner of the $V\gamma9V\delta2$ T cell Receptor (TCR) and while binding of its CFG-IgV face to the HV4 germline-encoded region of the $V\gamma9V\delta2$ TCR γ-chain is not sufficient for pAg-signaling, it is essential[12,13,16]. To explore if our antagonistic $\alpha - BTN2A1$ mAbs block pAg-signaling by competing for the $V\gamma9V\delta2$ TCR epitope on BTN2A1, we tested mAb-TCR competition by using High-Five insect cells expressing full-length BTN2A1 on their cell surface. These cells were incubated with 150nM saturating concentrations of our $\alpha - BTN2A1$ mAbs and were then stained with 120nM fluorescently tagged tetramers of the G115 $V\gamma9V\delta2$ TCR clone. TCR tetramer staining intensity was assessed relative to a no mAb, full TCR staining control group. G115 tetramer staining of

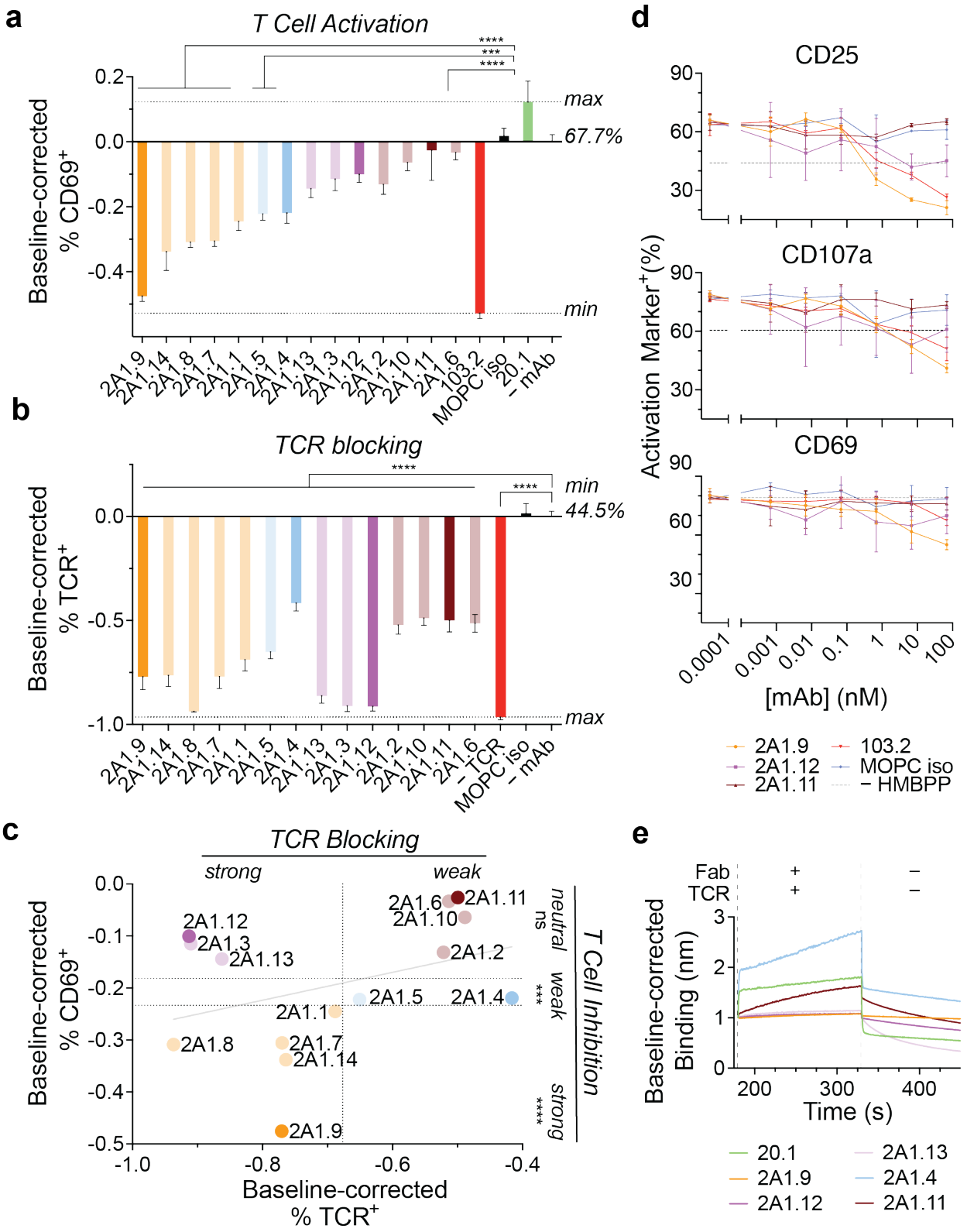

Figure 2.3: $V\gamma9V\delta2$ **activation can be inhibited by** α**-BTN2A1 mAbs**
(Continued on next page).

Figure 2.3: $V\gamma 9V\delta 2$ activation can be inhibited by α-BTN2A1 mAbs, continued

(Continued from previous page) **(A)** Inhibition of activation of G115-TCR expressing Jurkat Jrt-3.3 cells after co-incubation with DaudiWT cells pre-incubated with 5μg/mLM HMBPP and 6.8 nM (1μg/mLg/mL) α-BTN2A1 mAb or controls (MOPC isotype, 20.1 mAb, 103.2 mAb or Buffer + HMBPP). CD69 expression as a marker of T-cell activation was assessed by flow-cytometry (gated on isotype antibody) and normalized to Buffer + 5 μM HMBPP condition (Value-Baseline/Baseline). Mean + SD (n=6, 2 independent experiments). Dunnett test pairwise comparison to – mAb control: ****p<0.0001, ***p<0.0002. **(B)** Competition between α-BTN2A1 mAbs and the $V\gamma 9V\delta 2$ TCR for binding to BTN2A1 ectodomain was assessed in High-Five insect cells expressing full-length BTN2A1 stained with 150nM α-BTN2A1 mAbs or controls (20.1, 103.2, MOPC isotype or Buffer) followed by 120nM fluorescently-tagged $V\gamma 9V\delta 2$-TCR tetramers (G115 clone). TCR tetramer staining was assessed by flow-cytometry (gated on no TCR) and normalized to TCR tetramer, − mAb condition (Value-Baseline/Baseline). Mean + SD (n=6, 2 independent experiments). Dunnett test pairwise comparison to Buffer control: ****p<0.0001. **(C)** Correlation between α-BTN2A1 mAb $V\gamma 9V\delta 2$ antagonism (Baseline-corrected CD69 expression) and $V\gamma 9V\delta 2$ TCR-competition (Baseline-corrected TCR tetramer staining) as calculated by simple linear regression (R^2 =0.136, p = 0.1944). Strong and weak TCR blocking designated as lower and upper half of the range of TCR tetramer staining, respectively. TCR inhibition classified based on p values described in (A). **(D)** Inhibition of activation of $V\gamma 9V\delta 2$ T-cells expanded from primary PBMCs after co-incubation with DaudiWT cells pre-incubated with 5μM HMBPP and increasing concentrations of α-BTN2A1 mAb or controls (MOPC isotype, 103.2 mAb or Buffer + HMBPP). CD25 (top), CD107a (middle) and CD69 (bottom) expression as markers of T-cell activation were assessed by flow-cytometry (gated on isotype antibody). Mean + SD (n=3). **(E)** $V\gamma 9V\delta 2$ TCR competition with α-BTN2A1 Fab or control (20.1 Fab) with for binding to BTN2A1 ectodomain assessed by BLI, normalized. Immobilized Biotinylated BTN3A1 was exposed to 1.66μM Fab followed by 2.66μM Fab + 80μM TCR (G115 clone). Step 2 binding (nm) of TCR to Biotinylated BTN2A1 ectodomain in the presence of Fab was normalized to Fab alone binding (nm) at the end of Step 1.

BTN2A1 was reduced to varying degrees in the presence of every $\alpha - BTN2A1$ mAb 2.3. Addition of certain mAbs (2A1.9, 2A1.14, 2A1.8 and 2A1.7) had a greater effect on TCR tetramer staining of BTN2A1 2.3, potentially indicative of a larger overlapping mAb:TCR epitope on BTN2A1. Interestingly, a group of antibodies including 2A1.12 dramatically reduced TCR tetramer staining of BTN2A1 but did not exhibit G115 antagonism in our cellular assays. The G115 tetramer had no background staining on High-five insect cells expressing the control transmembrane protein ADLRG3 2.5.

The mAb:TCR competition for BTN2A1 binding was validated for representative Fabs

using BLI 2.3 2.5. BTN2A1 ectodomain was immobilized and exposed first (1) to $\alpha - BTN2A1$ Fab at 66μM for 150 seconds (s) followed by (2) 66μM Fab mixed with 80μM monomeric G115 $V\gamma 9V\delta 2$ TCR clone for 150s. Fab was included in the TCR association step (2.) to prevent Fab dissociation from masking TCR association. The 20.1 Fab, as control, was used to determine maximum TCR binding 2.5. The results from this biophysical epitope competition tracked with that assessed in High-Five insect cells: 2A1.9 completely blocked $V\gamma 9V\delta 2$ TCR association with BTN2A1 ectodomain 2.3 2.5 2A1.12 and 2A1.13 also dramatically reduced $V\gamma 9V\delta 2$ TCR association with BTN2A1 ectodomain 2.3 2.5 and 2A1.4 and 2A1.11 did not reduce $V\gamma 9V\delta 2$ TCR association with BTN2A1 ectodomain 2.3 2.5.

To understand the relationship between $V\gamma 9V\delta 2$ antagonism and TCR competition potency we classified the mAbs based on their potency of $V\gamma 9V\delta 2$ antagonism and TCR competition 2.3. A class of strongly antagonistic mAbs that dramatically reduce TCR:BTN2A1 staining emerged 2.3, represented by the 2A1.9 mAb. Another class of mAbs substantially reduced TCR staining of BTN2A1 but did not reduce $V\gamma 9V\delta 2$ activation 2.3) represented by the 2A1.12 mAb. The third class of mAbs weakly blocked TCR binding to BTN2A1 but had neutral effects on $V\gamma 9V\delta 2$ activation 2.3) represented by the 2A1.11 mAb. Although no mAbs had strong antagonistic properties without blocking the TCR 2.3, the 2A1.4 mAb significantly reduced $V\gamma 9V\delta 2$ activation and was the weakest TCR blocker 2.3 suggesting that it may have a mechanism of antagonism different from direct TCR competition for BTN2A1 binding. The largely nonlinear relationship between $V\gamma 9V\delta 2$ antagonism and TCR competition 2.3 prompted us to pursue structural determination of Fab:BTN2A1 complexes to assess how mAb epitopes contributed to $V\gamma 9V\delta 2$ antagonism.

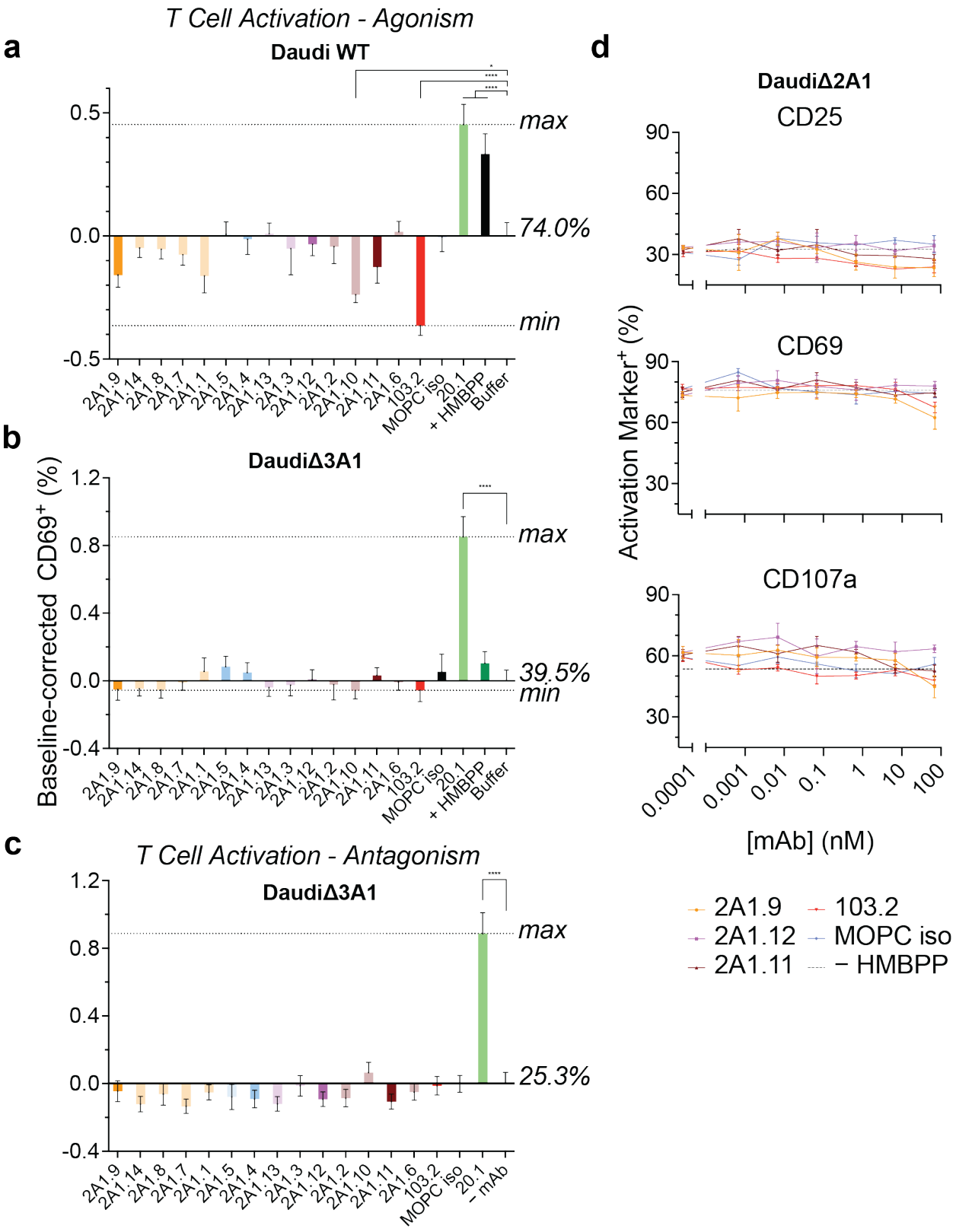

Figure 2.4: Supporting data for $V\gamma 9V\delta 2$ activation assays

Figure 2.4: Supporting data for $V\gamma 9V\delta 2$ activation assays, continued

(Continued from previous page) **(A)** Activation of G115-TCR expressing Jurkat Jrt-3.3 cells after co-incubation with DaudiWT cells pre-incubated with 6.8nM (1μg/mL) α-BTN2A1 mAb or controls (MOPC isotype, 20.1 mAb, 103.2 mAb, Pamidronate or Buffer + HMBPP). CD69 expression as a marker of T-cell activation was assessed by flow-cytometry (gated on isotype antibody) and normalized to Buffer condition (Value-Baseline/Baseline). Dunnett test pairwise comparison to Buffer control: *p<0.0332, ****p<0.0001. **(B)** Activation of G115-TCR expressing Jurkat Jrt-3.3 cells after co-incubation with DaudiΔ3A1 cells pre-incubated with 6.8nM (1μg/mL) α-BTN2A1 mAb or controls (MOPC isotype, 20.1 mAb, 103.2 mAb, Pamidronate or Buffer + HMBPP). CD69 expression as a marker of T-cell activation was assessed by flow-cytometry (gated on isotype antibody) and normalized to Buffer condition (Value-Baseline/Baseline).. Dunnett test pairwise comparison to Buffer control: ****p<0.0001. **(C)** Inhibition of activation of G115-TCR expressing Jurkat Jrt-3.3 cells after co-incubation with DaudiΔ3A1 cells pre-incubated with 5μg/mLM HMBPP and 6.8nM (1μg/mL) α-BTN2A1 mAb or controls (MOPC isotype, 20.1 mAb, 103.2 mAb or Buffer + HMBPP). CD69 expression as a marker of T-cell activation was assessed by flow-cytometry (gated on isotype antibody) and normalized to Buffer + 5 μM HMBPP condition (Value-Baseline/Baseline). Dunnett test pairwise comparison to – mAb control: ****p<0.0001. **(D)** Inhibition of activation of $V\gamma 9V\delta 2$ T-cells expanded from primary PBMCs after co-incubation with DaudiΔ2A1 cells pre-incubated with 5μg/mLM HMBPP and increasing concentrations of α-BTN2A1 mAb or controls (MOPC isotype, 103.2 mAb or Buffer + HMBPP). (D) CD25, CD107a, CD69 expression as markers of T-cell activation were assessed by flow-cytometry (gated on isotype antibody). Mean + SD (n=3).

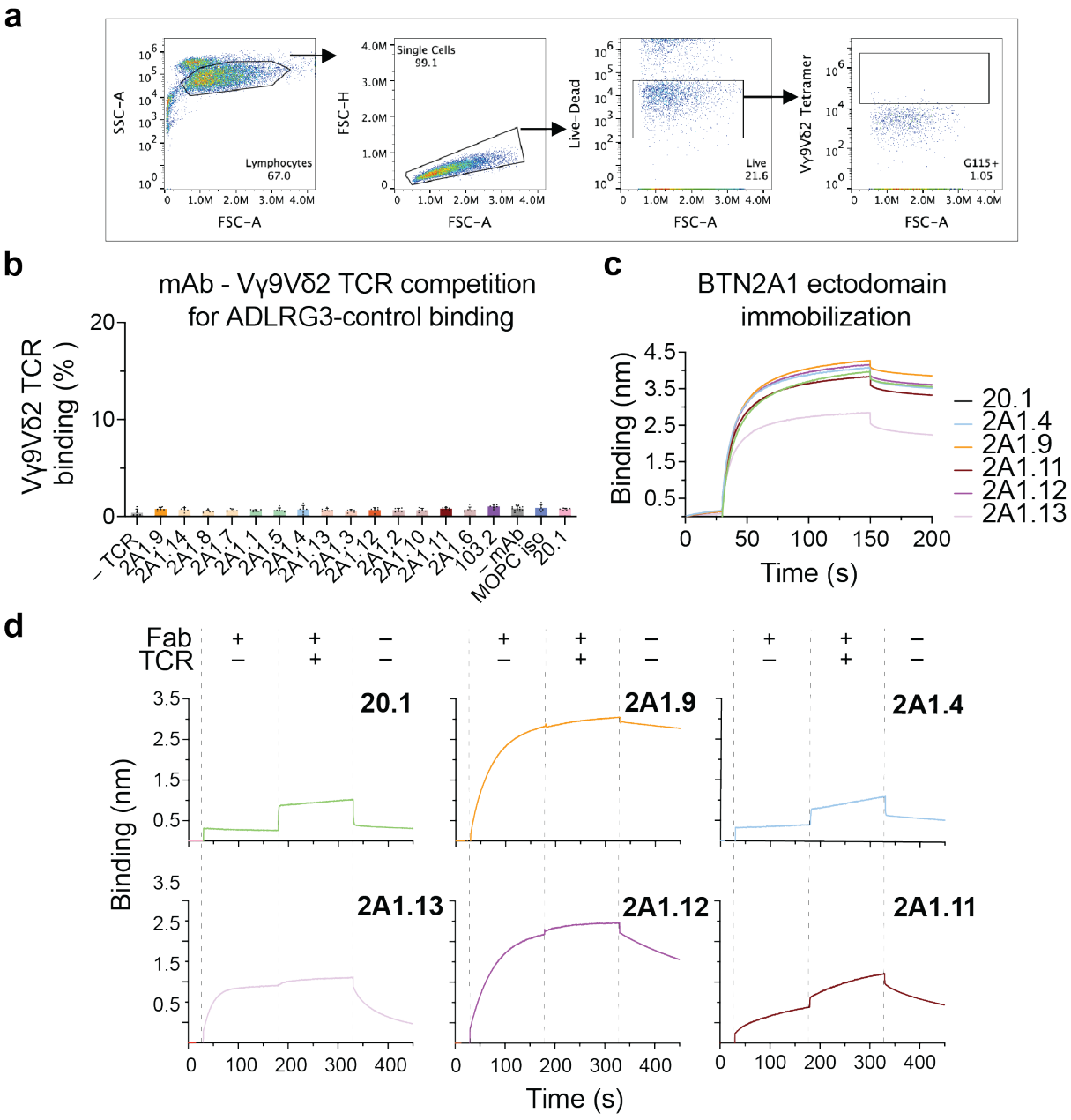

Figure 2.5: Supporting data for α-BTN2A1 reagent competition with $V\gamma9V\delta2$ TCR for binding to BTN2A1

(A) Gating strategy for α-BTN2A1 mAbs - $V\gamma9V\delta2$ TCR competition assays. $V\gamma9V\delta2$ TCR Tetramer positive gate drawn to˜1% positive staining in – mAb condition. **(B)** Competition between α-BTN2A1 mAbs and the $V\gamma9V\delta2$ TCR for binding to BTN2A1 ectodomain was assessed in High-Five insect cells expressing full-length ADLRG3 control transmembrane protein stained with 150nM α-BTN2A1 mAbs or controls (20.1, 103.2, MOPC isotype or Buffer) followed by 120nM fluorescently-tagged $V\gamma9V\delta2$-TCR tetramers (G115 clone). TCR tetramer staining was assessed by flow-cytometry (gated on no TCR). Mean + SD (n=6, 2 independent experiments).

Figure 2.5: Supporting data for competition assays between α-BTN2A1 reagent competition with $V\gamma9V\delta2$ TCR for binding to BTN2A1, continued

(Continued from previous page) **(C)** Biotinylated BTN3A1 immobilization on streptavidin biosensor assessed by BLI, colored by reagent subsequently tested (representative of 2 independent experiments). **(D)** α-BTN2A1 Fab or control (20.1 Fab) competition with $V\gamma9V\delta2$ TCR for binding to BTN2A1 ectodomain assessed by BLI. Immobilized Biotinylated BTN3A1 was exposed to 1. 66μM Fab followed by 2. 66μM Fab + 80μM TCR (G115 clone). 20.1 (top-left), 2A1.9 (top-middle), 2A1.4 (top-right), 2A1.13 (bottom-left), 2A1.12 (bottom-middle) and 2A1.11 (bottom-right) were assessed.

CHAPTER 3

MAPPING THE EXTRACELLULAR ARCHITECTURE OF THE PAG SIGNALING COMPLEX WITH α-BTN2A1 ANTIBODIES

3.1 Introduction

Understanding the overall binding orientation, docking angle and molecular contacts between α-BTN2A1 binders and the BTN2A1 extracellular domain can provide insight into the complex relationship between the $V\gamma9V\delta2$ antagonism potency and $V\gamma9V\delta2$ TCR blocking potency of the mAbs in my panel.

3.2 Results

3.2.1 Complex structure shows 2A1.9 Fab sequestering critical residues in the $V\gamma9V\delta2$ TCR epitope on BTN2A1

To better understand the molecular underpinnings of mAb antagonism of $V\gamma9V\delta2$ TCR, a 2.8Å structure of 2A1.9 Fab in complex with monomeric BTN2A1 ectodomain C219S (BTN2A1 ectodomain) was solved by X-ray crystallography 3.1 3.1a. Specific molecular contacts between the 2A1.9 Fab and the BTN2A1 ectodomain were identified using PDB-ePISA[43] and ccp4-Contact[44]. 2A1.9 Fab bound to the IgV-like domain of BTN2A1 ectodomain utilizing all CDR loops except CDRL2 to make molecular contacts with residues located throughout BTN2A1 C", C', C, F, and G */beta* strands (CFG-face) 3.1. The total Buried Surface Area (BSA) on the BTN2A1 ectodomain was 964.6 Å, the Fab heavy chain contributing 658.6 Å and Fab light chain contributing 306.0 Å. The 2A1.9 Fab formed 15 Hydrogen-bonds (HB) and salt-bridges (SB) with BTN2A1 ectodomain 3.2, 7 of which in-

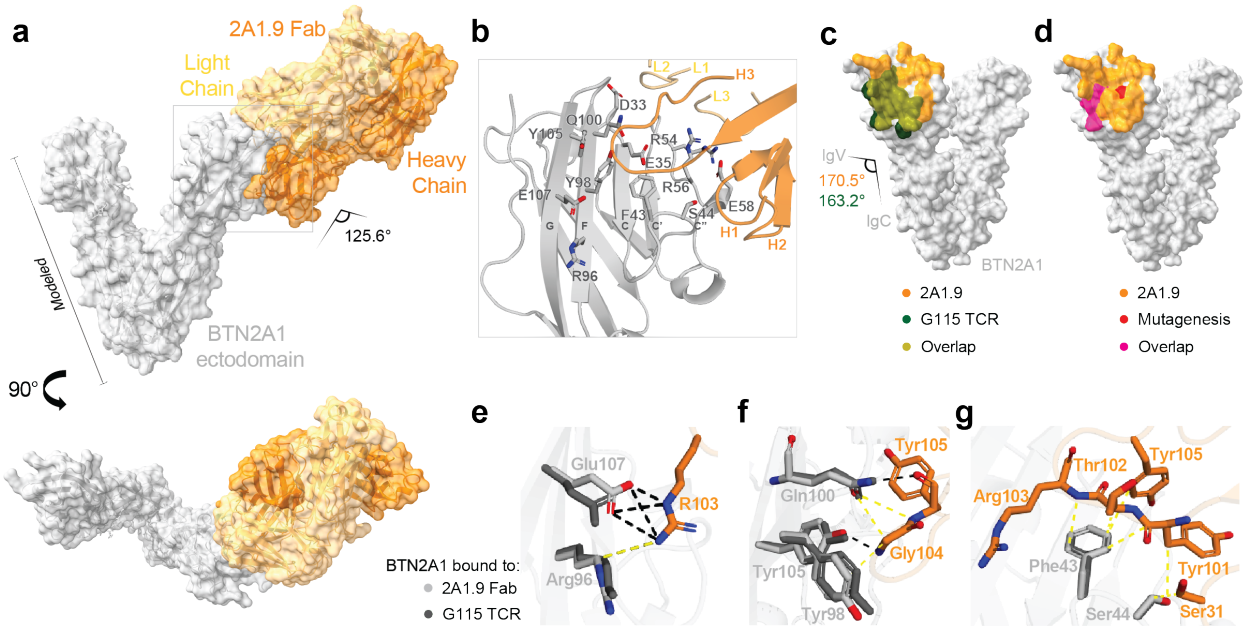

Figure 3.1: Structure of 2A1.9 Fab in complex with BTN2A1 ectodomain provides insight into TCR-competition mechanism of $V\gamma9V\delta2$ Antagonism.
(A) Structure and surface representation of BTN2A1 ectodomain complexed with antagonistic 2A1.9 Fab as determined by X-ray Crystallography (PDB: 8VC7) **(B)** CFG Face of BTN2A1 ectodomain showing key residues implicated in $V\gamma9V\delta2$ activation[13] or TCR binding[32] and docking orientation of 2A1.9 Fab CDR loops. **(C)** Surface representation of BTN2A1 ectodomain with residues contacting 2A1.9 Fab (orange), $V\gamma9V\delta2$ TCR (PDB:8DFW)[32] (green) or both (olive) highlighted. **(D)** Surface representation of BTN2A1 ectodomain with residues contacting 2A1.9 Fab (orange), crucial for $V\gamma9V\delta2$ activation as assessed by mutagenesis[13] (red) or both (pink) highlighted. **(E-G)** Molecular contacts of 2A1.9 Fab with BTN2A1 residues implicated in $V\gamma9V\delta2$ activation[13] or TCR binding[32] as assessed by PDB-ePISA and Contact-ccp4. Highlighted residues of BTN2A1 IgV domain bound to 2A1.9 Fab (light grey) or $V\gamma9V\delta2$ TCR (dark grey) are shown. **(E)** Glu107 and Arg96 **(F)** Tyr98, Gln100 and Tyr105 **(G)** Phe43 and Ser44 are shown. HB (distance <3.5Å) and SB (distance <4.5Å) depicted in black, vdW (distance <4Å) depicted in yellow. If residue contact involves both HB/SB and vdW only HB/SB is shown.

Table 3.1: Crystallography data collection and refinement statistics

(a) [vdW: van der Waal contact (distance < 4 Å); H: hydrogen bond (distance < 3.5 Å) SB: salt bridge (distance < 4.5 Å, polar interaction between oppositely charged atoms)]

	2A1.9 - 2A1 ecto
PDB ID code	8VC7
Data Collection	
Radiation Source	SSRL 14-1
Wavelength (Å)	1.195
Resolution range (Å)	39.46 - 2.76 (2.83 - 2.76)
Space group	P 21 21 21
Unit cell	44.915 200.976 206.684 90 90 90
Data Processing	
Total reflections	441063
Unique reflections	49406 (3511)
Multiplicity	8.9
Completeness (%)	99.80 (100.00)
Mean I/sigma(I)	7.2
Wilson B-factor	42.85
R-merge	0.272
R-meas	0.289
R-pim	0.095
CC1/2	0.99
CC*	
Data Refinement	
Reflections used in refinement	49406 (3511)
Reflections used for R-free	1998 (136)
R-work	0.2184 (0.3430)
R-free	0.2602 (0.3822)
CC(work)	
CC(free)	
Number of non-hydrogen atoms	9797
macromolecules	9727
ligands	70
solvent	0
Protein residues	1288
Nucleic acid bases	
RMS(bonds)	0.009
RMS(angles)	1.14
Ramachandran favored (%)	96.86
Ramachandran allowed (%)	2.91
Ramachandran outliers (%)	0.24
Rotamer outliers (%)	3.83
Clashscore	6.12
Average B-factor	38.63
macromolecules	38.46
ligands	62.13
solvent	
Number of TLS groups	

volved residues in the CDRH3 loop. These stable contacts were strengthened through 154 calculated van der Waals (vdW) interactions between both sidechain and main-chain atoms of 2A1.9Fab CDR loop and BTN2A1 ectodomain CFG-face residues 3.2. Due to the abundance of vdW interactions, representative contacts were chosen for each residue pair when multiple atoms formed vdW interactions for visual clarity.

We first mapped the binding footprints of the 2A1.9 Fab and the $V\gamma9V\delta2$ TCR[32] on the BTN2A1 ectodomain 3.1. Consistent with our cellular and biophysical results, the epitopes of the 2A1.9 Fab and the $V\gamma9V\delta2$ TCR overlapped substantially, with the 2A1.9 Fab sequestering all but 3 residues in the interface between the $V\gamma9V\delta2$ TCR and the BTN2A1 ectodomain 3.1. The 2A1.9 binding footprint also included critical residues for

Table 3.2: Molecular contacts between 2A1.9 Fab and BTN2A1 ectodomain

2A1.9 Fab Residue	BTN2A1 residue	Type
CDR1 Light		
Ser30 (OG)	Asp33 (OD1)	HB
Ser30 (OG)	Glu32, Asp33, Gly52, Gly53	VdW
Ser31	Asp33	VdW
Ala32	Gly52	VdW
CDR2 Light		
Tyr49	Gly102, Arg103	VdW
Ser53	Gly102, Arg103	VdW
CDR3 Light		
Ser91 (O)	Arg56 (NH2)	HB
Ser91 (O)	Arg56	VdW
Ser92 (O)	Arg54 (NE)	HB
Ser92 (OG)	Gly52 (O)	HB
Ser92	Gly52, Arg54	VdW
Other Light		
Arg66 (NH1)	Asp33 (OD2)	HB, SB
Arg66 (NH1)	Asp33	VdW
CDR1 Heavy		
Tyr30	Gln42, Pro45	VdW
Ser31	Ser44	VdW
CDR2 Heavy		
Tyr50 (OH)	Glu58 (OE2)	HB
Tyr50 (OH)	Glu58	VdW
Tyr52 (OH)	Glu58 (OE2)	HB
Tyr52 (OH)	Glu58, Glu59	VdW
Ser54	Pro45	VdW
Ser55 (OG)	Glu58 (O)	HB
Ser55 (OG)	Glu58, Arg65	VdW
Tyr57	Thr57, Glu58, Arg65	VdW
CDR3 Heavy		
Tyr101	Phe43, Ser44, Glu59	VdW
Thr102	Phe43	VdW
Arg103 (NE)	Glu107 (OE1, OE2)	HB, SB
Arg103 (NH2)	Glu107 (OE1, OE2)	HB, SB
Arg103	Phe39, Phe43, Arg96, Tyr98, Glu107	VdW
Gly104 (N)	Tyr98 (OH)	HB
Gly104 (N)	Tyr98, Gln100, Tyr105	VdW
Tyr105 (OH)	Glu35 (OE1)	HB
Tyr105 (OH)	Lys 51 (NZ)	HB
Tyr105 (O)	Gln100 (NE2)	HB
Tyr105	Glu35, Phe43, Gln100	VdW
Asp107 (OD1, OD2)	Lys51 (NZ)	SB

pAg-signaling 3.1 identified through rational mutagenesis based on structural models of the BTN2A1:TCR complex[13]. To compare the structural and molecular differences in BTN2A1 when bound to either the 2A1.9 Fab or the $V\gamma9V\delta2$ TCR I aligned the BTN2A1 IgV domain in our complex structure with that in the structure of the BTN2A1 ectodomain in complex with the $V\gamma9V\delta2$ TCR (PDB: 8DFW)[32]. The angle between the BTN2A1 ectodomain IgV and IgC domains was altered 7.3° when bound to the 2A1.9 Fab versus the $V\gamma9V\delta2$ TCR 3.1. I then analyzed critical BTN2A1 residue side chain orientations and molecular contacts with the 2A1.9 Fab. Residues that formed electrostatic interactions with the $V\gamma9V\delta2$ TCR[32] or had been shown by mutagenesis to be critical for pAg-signaling[13] were highlighted. R96 and E107 bind the $V\gamma9V\delta2$ TCR[32] and mutagenesis of these residues abrogates pAg-signaling[13].

The 2A1.9 Fab residue R103 forms a network of HB and vdW interactions with these residues and alters the position of E107 3.1, likely contributing to the high affinity of the 2A1.9 Fab for BTN2A1 as well as its antagonism potency. BTN2A1 Y98, Q100, and Y105 contact the $V\gamma9V\delta2$ TCR and the mutagenesis of residues Y98 and Y105 either abrogate or reduce pAg-signaling, respectively[13]. The 2A1.9 Fab contacts these three residues through G104 and Y105 in its CDRH3 loop via main and sidechain HB and vdW interactions 3.1. BTN2A1 F43 and S44 bind the $V\gamma9V\delta2$ TCR[32] and S44 has been implicated in pAg-signaling through mutagenesis[13]. The 2A1.9 Fab uses side- and main-chain atoms in CDRH3 and CDRH1 residues to sequester F43 and S44 through extensive vdW interactions 3.1. Altogether these data establish that the mechanism by which 2A1.9 antagonizes $V\gamma9V\delta2$ activation is by direct competition with the $V\gamma9V\delta2$ TCR for BTN2A1 binding.

3.2.2 Preliminary Complex Structures of BTN2A1 with 2A1.4 and 2A1.11 Fabs reveal insight into molecular features governing BTN2A1's role in pAg-signaling

	2A1.9	**2A1.4**	**2A1.11**	**2A1.12**
Data Collection				
Microscope	Krios	Krios	Krios	Glacios
Magnification	81,000	81,000	81,000	
Voltage (kV)	300	300	300	200
Electron Exposure (e-/A2)	1.12	1.12	1.12	1.12
Pixel Size (Å)	1.068	1.065	1.065	0.868
Data Processing				
Symmetry	C1	C1	C1	C1
Micrographs Used	500	1988	5438	542
Initial Particle Images (No.)	138,922	2,070,171	3,051,337	221026
Final Particle Images (No.)	32,636	178,142	289,154	N/A
Reference map (PDB ID)	8DFW	8DFW	8DFW	N/A
Estimated resolution (Å)	9.6	10.7	9.5	N/A

Having verified the importance of the BTN2A1 epitope shared between 2A1.9 and the

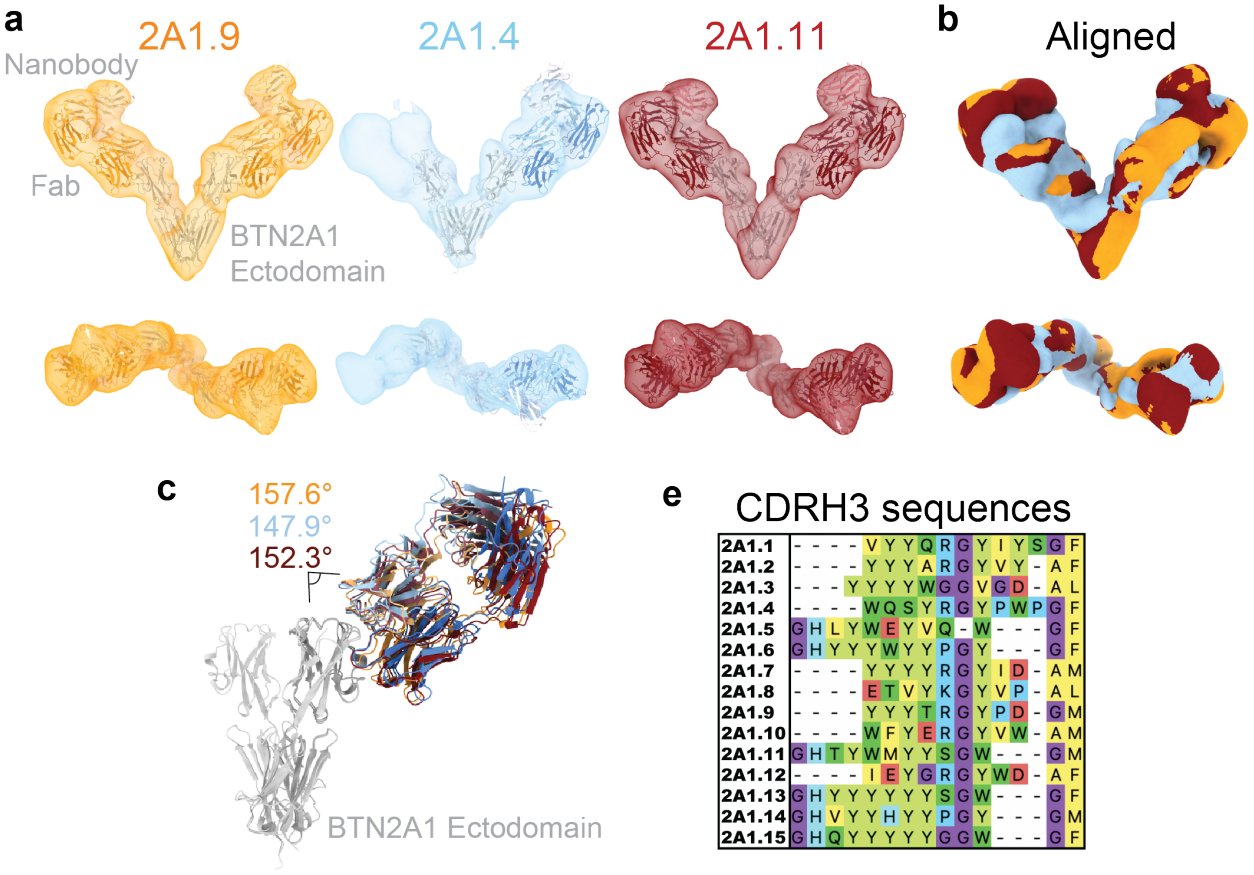

Figure 3.2: Docking orientations of 2A1.4 and 2A1.11 α-BTN2A1 Fabs on BTN2A1 are similar to 2A1.9.
(A) Models of Fabs 2A1.9 (left), 2A1.4 (middle) and 2A1.11 (right) in complex with the BTN2A1 ectodomain dimer. Models were generated by fitting the BTN2A1 dimer (PDB ID: 8DFW; Chain A,B) and a muIgG1 Fab complexed with a nanobody (PDB ID: 7PIJ) into respective volume maps at 9.3Å, 10.7Å, and 9.5Å, respectively, acquired by single-particle cryo-electron microscopy. **(B)** Alignment of 2A1.4 and 2A1.11 with 2A1.9 Fab Complex volume maps. **(C)** Putative docking angles of models of the 2A1.9, 2A1.4 and 2A1.11 Fabs on the BTN2A1 ectodomain with nanobodies and one Fab removed for clarity aligned by the BTN2A1 IgV domain. Docking angles in the plane perpendicular to the cell membrane were calculated using the CA of BTN2A1 Cys97, Gln100 and Fab heavy-chain Cys92 in ChimeraX. **(D)** Alignment of α-BTN2A1 CDRH3 loops.

$V\gamma9V\delta2$ TCR in $V\gamma9V\delta2$ activation, I wished to understand whether other epitopes on BTN2A1 were critical for pAg signaling. I thus pursued structural determination of 2 additional Fabs in complex with the BTN2A1 ectodomain dimer (BTN2A1 dimer) and an anti-Fab nanobody via single-particle Cryo-electron microscopy **??**. I prioritized the mAbs most likely to have a non-overlapping epitope with the $V\gamma9V\delta2$ TCR due to discrepancies in their $V\gamma9V\delta2$ antagonism and TCR blocking abilities. The 2A1.4 mAb is the poorest TCR blocker but significantly inhibits $V\gamma9V\delta2$ activation more potently than stronger TCR blockers and the TCR blocking mAb 2A1.11 has insignificant effects on $V\gamma9V\delta2$ activation 2.3. I collected datasets of the 2A1.4, 2A1.11 and 2A1.9 Fabs in complex with the BTN2A1 dimer and a stabilizing/bulking anti-Fab nanobody and generated maps at 9.3, 10.65 and 9.5Å resolutions, respectively 3.2. Structures of the BTN2A1 ectodomain (PDB ID: 8DFW, Chain A-B) and a muIgG1 Fab complexed with a nanobody (PDB ID: 7PIJ) were then modeled into the low resolution maps using ChimeraX[45]. At these resolutions I are able to compare the Fab docking angles and overall conformation of binding to BTN2A1 3.2. The docking orientation and angle of both the 2A1.11 and 2A1.4 Fabs are remarkably similar to that of the 2A1.9 Fab 3.2. The 2A1.9, 2A1.4 and 2A1.11 Fabs bind to BTN2A1 at an angle of 157.6°, 147.9° and 152.3° respectively in the plane perpendicular to the cell membrane 3.2. These data suggest that the epitopes of 2A1.4 and 2A1.11 on BTN2A1 likely overlap with that of 2A1.9 and subsequently the $V\gamma9V\delta2$ TCR. However, the different abilities of 2A1.4, 2A1.11 and 2A1.9 mAbs to antagonize $V\gamma9V\delta2$ activation and block TCR recognition of BTN2A1 cannot be explained by the overall docking location of Fabs on BTN2A1.

3.2.3 Molecular intricacies in Fab:BTN2A1 interface may drive the potency of mAb $V\gamma9V\delta2$ antagonism

I was curious as to how various mAbs had the ability to sequester the $V\gamma9V\delta2$ TCR epitope on BTN2A1 with variable effects on $V\gamma9V\delta2$ activation ranging from strong inhibition to

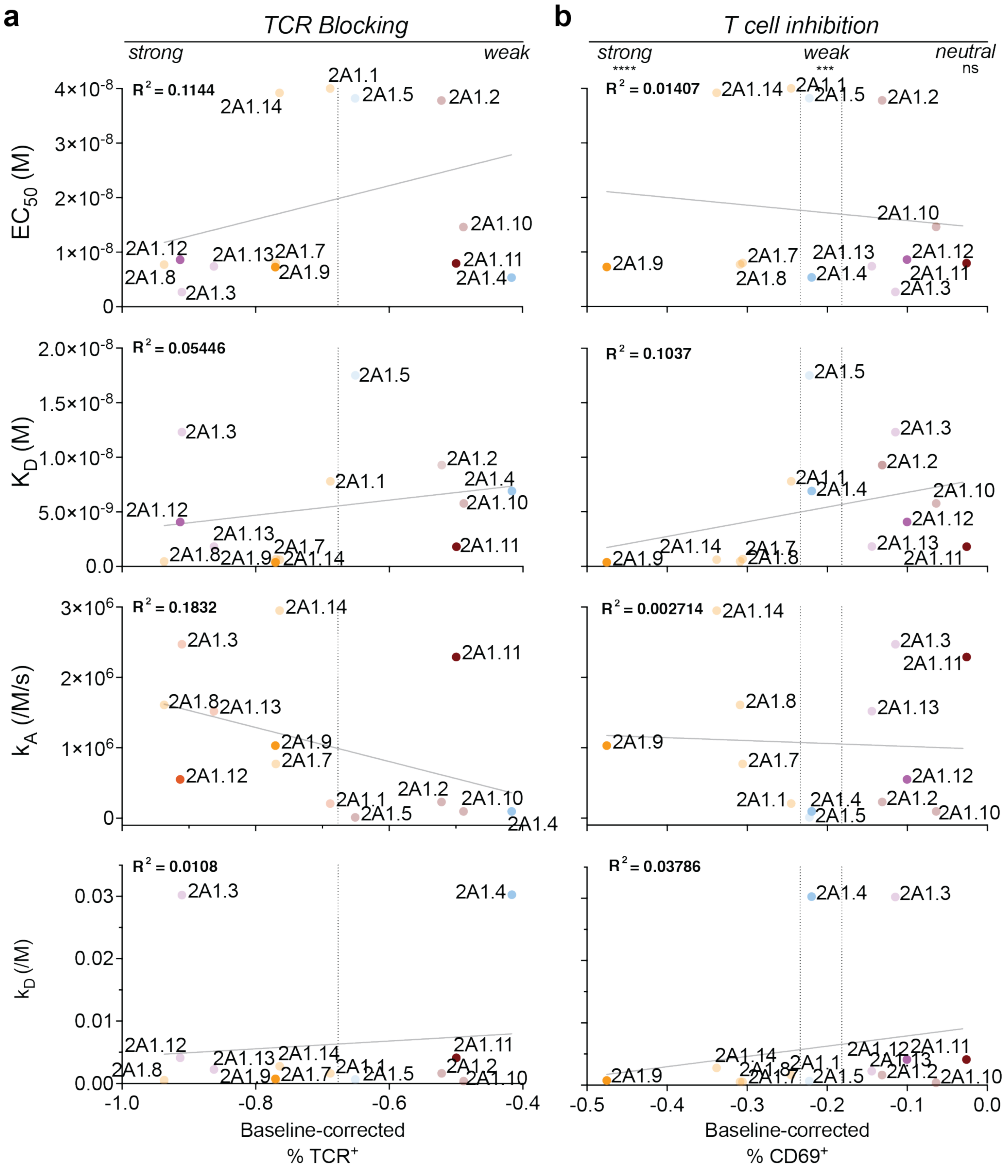

Figure 3.3: Analysis of the relationship between reagent affinity and mAb physiological property

(A) Baseline-corrected TCR blocking from 2.3 plotted against mAb or Fab affinity properties including mAb EC_50 of binding to DaudiWT cells, Fab K_D, Fab k_A and Fab k_D from 2.1. **(B)** Baseline-corrected CD69 expression from 2.3 plotted against mAb or Fab affinity properties including mAb EC_50 of binding to DaudiWT cells, Fab K_D, Fab k_A and Fab k_D from (Supplementary Figure 2). Simple linear regression was calculated with R^2 values indicated.

neutral. To probe whether the physiological properties of mAbs could be characterized by differences in cellular or biophysical affinity, EC_50, K_D, k_A and k_D were plotted as a function of mAb $V\gamma9V\delta2$ antagonism or TCR blocking potency 3.3. I observed that 2A1.11 and 2A1.4 have 10.7X and 1.7X faster respective $k_D$properties than 2A1.9 (Supplementary Table 1) and the strongest antagonists tended to have biophysical affinities (KD) below 1 nM (Supplementary Fig. 11H). However there was no overall correlation between mAb affinity for BTN2A1 and $V\gamma9V\delta2$ antagonism or TCR blocking (Supplementary Fig. 11). I then aligned the CDRH3 loop sequences of α-BTN2A1 mAbs and observed that the R103 and GY motif 3.1 used by the 2A1.9 Fab to sequester critical BTN2A1 residues from the $V\gamma9V\delta2$ TCR were highly conserved in our panel 3.2. Thus, subtle molecular differences in the interactions between Fab CDR loops and BTN2A1 may play a role in mAb antagonism potency controlling whether Fab contact with BTN2A1 persists on the time scale necessary to compete with $V\gamma9V\delta2$ TCR binding in a physiological context. Overall our data highlights the complicated mechanisms by which antibodies bind to and influence the behaviors of their targets with important implications in the development of antibody-based therapeutics and research tools.

3.3 Discussion and Conclusions

Our novel BTN2A1 antibodies either antagonized or had no effect on $V\gamma9V\delta2$ antagonism, consistent with reagents developed by the Uldrich[12] and Olive[30] groups. This suggests that the primary role BTN2A1 serves is to coordinate the formation of the pAg signaling complex as a central protein covered in critical epitopes for binding the $V\gamma9V\delta2$ TCR. Our high resolution structure of the 2A1.9 Fab bound to BTN2A1 shows 2A1.9 utilizing a complex network of electrostatic interactions to bind residues critical for the interaction between the $V\gamma9V\delta2$ TCR and BTN2A1. This extensive network of hydrogen bonds and van der Waals interactions allows 2A1.9 mAb to potently antagonize $V\gamma9V\delta2$ activation by sequestering

the $V\gamma 9V\delta 2$ TCR epitope on BTN2A1. Our low resolution structural data on the 2A1.4 and 2A1.11 Fabs in complex with BTN2A1 suggest a similar binding location and angle to 2A1.9 which is intriguing considering that neither 2A1.4 nor 2A1.11 blocks $V\gamma 9V\delta 2$ TCR binding and 2A1.11 does not antagonize $V\gamma 9V\delta 2$ activation. The affinity between BTN2A1 and the $V\gamma 9V\delta 2$ TCR is$\tilde{}$40 μM[12,13] and affinities between TCR hypervariable loops are considered to be low affinity[46] as well. It is surprising that our neutral or weakly antagonistic α-BTN2A1 Fabs had nM range affinities and yet could not compete with the $V\gamma 9V\delta 2$ TCR for binding to BTN2A1 even as bivalent antibodies which should boost binding strength considerably due to avidity effects. Though the biophysical principles underlying TCR-signaling are still poorly understood, it is possible that antibodies with fast off-rates provide enough of an opportunity for the $V\gamma 9V\delta 2$ TCR to bind to BTN2A1 and initiate TCR-mediated signaling. None of our tested antibody reagents bound non-overlapping epitopes with the $V\gamma 9V\delta 2$ TCR, therefore the roles of the ABE face and top membrane distal face of the BTN2A1 IgV ectodomain as well as the IgC domains remain undetermined. It is possible that additional epitopes exist to coordinate binding with BTN3A[14,16] or another TCR CDR loop ligand. Indeed, an interaction between BTN3A and the BTN2A1 IgV have been suggested through NMR and FRET experiments conducted by the Willcox[16] and Olive[30] groups though the role and necessity of this interaction for pAg signaling is unclear[16].

CHAPTER 4

THE ROLE OF BTN3A CLUSTERING IN $V\gamma 9V\delta 2$ ACTIVATION

4.1 Introduction

The Scotet and Adams groups initially observed immobilization of BTN3A in target cell membranes prior to target cell – T cell contact dependent on the addition of pAg or 20.1 agonist[27,47]. The addition of pAg or 20.1 to target cells also drives the formation of BTN3A puncta on the cell membrane, indicating the formation of BTN3A clusters that may drive the formation of early immunological synapses[27,47]. Indeed, BTN3A dramatically localizes to the target cell - T cell interface in the presence of activating reagents[47]. Structural data from the Adams lab has supported the clustering hypothesis, showing 20.1 binds the IgV C' and C" strands of BTN3A dimers in a lateral and downward orientation necessitating that one 20.1 mAb must cluster two BTN3A dimers on the cell membrane in close proximity[27,48]. However, the Adams group also found that the 20.1 Fab and scFv could stimulate $V\gamma 9V\delta 2$ activation[27], complicating our understanding of the role of 20.1 valency and subsequently BTN3A clustering in $V\gamma 9V\delta 2$ activation. I thus set out to learn more about how 20.1 mimics pAg signaling to stimulate $V\gamma 9V\delta 2$s.

4.2 Results

4.2.1 Rational engineering of α-BTN3A mAb 20.1 to probe the role of BTN3A clustering in pAg-signaling

It has been hypothesized that 20.1 must multimerize BTN3A dimers when binding BTN3A bivalently due to its lateral binding orientation[27,48] 4.1. This model suggests that 20.1 mimics what happens physiologically, where pAg binding to the intracellular B30.2 domain

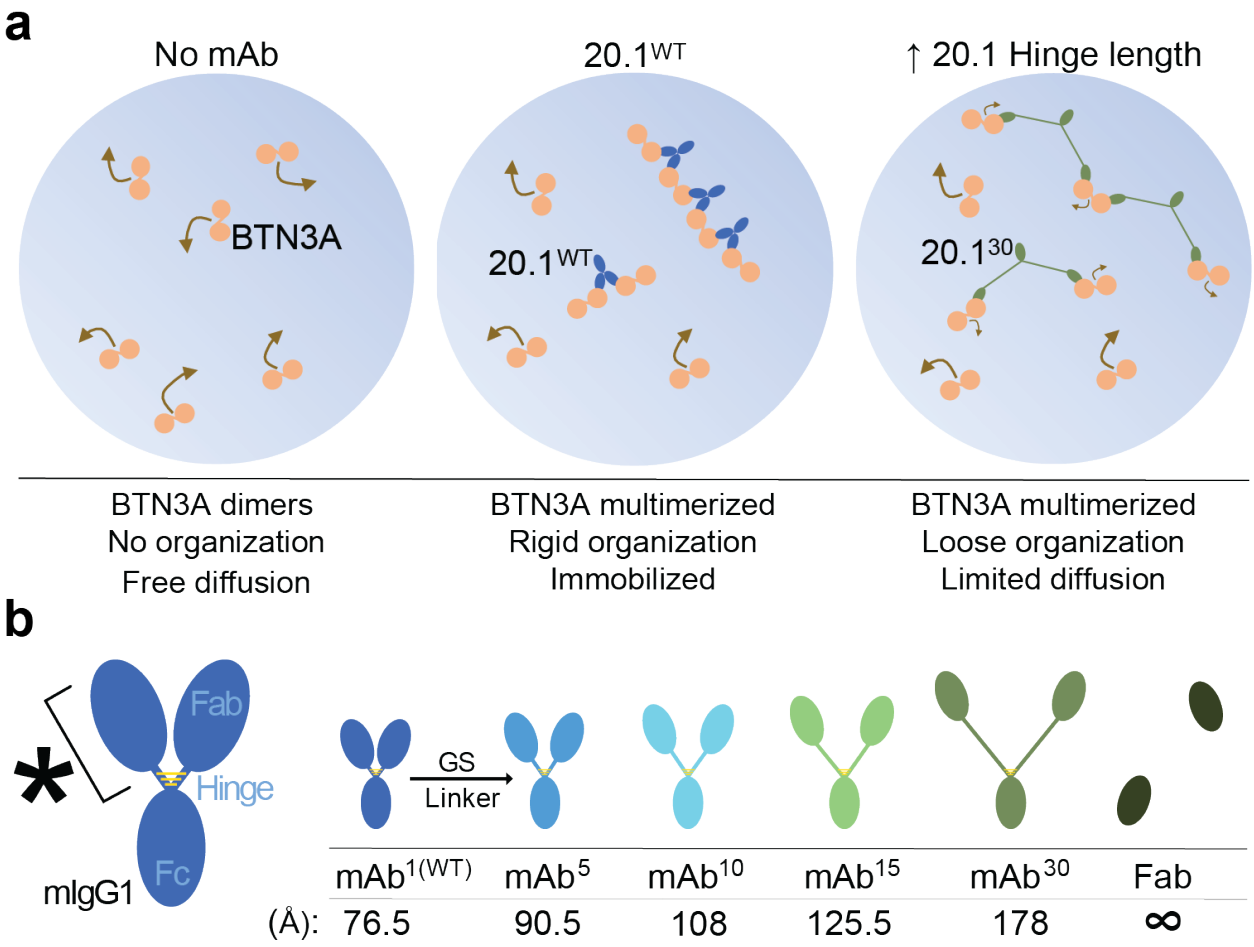

Figure 4.1: Rationally engineered 20.1 agonist mAbs may alter BTN3A multimerization

(A) Schematic representing the putative effects of increasing 20.1 inter-Fab distance on BTN3A1 membrane organization. Left: BTN3A membrane organization under resting conditions. Middle: 20.1WT may cluster and immobilize BTN3A. Right: 20.1 mAb hinge variants restore BTN3A disorder and diffusion.**(B)** Schematic representing key features of modified mAb constructs with hinge-regions lengthened using Glycine-Serine linkers. Left: Annotated mAb domains. Right: 20.1 and 103.2 variants developed for this study with total linker lengths (top) and number of added amino acids (bottom). Distances between mAb inter-heavy chain cysteine bond and Fab CDR loops were estimated as following. The IgV domains of a muIgG1 Fab (PDB ID:1OPG) were aligned to the 20.1 scFv structure (PDB ID:4F9L). The distance tool in Pymol was then utilized to calculate Fab length between C-terminal cysteine bond and longest CDR loop of 20.1 (73Å). 3.5Å was then added to this value for each hinge amino acid.

of BTN3A1 may drive BTN3A multimerization, seeding early immunological synapses that recruit BTN2A1 and ultimately stimulate $V\gamma9V\delta2$ activation. In order to test this hypothesis, I engineered variants of the 20.1 agonist antibody with increasing hinge region lengths to test the role of pAg-induced BTN3A1 clustering in pAg signaling 4.1.

I hypothesized that 20.1 derivatives with longer hinge regions would affect the potency of $V\gamma9V\delta2$ agonism due to increasing inter-BTN3A flexibility, membrane-mobility and cluster-disorder within BTN3A multimers 4.1. 20.1WT is a murine IgG1 antibody with 1 glycine in its hinge region between the Cys102 forming a disulfide bond with the Fab light chain and Cys104 forming the first of 3 inter-heavy chain disulfide bonds. Glycine-serine (GS) linkers ranging from 4 to 29 amino acids were added to the 20.1 heavy chain hinge region between Cys102 and Cys104 to generate 20.1 variants (20.1^5, $20.1^(10)$, $20.1^(15)$, $20.1^(30)$) 4.1. Each additional hinge-linker amino acid added 3.5Å to the radius of diffusion between two 20.1 Fab:BTN3A complexes, incrementally increasing the radius of diffusion from˜150Å in 20.1WT to˜360Å in 20.1^30 by a maximum factor of˜2.3X 4.1. GS linkers in these engineered variants did not affect protein stability nor mAb affinity for biotinylated BTN3A ectodomain as assessed by Bio-Layer Interferometry (BLI), respectively 7.1 4.2.

4.2.2 20.1 mAb does not trigger $V\gamma9V\delta2$ by clustering BTN3A

Increasing concentrations of the WT 20.1 mAb, the 20.1 mAb hinge variants or the 20.1 Fab were added to Daudi-Cas9-ΔAAVS1 (DaudiWT), a B-cell lymphoma target-cell line that readily activates $V\gamma9V\delta2$ T cells, or Daudi-Cas9-ΔBTN3A1 (DaudiΔ3A1). Jurkat JRT3.3 T cells expressing the G115 $V\gamma9V\delta2$ TCR[49] (G115 Jurkats) were then co-incubated with these mAb-pulsed target-cells overnight and assayed for activation by analysis of CD69 expression via flow cytometry. Increasing inter-Fab distances in engineered 20.1 mAb hinge variants had minor effects on the EC_50 of $V\gamma9V\delta2$ agonism 4.3 but there was no obvious trend between the 20.1 mAb hinge region length and $V\gamma9V\delta2$ activation 4.3 4.4 indicating

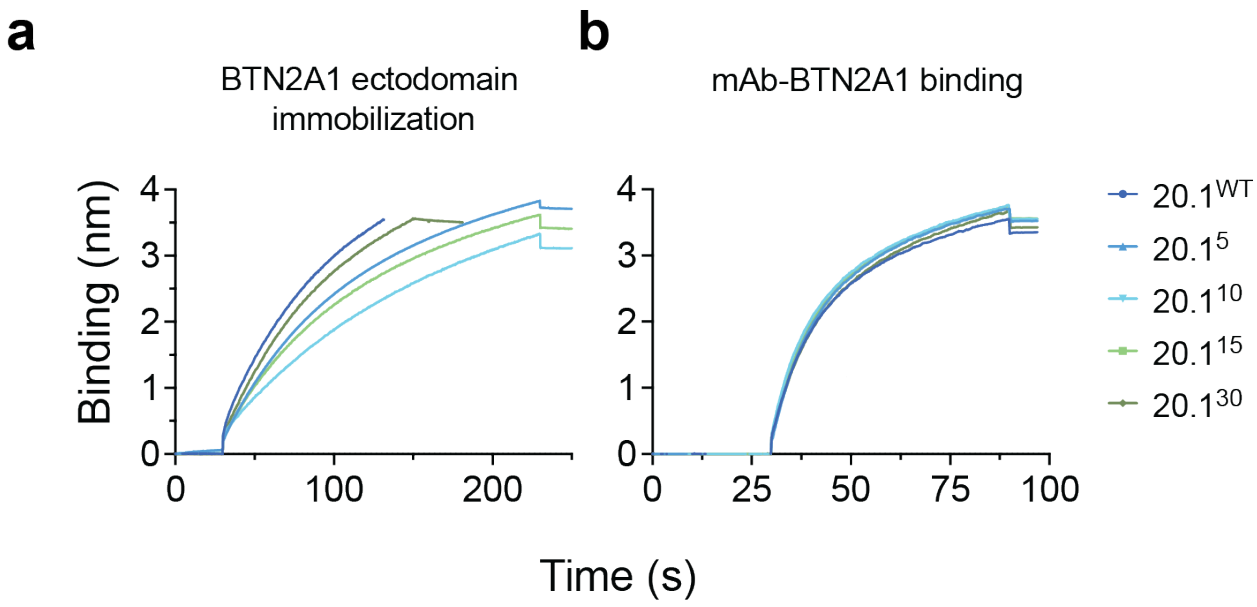

Figure 4.2: Modifying 20.1 hinge region does not affect relative affinity for BTN3A1

(A) Biotinylated BTN3A1 immobilization on streptavidin biosensor assessed by BLI, colored by 20.1 variants reagent subsequently tested (representative of 3 independent experiments). **(B)** Relative 20.1 variants affinity for Biotinylated BTN3A1 was probed at 1.3 μM by BLI (representative of 3 independent experiments).

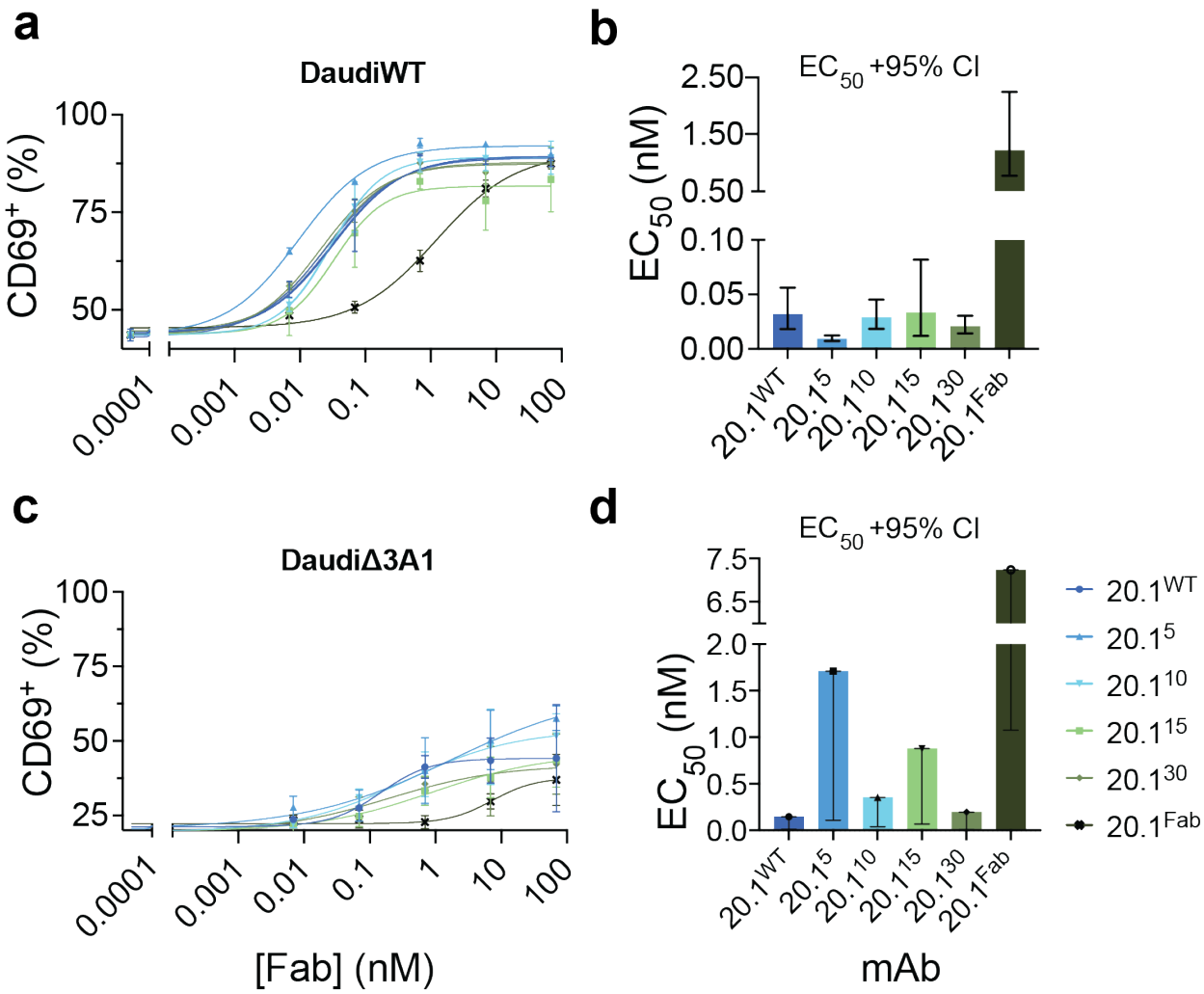

Figure 4.3: $V\gamma 9V\delta 2$ **activation by 20.1 does not depend on BTN3A clustering** **(A-B)** Activation of G115-TCR expressing Jurkat Jrt-3.3 cells after co-incubation with **(A)** DaudiWT or **(B)** Daudi$\Delta 3A1$ cells pre-incubated with 20.1 variants at increasing concentrations or control (Buffer). CD69 expression as a marker of T-cell activation was assessed by flow-cytometry (gated on isotype antibody). Means + SD and non-linear regression with variable slope - four parameters (n=3). **(C-D)** EC50 and 95% confidence intervals of $V\gamma 9V\delta 2$ activation for 20.1 variants incubated with **(C)** DaudiWT or **(D)** Daudi$\Delta 3A1$ was calculated by non-linear regression with variable slope - four parameters (R^2=0.9706, 0.9920, 0.9744, 0.8868, 0.9843, 0.9857, respectively).

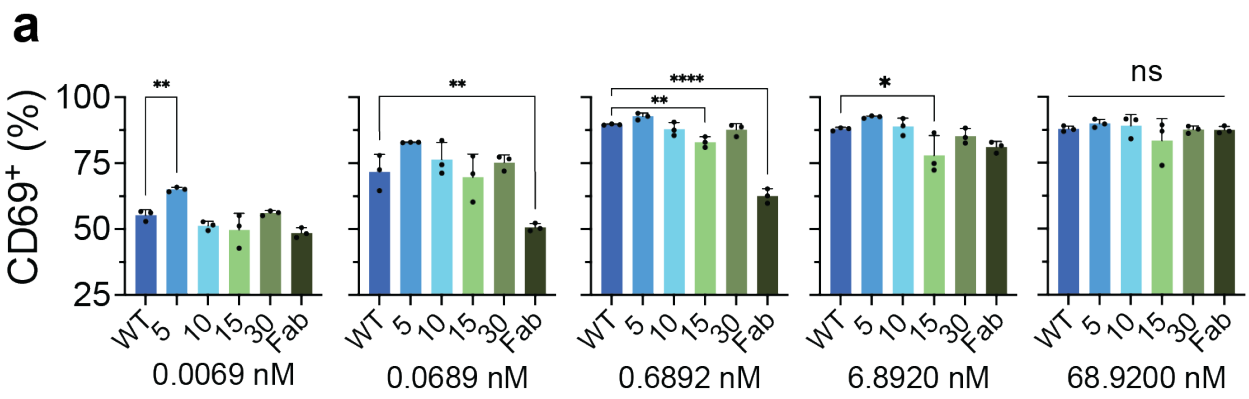

Figure 4.4: $V\gamma9V\delta2$ activation by specific concentrations of 20.1 variants **(A)** Activation of G115-TCR expressing Jurkat Jrt-3.3 cells after co-incubation with DaudiWT cells pre-incubated with 20.1 variants at specific concentrations from 4.3. Mean + SD (n=3). Dunnett test pairwise comparison to 20.1WT: ****p<0.0001, ***p<0.0002, **p<0.0021, *p<0.0332, ns p>0.1234.

that tight clustering and multimerization of BTN3A likely is not the driving factor in 20.1 mAb agonism of $V\gamma9V\delta2$ activation. The 20.1 Fab has an infinite radius of diffusion and, as previously reported[27], retains the ability to activate $V\gamma9V\delta2$ T cells with reduced potency 4.3 4.4. The WT 20.1 mAb, 20.1 mAb hinge variants and the 20.1 Fab were mildly agonistic when incubated with DaudiΔ3A1 target cells, likely due to interactions with BTN3A2 and BTN3A3 4.4, expression of which was retained in this cell line. These data suggest that 20.1 agonism of $V\gamma9V\delta2$ activation is driven by the molecular or steric effects of 20.1 contact with BTN3A. Indeed, BTN3A1 residues bound by both the 20.1 agonist mAb and α-BTN3A agonist mAb CTX2026 are directly adjacent to a recently reported pAg-signaling hotspot[16].

4.3 Discussion and Conclusions

Prior to this work, it was unclear whether antibody valency or steric hinderance enabled 20.1 to stimulate $V\gamma9V\delta2$ activation. To tease apart two potential mechanisms by which 20.1 mAb stimulates possibilities, I engineered the hinge region of 20.1 to generate variants with increasingly longer inter-Fab distances. I hypothesized that if clustering of BTN3A was

critical for pAg signaling, altering the architecture of BTN3A clusters with 20.1 variants would affect $V\gamma9V\delta2$ activation. I found lengthening the 20.1 hinge region had no effect on $V\gamma9V\delta2$ activation and confirmed that 20.1 Fab was a less potent agonist of $V\gamma9V\delta2$ activation. Altogether, this suggests that 20.1 mAb may indeed cluster and immobilize BTN3A1 on the cell membrane, but these are not the mechanisms by which 20.1 mimics pAg-induced changes in BTN3A to trigger $V\gamma9V\delta2$ activation. Instead, an allosteric mechanism in which contact between 20.1 and the BTN3A ectodomain alone is crucial for 20.1 agonism or a steric mechanism by which 20.1 occludes an inhibitory epitope on BTN3A may be more likely. Indeed, this model is supported by data recently published by the Willcox group in which an antigenic hotspot on BTN3A1 critical for pAg signaling to the MOP clone of the $V\gamma9V\delta2$ TCR lies directly adjacent to the 20.1 epitope on BTN3A1[16]. 20.1 binding to BTN3A1 may allosterically alter this antigenic hotspot enabling the recruitment of a $V\gamma9V\delta2$ TCR ligand or binding to the $V\gamma9V\delta2$ TCR itself. I have utilized the reagents developed in this work to improve our understanding of the molecular events driving pAg signaling. While this knowledge may eventually aid in the improvement of $V\gamma9V\delta2$ immunotherapies, these reagents themselves can be useful in a clinical setting. The 20.1 antibody is already being explored as an immunotherapy adjuvant[22] and I report a small but significant improvement on its agonist properties with the addition of 4 amino acids to its hinge region (4.4).

CHAPTER 5

THE ROLE OF BTN3A CONFORMATIONAL CHANGE IN $V\gamma 9V\delta 2$ ACTIVATION

5.1 Introduction

Understanding how 103.2 mAb antagonizes $V\gamma 9V\delta 2$ activation will provide critical insights into the mechanism of pAg signaling. Structural data suggests that 103.2 binds the top of V-shaped BTN3A dimers in a 1:1 orientation, potentially sterically hindering a critical interaction with a T cell binding partner. Complicating this theory is the fact that the 103.2 single-chain version (103.2scFv) cannot antagonize $V\gamma 9V\delta 2$ activation[27]. Though the bulkiness of the Fc domain in 103.2WT may be necessary for steric hindrance, it is also possible that valency is key to 103.2 antagonism.

5.2 Results

5.2.1 Rational engineering of α-BTN3A mAb 103.2 to probe the role of BTN3A extracellular conformation in pAg-signaling

Our previous structural analysis[27] demonstrated that the 103.2 Fab binds to the top of a BTN3A monomer potentially sterically hindering a critical interaction with a T cell binding partner. Complicating this theory is the fact that the 103.2 single-chain version (103.2 scFv) cannot antagonize $V\gamma 9V\delta 2$ activation.[27] Though the bulkiness of the Fc domain in the 103.2 mAb may be necessary for steric hindrance, it is also possible that valency is key to 103.2 antagonism due to its overall low binding affinity of 15 nM.[27] Our original analysis of our complex structure between the 103.2 scFv and BTN3A (PDB ID: 4F9P) used a model derived from IgGs that had long, flexible linkers between the Fab and Fc domains.[27] Based on this analysis, we concluded that the 103.2 mAb would be able to

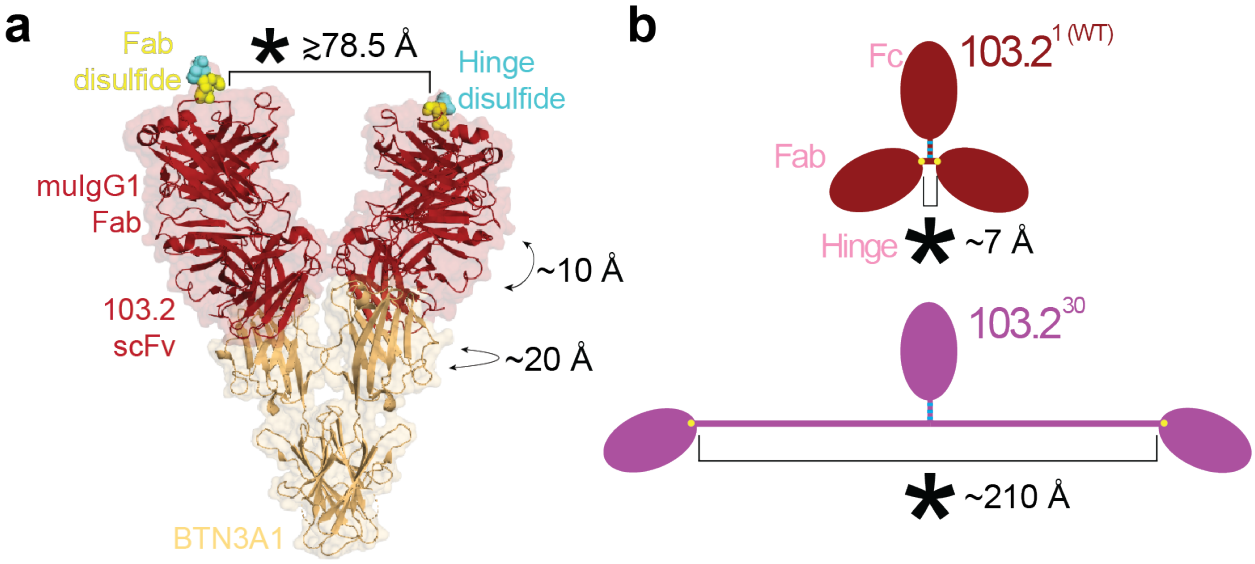

Figure 5.1: Monovalent binding of 103.2 to BTN3A1 likely induces conformational torsion

(A) Structural alignment of BTN3A1 in complex with the 103.2 single-chain-variable-fragment (scFv) (PDB ID: 4F9P) with 2 mouse IgG1 Fragment antibodies (Fab) (PDB ID: 1BAF) and ColabFold models of the murine IgG1 Hinge region. Distance between heavy-chain cysteine residues forming each terminal Fab disulfide bond (yellow) is denoted by *. The first hinge-region inter heavy-chain cysteine residues shown in blue. The range of orientations of BTN3A1 IgV in relation to BTN3A1 IgC and Fab IgV in relation to Fab IgC determined by structural alignment are indicated. (B) Schematic representing key features of modified mAb constructs with hinge-regions between Fab and hinge disulfide bonds lengthened using Glycine-Serine linkers.

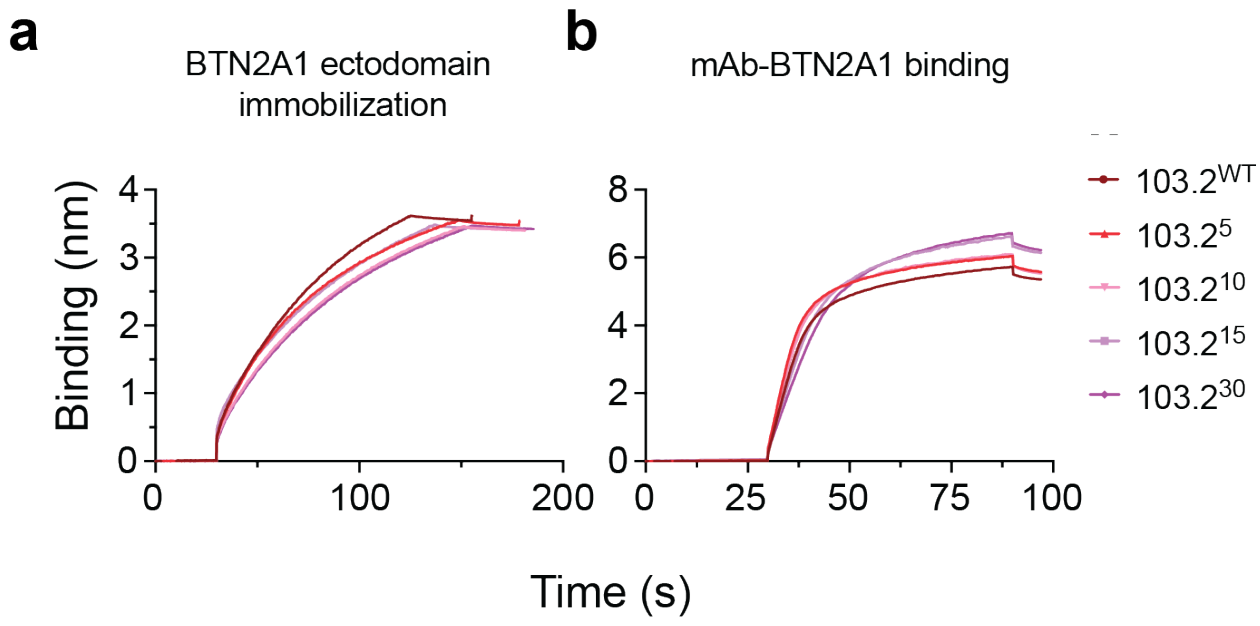

Figure 5.2: Modyfing 103.2 hinge region has subtle effects on relative affinity for BTN3A1.
(A) Biotinylated BTN3A1 immobilization on streptavidin biosensor assessed by BLI, colored by 103.2 variants reagent subsequently tested (representative of 3 independent experiments). **(B)** Relative 103.2 variants affinity for Biotinylated BTN3A1 was probed at 1.3 μM by BLI (representative of 3 independent experiments).

bind one BTN3A dimer, with each Fab engaging with one BTN3A monomer in an overall 1:1 stoichiometry (mAb to BTN3A dimer). We have since re-analyzed this complex in the context of the functional 103.2 IgG isotype (muIgG1), which has a much more restricted length and flexibility of 7Å in the hinge region between the Fab and Fc domains (Fig. 2A). To do this, we aligned the 103.2 scFv with 5 full-length murine IgG1 Fabs 7.1 and observed that the distance between the heavy chain cysteines that form the final interchain disulfide bond of the Fab are between 79-113Å apart 5.1 7.1, a distance that the hinge region must bridge in a bi-valent mAb. Therefore there is either significant flexibility in the BTN3A monomers between their IgV and IgC domains, or the 103.2 mAb must engage the BTN3A dimer with a 1:2 stoichiometry (one 103.2 mAb to 2 BTN3A dimers). In the first scenario, we have previously shown that while the IgC domains of BTN3A have negligible structural flexibility when dimerized, the IgV domains can rotate up to 20 Å at the point of the linker between the IgV and IgC[27] 5.1. Including the general flexibility of 10Å between Fab IgV and IgC domains 5.1 7.1, our model positions the 103.2 mAb within 11.5Å of being capable of monovalently binding to BTN3A. If monovalent (1:1) binding between 103.2 and BTN3A is possible, substantial torsional force on the BTN3A IgV domains would be required, potentially locking them in an inactive conformation. Alternatively, bivalent 103.2 binding to BTN3A may also influence the conformational flexibility of BTN3A dimers preventing the propagation of intracellular pAg-binding information through JMs to BTN3A extracellular domains, ultimately influencing BTN3A interactions between heterodimers[10] or with other proteins such as 2A1.

5.2.2 α-BTN3A mAb 103.2 does not antagonize Vγ9Vδ2 activation through BTN3A conformational constraint

To test these models, we hypothesized that 103.2 variants with longer hinge regions (103.25, 103.210, 103.215, 103.230) would reduce conformational torsion on BTN3A extracellular do-

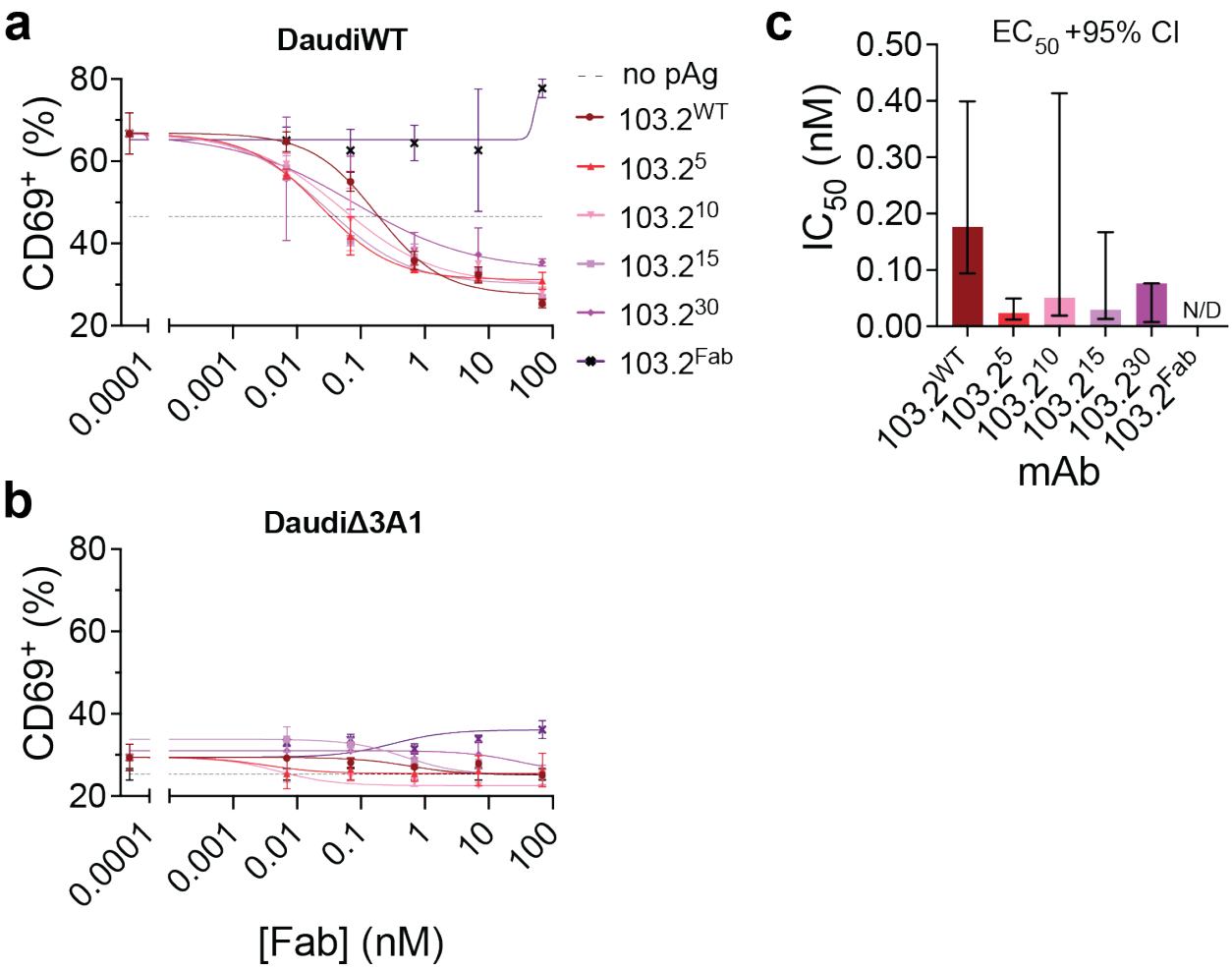

Figure 5.3: $V\gamma 9V\delta 2$ activation by 103.2 does not depend on BTN3A conformational constraint

(a-b) Inhibition of activation of G115-TCR expressing Jurkat Jrt-3.3 cells after co-incubation with **(a)** DaudiWT or **(b)** Daudi Δ3A1 cells pre-incubated with 5μM HMBPP and 103.2 variants at increasing concentrations or controls (Buffer + HMBPP). CD69 expression as a marker of T cell activation was assessed by flow-cytometry (gated on isotype antibody). Means + SD and non-linear regression with variable slope - four parameters (n=3). **(c)** IC_50 of inhibition and 95% confidence intervals for 103.2 variants was calculated by non-linear regression with variable slope - four parameters (R^2=0.9501, 0.9508, 0.9273, 0.9396, 0.8086, 0.3131 respectively).

mains 5.1, potentially altering the potency of 103.2 antagonism of $V\gamma 9V\delta 2$ T cells. Therefore, the 103.2 mAb hinge region was modified as described for the 20.1 mAb hinge variants 4.1 5.1. As with the 20.1 mAb hinge variants, GS linkers in the 103.2 mAb hinge variants did not affect protein stability as assessed by SDS-PAGE gel electrophoresis although we noted a minor increase in their relative affinity for biotinylated BTN3A1 ectodomain as assessed by BLI 7.1.

Increasing concentrations of the 103.2 mAb hinge variants or the 103.2 Fab were added to DaudiWT or DaudiΔ3A1 in the presence of $5/mu$M HMBPP. While DaudiWT are capable of activating $V\gamma 9V\delta 2$s without exogenous pAg[24], addition of exogenous pAg boosts the potency with which DaudiWT stimulate $V\gamma 9V\delta 2$ activation thus increasing the dynamic range of inhibition assays. G115 Jurkats were then co-incubated with mAb + pAg-pulsed target-cells overnight and assayed for activation by analysis of CD69 expression via flow cytometry. Increased inter-Fab distances in 103.2 hinge variants had no significant effect on the potency or maximum 5.3 of $V\gamma 9V\delta 2$ activation. The 103.2 Fab has an infinite radius of diffusion and cannot antagonize $V\gamma 9V\delta 2$ activation 5.3. Our data suggest that the mechanism of 103.2 antagonism does not involve releasing conformational constraint on BTN3A ectodomains or multimerizing BTN3A. We therefore posit that the importance of the 103.2 mAb bivalent engagement of BTN3A in $V\gamma 9V\delta 2$ antagonism may be due to its higher avidity or the added steric bulk of a mAb over Fab or scFv reagents. Higher avidity or steric hindrance may enable the 103.2 mAb to successfully compete with a yet unknown ligand of BTN3A.

5.3 Discussion and Conclusions

In contrast to 20.1, the 103.2 mAb cannot function as an scFv and is incapable of antagonizing $V\gamma 9V\delta 2$ activation[27]. We hypothesized that valency was thus critical to the function of 103.2 as an antagonist and that antagonism may occur through conformational constraint imposed

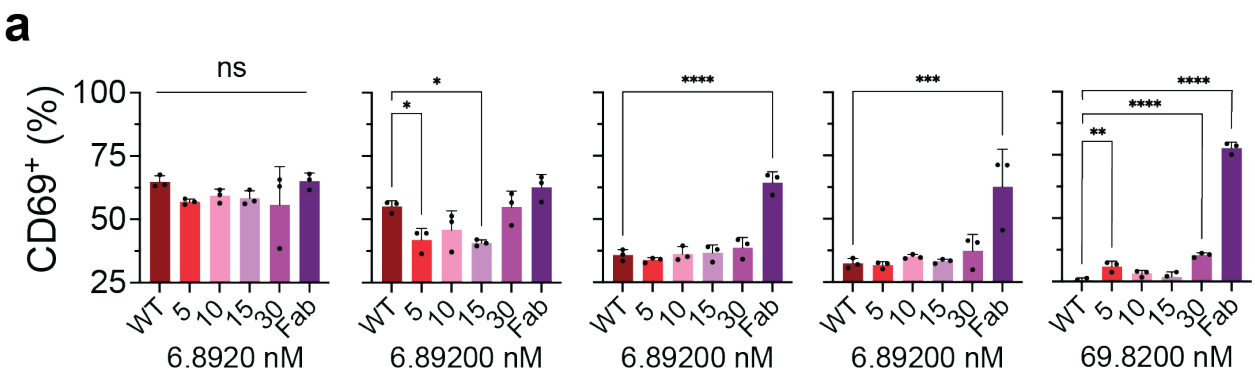

Figure 5.4: $V\gamma9V\delta2$ activation by specific concentrations of 103.2 variants **(a)**Activation of G115-TCR expressing Jurkat Jrt-3.3 cells after co-incubation with DaudiWT cells pre-incubated with 103.2 variants at specific concentrations from 5.3. Mean + SD (n=3). Dunnett test pairwise comparison to 103.2WT: ****p<0.0001, ***p<0.0002, **p<0.0021, *p<0.0332, ns p>0.1234.

on the ectodomains of BTN3A dimers by 103.2 5.1. To test this hypothesis, I engineered the hinge region of 103.2 to generate variants with increasingly longer inter-Fab distances 4.1. We hypothesized that if the conformational constraint of BTN3A by 103.2 prevents pAg signaling, releasing this conformational constraint with 103.2 variants would restore $V\gamma9V\delta2$ activation. The potency of 103.2 antagonism was unaffected by the modification of inter-Fab distances 5.3 even at distances predicted to apply no torsional force to the BTN3A ectodomain 5.1. Thus 103.2 does not antagonize $V\gamma9V\delta2$ activation by locking BTN3A ectodomains in an inactive conformation. The inability of 103.2 Fab 5.3 and scFv[27] to antagonize $V\gamma9V\delta2$ activation suggests an antagonism mechanism of steric hindrance of rather than direct competition for a critical epitope on BTN3A. 103.2 binds to the top of the IgV domain of BTN3A dimers 5.1 6.1[27] suggesting that 103.2 sterically occludes access to epitopes on the rest of the BTN3A ectodomain when bound. Indeed, the loss of the Fc domain and bivalent avidity may explain why the 103.2 Fab and scFv are incapable of steric occlusion and subsequent $V\gamma9V\delta2$ antagonism in contrast to full-length 103.2. Together my findings suggest that the tertiary extracellular structure of the pAg signaling complex is quite sensitive to both allosteric and steric perturbation.

CHAPTER 6

CONCLUSION AND FUTURE DIRECTIONS

6.1 Key findings

6.1.1 Summary of findings

Disentangling the cellular and molecular events of pAg signaling has challenged molecular immunologists for over a decade[17]. In this work, I utilize rationally modified in addition to novel antibodies against key proteins in the pAg signaling complex to resolve long-standing questions about the cellular and molecular events that trigger $V\gamma9V\delta2$ activation. First, I demonstrate that BTN3A1 multimerization and clustering does not drive pAg signaling. Second, I show that antagonism of $V\gamma9V\delta2$ activation with the 103.2 mAb is not driven by the conformational constraint of BTN3A1. We then developed novel antibodies against BTN2A1 to better understand the extracellular contribution of BTN2A1 to the pAg signaling complex. Antibodies binding to BTN2A1 had either antagonistic or neutral effects on $V\gamma9V\delta2$ activation. Our 2.8Å crystal structure of the 2A1.9 Fab with BTN2A1 ectodomain shows that the 2A1.9 mAb antagonizes $V\gamma9V\delta2$ activation by blocking the $V\gamma9V\delta2$ TCR epitope on BTN2A1. Intriguingly, other α-BTN2A1 binders competed with the $V\gamma9V\delta2$ TCR for BTN2A1 binding but did not antagonize $V\gamma9V\delta2$ activation and the 2A1.4 binder $V\gamma9V\delta2$ antagonist did not block TCR binding. We thus pursued structural determination of additional α-BTN2A1 Fabs in complex with the BTN2A1 ectodomain to better map critical epitopes on BTN2A1. Our preliminary, low resolution structural data of the weak antagonist 2A1.4 and neutral 2A1.11 Fabs in complex with BTN2A1 ectodomain show intriguingly similar docking angles of Fab on BTN2A1. This suggests that unique molecular interfaces and subsequent affinities between antibodies and BTN2A1 drives antagonism potency and that the primary role of BTN2A1 in pAg signaling is to bind the $V\gamma9V\delta2$ TCR. BTN2A1 may ultimately serve to propagate information about pAg-BTN3A1 binding from the target

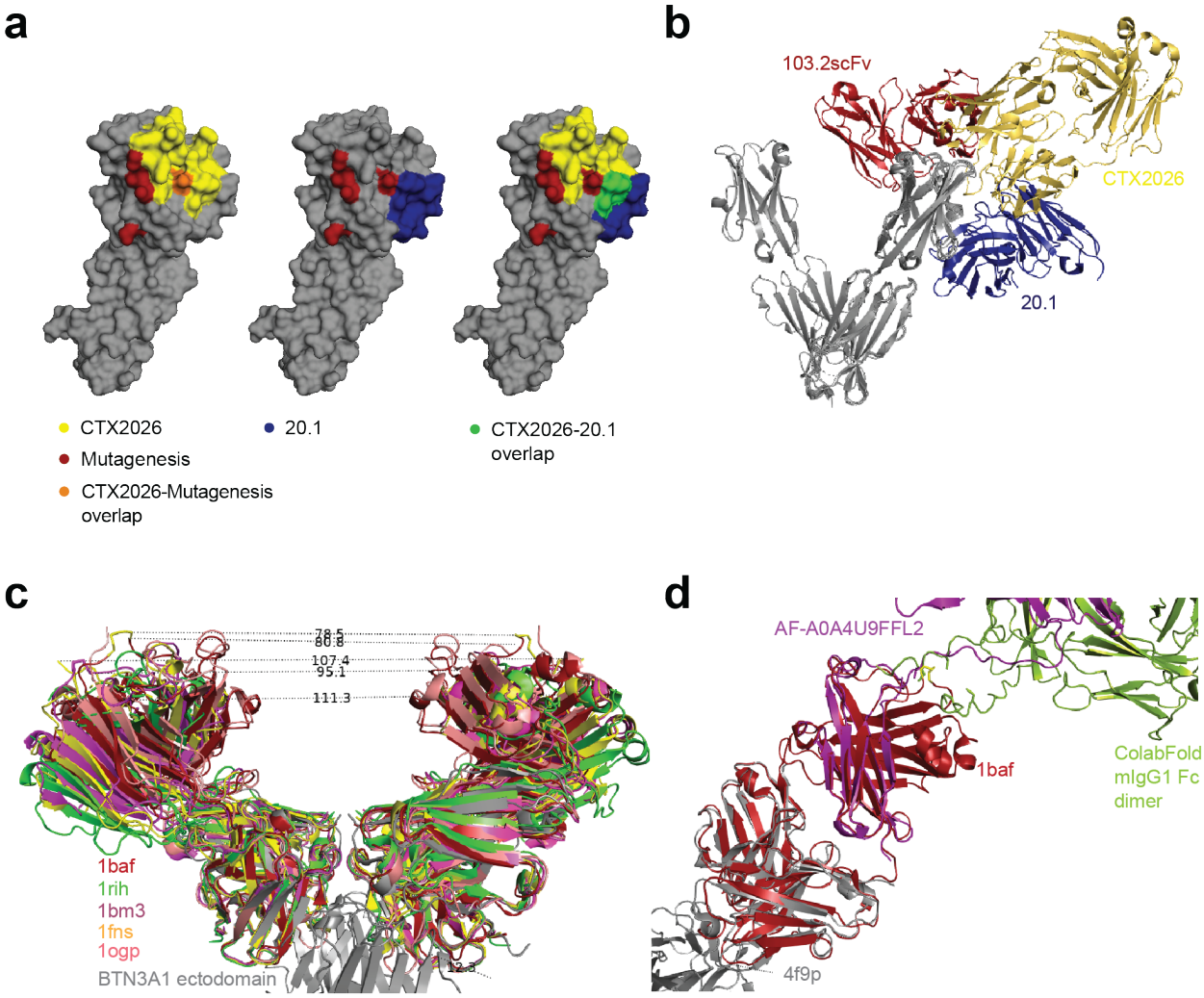

Figure 6.1: Epitopes of interest on BTN3A1 ectodomain

(a) Epitopes for residues that abrogate pAg signaling (red)[16], CTX2026 Fab (yellow)[50], 20.1 scFv (blue)[27], CTX2026-20.1 overlap (green), and CTX2026-mutagenesis overlap (orange). **(b)** Complex orientations for BTN3A1 binders that modulate pAg signaling. **(c)** Alignment of PDB structures with 103.2 scFv in complex with BTN3A1 (PDB ID:49fp). Distances measured between CA of cysteine residues forming disulfide bonds with Fab light chain in Pymol. **(d)** All aligned structures used to generate the model in 5.1. BTN3A1 in complex with the 103.2 single-chain-variable-fragment (scFv) (PDB ID: 4f9p) was aligned with a mouse IgG1 Fragment antibody (Fab) (PDB ID: 1baf). The AlphaFoldREF model of the murine IgG1 heavy chain (AF-A0A4U9FFL2) was then aligned to the CH1 domain of PDB ID: 1baf. Finally, a model of the murine IgG1 Fc dimer was generated using ColabFoldREF. Briefly, two murine IgG1 Hinge-CH2-CH3 domains were linked with 30 glycine residues. This model was then aligned to the CGC motif in the hinge region of ID: AF-A0A4U9FFL2.

cell to the T cell or as a costimulatory signal involved in coordinating the orientation of a true $V\gamma 9V\delta 2$ TCR ligand.

6.1.2 Future Directions

Therapeutic development surrounding BTN3A has focused on reagents with agonistic properties. An intriguing idea is the use of antagonist antibodies in clinical contexts where the expression of BTNs is a poor prognostic marker. The data surrounding the association between BTN expression in tumors and clinical outcomes is complicated and tumor-dependent and. High expression of BTN3A1 in ovarian and pancreatic cancers[23] and BTN2A1 in metastatic renal cell carcinoma[51?] has been associated with reduced patient survival. Indeed, the Conejo-Garcia group has shown that BTN3A1 can operate to suppress T cell TCR signaling by preventing the segregation of CD45 from the immune synapse[50]. Thus the role of tumor-infiltrating $V\gamma 9V\delta 2$ T cells as well as how BTN3A and BTN2A1 operate outside of pAg signaling is poorly understood. In contexts where $V\gamma 9V\delta 2$ T cells or BTNs play immunosuppressive roles, targeting BTN2A1 with antagonistic antibodies may sensitize tumors to immunotherapy.

CHAPTER 7

METHODS

7.1 Protein expression and purification

7.1.1 Fragment antibodies

α-BTN2A1 Fabs with a human-IgG1 Herceptin scaffold were cloned into the RH2.2 vector. Fab Heavy and Light chains were on the same plasmid. Fab overexpression was induced in Escheria coli BL21 Gold (DE3) cells in 2xYT media using 1mM isopropyl β-d-1-thiogalactopyranoside (IPTG) for 4 hr at 37C. Bacterial cells were centrifuged, resuspended and lysed by homogenization and sonication. Bacterial lysate was spun at 20,000 x g for 45'. Fabs were purified from the periplasmic fraction with Protein Ga1 or G-F resin (Kossiakoff Lab, U.Chicago), eluted with 0.1 M Glycine pH 2.3 and neutralized with a 1:5 volume ratio of 1 M Tris Buffer pH 8.0. Fabs were then dialyzed into Phosphate Buffered Saline (PBS). α-BTN3A1 Fab 20.1 and 103.2 Heavy and Light chains with a hybrid murine-IgG1 Fab IgV and human-IgG1 Herceptin Fab IgC scaffold were cloned into the pAcGP67a Vector containing a C-terminal human rhinovirus 3C protease cleavage site, acid- and basic-zipper, respectively, and hexa-histidine tag. Baculovirus was generated by transfection of plasmid and linearized baculovirus DNA into Sf9 insect cells using Cellfectin transfection reagent. Baculovirus was then added to High-Five insect cells and proteins were expressed for 60-68 hrs at 27°C. Supernatant was isolated by centrifugation at 1700 rpm for 15' and filtered through glass-fibre. Proteins were purified using Protein-G resin, eluted with 0.1 M Glycine pH 2.3 and neutralized with a 1:5 volume ratio of 1 M Tris Buffer pH 8.0. Fabs were then dialyzed into Phosphate Buffered Saline (PBS).

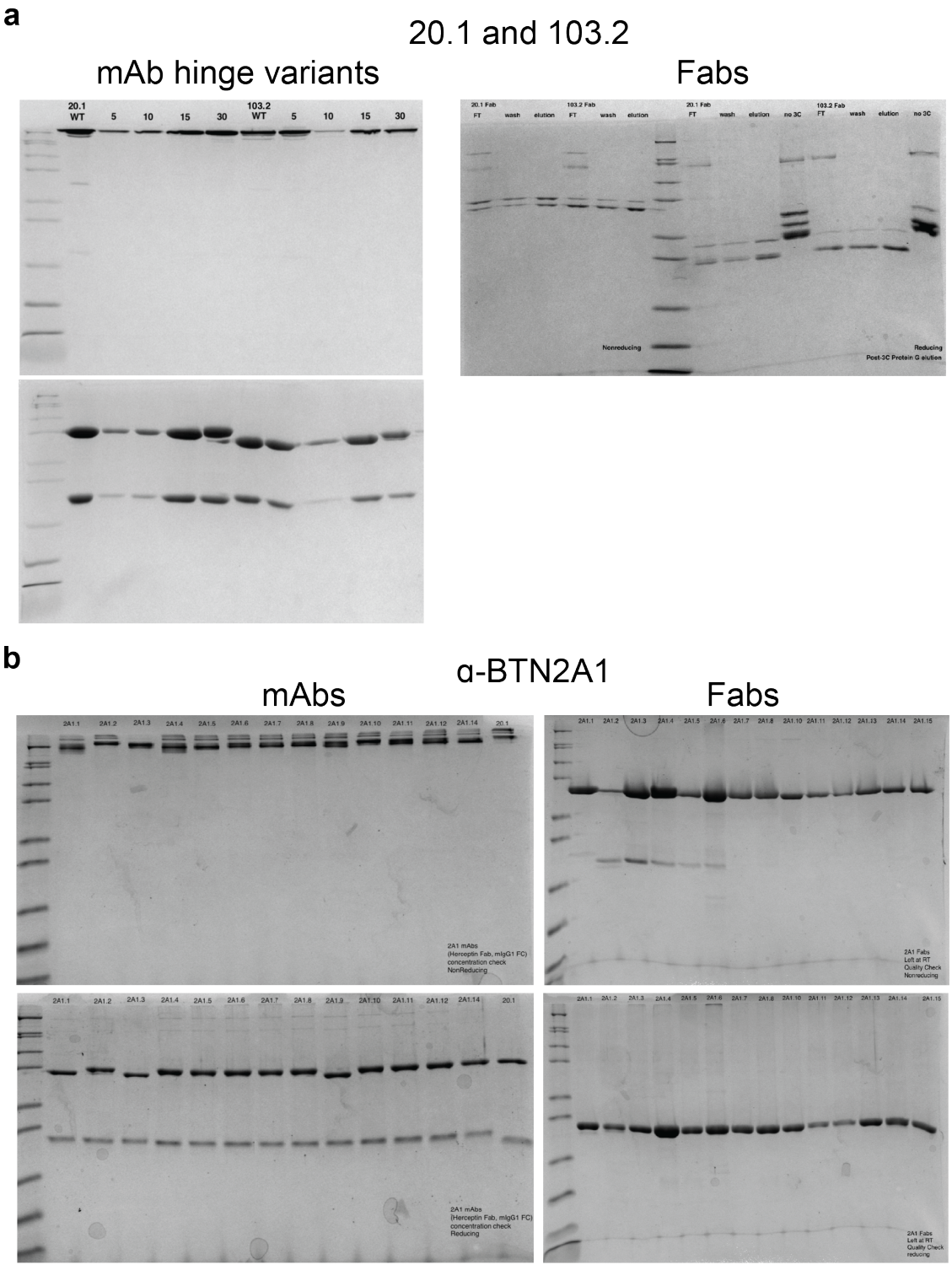

Figure 7.1: Protein expression and purification

(Continued on next page)

Figure 7.1: Protein expression and purification, continued)

(Continued from previous page) **(A)** Non-reducing (top-left) and reducing (bottom-left) SDS-PAGE gels showing 20.1 and 103.2 mAb hinge variants expressed in Expi293 cells and purified using Protein-G resin. Non-reducing and reducing (right) SDS-PAGE gels showing 20.1 and 103.2 Fabs expressed in BL21 (DE3) competent cells and purified using Protein-Ga1 resin (Kossiakoff Lab, Univ. of Chicago). **(B)** Non-reducing (top-left) and reducing (bottom-left) SDS-PAGE gels showing /*alpha*-BTN2A1 mAb constructs expressed in Expi293 cells, purified using Protein-G resin, dialyzed into PBS and normalized to 878 nM (130 /*mu*g/mL). Non-reducing (top-right) and reducing (bottom-right) SDS-PAGE gels showing /*alpha*-BTN2A1 Fab constructs expressed in BL21 (DE3) competent cells and purified using Protein-Ga1 resin (Kossiakoff Lab, Univ. of Chicago).

7.1.2 Monoclonal antibodies

α-BTN2A1 mAb sequences with a hybrid human-IgG1 Herceptin Fab IgV and murine-IgG1 IgC-Hinge-Fc scaffold were cloned into the AbVec vector. Heavy and Light chains were on separate plasmids. α-BTN3A1 mAbs with a murine-IgG1 scaffold were cloned into the AbVec vector. MAbs were expressed in Expi293 cells at 37C using the ExpiFectamineTM transfection system with 0.5 μg each of Heavy and Light chain plasmids per 1 mL of culture. 7 days after transfection, supernatant was isolated by centrifugation at 3000 x g for 10'. mAbs were then purified using Protein G or Protein Ga1 resin, eluted with 0.1 M Glycine pH 2.3 and neutralized with a 1:5 volume ratio of 1 M Tris Buffer pH 8.0. MAbs were then dialyzed into PBS.

7.1.3 BTN2A1 ectodomain, BTN2A1 ectodomain C219S

BTN2A1 ectodomain (residues 1-219) and BTN2A1 ectodomain C219S (residues 1-219) were cloned into the pAcGP67a Vector containing a C-terminal human rhinovirus 3C protease cleavage site and hexa-histidine tag. Proteins were expressed in High-Five insect cells with the baculovirus expression system as previously described. Proteins were purified using Ni-NTA resin and eluted with Hanks Buffered Saline (HBS) + 200 mM and 500 mM imidazole. Proteins were de-glycosylated for 2hrs at 37C using Endo-F3 in HBS + 15mM imidazole at

a concentration of ~1 mg/mL. Proteins were repurified using Ni-NTA resin and HBS + 200 mM imidazole elution to remove Endo-F3 and incubated with 3C protease overnight in HBS + 75 mM imidazole for the removal of the hexa-histidine tag. Proteins were purified further using anion-exchange chromatography over the MonoQ column in 20 mM Tris pH 8.0 with a 20 mL gradient of 30-700 mM NaCl. Proteins were subsequently utilized for structural determination.

7.1.4 Biotinylated BTN2A1 and BTN3A1 ectodomains + avitag

BTN2A1 ectodomain (residues 1-217) and BTN3A1 ectodomain (residues 1-217) were cloned into the pAcGP67a Vector containing a C-terminal BirA biotinylation sequence, human rhinovirus 3C protease cleavage site and hexa-histidine tag. Proteins were expressed in High-Five insect cells with the baculovirus expression system as previously described. Proteins were purified using Ni-NTA resin as previously described. Proteins were then incubated with 3C protease overnight in HBS + 75mM Imidazole for the removal of the hexa-histidine tag. Proteins were buffer exchanged to HBS + 15 mM Imidazole with 0.05 M bicine buffer pH 8.3, 10 mM ATP, 10 mM MgOAc and 50 μM d-biotin and biotinylated overnight using the BirA protein. Proteins were then purified using size-exclusion chromatography over the S200 column in HBS and verified for biotinylation by size-shift on an SDS-PAGE gel following coincubation with Traptavidin.

7.1.5 G115 and DP 10.7 TCRs

The γ chain of the G115 or DP-alpha constant-region TCR was cloned into the pAcGP67a Vector containing a C-terminal human rhinovirus 3C protease cleavage site, acidic-zipper and hexa-histidine tag. The δ chain of the G115 or DP-beta constant-region TCR was cloned into the pAcGP67a Vector containing a C-terminal BirA biotinylation sequence, human rhinovirus 3C protease cleavage site, basic-zipper and hexa-histidine tag. TCRs were

expressed in High-Five insect cells with the baculovirus expression system as previously described. TCRs were purified using Ni-NTA resin and eluted as previously described. TCRs were then incubated with 3C protease overnight in HBS and 75 mM Imidazole for the removal of the hexa-histidine tag. For TCR being used for tetramerization, TCR was buffer exchanged to HBS + 15 mM Imidazole HBS + 15 mM Imidazole with 0.05 M bicine buffer pH 8.3, 10 mM ATP, 10 mM MgOAc and 50 μM d-biotin and biotinylated overnight using the BirA protein. Unbiotinylated and biotinylated TCR were then purified using size-exclusion chromatography over the S200 column in HBS and verified for biotinylation by size-shift on an SDS-PAGE gel following coincubation with Traptavidin, if applicable. Biotinylated TCR was tetramerized by co-incubation with Streptavidin-PE at a ratio of 1:1.1 streptavidin monomer to biotinylated TCR monomer.

7.1.6 Nanobody

Histidine-tagged anti-Fab nanobody[52] was expressed in E. coli BL21 (DE3) cells overnight at 20°C post induction with 1mM IPTG at OD600 = 0.6-0.8. The cells were harvested by sonication in 25 mM TRIS, pH 8.0, 300 mM NaCl and 10% glycerol. After centrifugation, the supernatant was passed over a 10mL HisTrap HP column (GE Healthcare) and eluted with 25 mM TRIS, pH 8.0, 300 mM NaCl, 150 mM imidazole and 10% glycerol. The protein was further purified by SEC in 20 mM HEPES, pH 7.4, and 200 mM NaCl.

7.2 Phage display selection

To obtain high-affinity binders, five rounds of selection were performed using the phage display selection protocol previously described[29,42]. Briefly, Biotinylated BTN2A1 was immobilized onto streptavidin-coated paramagnetic beads (Promega) for five rounds of phage selection. In the first round, 1 μM of BTN2A1 was immobilized on 200 μl SA magnetic beads and was incubated with 1 mL phage library (1010 CFU) for 1 hour at room temperature

with gentle shaking. The beads were washed three times to remove nonspecific phage, added to log phase E. coli XL-1 blue cells (Stratagene), and incubated for 20' at room temperature. Then, media containing 100 μg/mL ampicillin and 10 9 p.f.u./mL of M13K07 helper phage (NEB) was added for overnight phage amplification at 37°C. The amplified phage was precipitated in 20% PEG/2.5 M NaCl for 20' on ice for subsequent rounds. Before each round, the phage pool was negatively selected against empty paramagnetic beads for 30' with shaking to eliminate nonspecific binders. The final antigen concentration was dropped systematically from 1 μM to 10 nM from the first to the fifth round (2nd round: 200 nM, third round: 50 nM, fourth round 20 nM, and fifth-round 10 nM). After phage binding, the beads were subjected to five washing rounds with 0.5% BSA/PBST. The bound phages were eluted using 0.1 M Glycine, pH 2.6, and neutralized with TRIS-HCl, pH 8. Then, the phage eluate was used for E. coli infection and phage amplification, as described above. Additional selection pressure using 1 μM of not biotinylated BTN3A1 in all washes was applied to ensure specificity to BTN2A1. After the fourth and fifth rounds the infected cells were plated on ampicillin agar and 192 colonies were picked to produce phage clones for single-point phage ELISA assay. The promising clones demonstrating high specificity were sequenced and reformatted into a RH2.2 expressing vector.

7.3 Affinity analyses

7.3.1 Cellular affinity

For determination of α-BTN2A1 mAb cellular affinity, Daudi cells were resuspended in PBS + 2% fetal bovine serum and incubated with increasing concentrations of α-BTN2A1 mAb. α-BTN2A1 mAbs were stained with 1:200 fluorescently-tagged secondary mAb and staining was assessed by flow-cytometry.

7.3.2 Enzyme-Linked Immunosorbent Assay

Single-point phage ELISA was used to test specificity of α-BTN2A1 Fabs for BTN2A1 binding. 50 nM of BTN2A1 or BTN3A1 protein was directly immobilized on high-binding experimental wells for 30', followed by extensive blocking with 2% BSA for 1 hour. After 15' of incubation with phage, the wells were extensively washed three times with 0.5% BSA/PBST and incubated with Protein L-HRP (1:5000 dilution in HBST) for 20'. The plates were again washed and developed with TMB substrate and quenched with 10% H_3PO_4, followed by determination of absorbance at A450. To probe for IFN-γ release by primary Vγ9Vδs2, the Invitrogen ebioscience Human IFN-γ ELISA Ready-SET-Go! Kit was used. Briefly, supernatants from primary Vγ9Vδ2 activation assays were frozen at -20C for 14 days. ELISA plates were coated for 2 hours at Room temperature (RT) followed by 3 washes with PBS. Plates were then blocked with diluent for 1hr15' and washed 2X with 300μL PBS. Supernatants were diluted 1:2 with diluent and added to the plate. Plates were incubated overnight rocking at 4C in saran-wrap to prevent evaporation. Plates were washed 3X with PBS and incubated with α-IFN-γ antibody conjugated to HRP for 1hr. Plates were then washed 3X and developed with TMB substrate. Plates were quenched with 10% H_3PO_4, followed by the determination of absorbance at A450.

7.3.3 Bio-layer interferometry

For 20.1 and 103.2 engineered variants relative affinity determination, biotinylated BTN3A1ecto-avi in HBS was immobilized on Streptavidin biosensor tips until Binding reached between 3 and 4 nm. Tips were blocked with 1 μM biotin for 30". After baseline was established in PBS for 30", the biosensor tip was exposed to 1.3 μM mAb for 90". Dissociation in PBS was then assessed for 120". For α-BTN2A1 Fab competition with the Vγ9Vδ2 TCR experiments, BTN2A1ecto-avi in HBS was immobilized for 150" on Streptavidin biosensor tips. Tips were blocked with 1 μM biotin in HBS for 30s followed by 2 mg/mL BSA for 180". The biosensor

tip was exposed to 66 μM α-BTN2A1 Fab concentration for 120". Tips were immediately placed into 66 μM α-BTN2A1 Fab + 80 μM Vγ9Vδ2 TCR for 120", in HBS. Dissociation in HBS was then assessed for 120".

7.3.4 Surface plasmon resonance

All Surface plasmon resonance (SPR) analyses were performed on a MASS-1. BTN2A1 was immobilized via a 6x His-tag to a Ni-NTA sensor chip. Fabs in two-fold dilutions were run as analytes at 30 μl/min flow rate at 20°C. Sensograms were corrected through double referencing, and a 1:1 binding model fit using Sierra Analyzer.

7.4 Cells

7.4.1 Cell lines

The γ and δ chain of the G115 Vγ9Vδ2 TCR clone were cloned into the pMSC-V vector with puromycin and zeocin selection genes, respectively. Jurkat JRT3.3 cells were transfected with these plasmids and selected first for γ chain expression for 7-14 days using 1 mg/mL puromycin. Cells were then selected for ≈4 weeks with 200 mg/mL zeocin. Cells were stained with α-γ9 and α-δ2 antibodies and sorted on TCR expression both at 1 week and 4 weeks. Daudi-Cas9 ΔAAVS1, ΔBTN2A1, ΔBTN3A1 cell lines were generated as described[53]. JRT3.3 Jurkat cells expressing the G115 TCR, DaudiWT, DaudiΔ2A1, and DaudiΔ3A1 were cultured in RPMI-1640 supplemented with 2 mM L-glutamine and 10 U/mL Penicillin/Streptomycin (R10). Cells were split to 0.3E6 cells/mL daily and split 24 hours prior to the start of an activation assay.

7.4.2 Isolation and expansion of $V\gamma9V\delta2$ T cells from peripheral blood

Peripheral blood was isolated from healthy donors through the IRB13-0666 protocol and subjected to density gradient centrifugation using Ficoll. Lymphocytes were isolated and brought to 1E6 cells/mL in RPMI-1640 supplemented with 2 mM L-glutamine, 0.1% β-me, 0.5X non-essential amino acids (Corning), 1 mM sodium pyruvate and 10 U/mL Penicillin/Streptomycin (R10+). Cells were pulsed with 5 μM Zoledronate and 100 U/mL IL-2 and incubated at 37°C. 100 U/mL IL-2 was supplemented into the media every 2-3 days and the culture volume was doubled on day 6 with fresh R10+ media supplemented with 100 U/mL IL-2. One day prior to use in activation assays, 100 U/mL IL-2 was pulsed into the media. Vγ9Vδ2 T cells were utilized on Day 9-10 for activation assays and assayed via flow-cytometry for expansion at such time.

7.5 $V\gamma9V\delta2$ activation assays

7.5.1 Agonist/Antagonist assay

In 96-well round-bottom plates with edge-wells containing 200 μL PBS, 0.05E6 Daudi target cells were incubated with PBS, mAb, or Fab +/- HMBPP, Pamidronate or MOPC isotype mAb in R10 for 2 hours in 100 μL. Target cells were washed with 200 μL warm PBS and centrifuged at 300 x g for 5' 3 X. Target cells were then co-incubated with 0.1E6 Jurkat or Primary Vγ9Vδ2 T cells per condition overnight in 200 μL R10. 1.6 μg/mL PHA was added to wells with T cells alone prior to overnight incubation as a positive control for activation. T Cell activation was assessed via flow-cytometry.

7.6 Cellular mAb:TCR Competition for BTN2A1 Binding Assay

Full-length BTN2A1 was cloned into the pAcGP67a Vector containing a C-terminal human rhinovirus 3C protease cleavage site and hexa-histidine tag. BTN2A1 was expressed in High-

Five insect cells with the baculovirus expression system as previously described. BTN2A1-expressing Insect cells were seeded at 1.5E5 cells/well in 96-well round-bottom plates with edge-wells containing 200 μL PBS and incubated with 150nM α-BTN2A1 mAb for 30'. Insect cells were washed with 200 μL PBS and centrifuged at 300 x g for 5'. Insect cells were then sequentially stained with DAPI followed by additional washes and stained with 120 nM G115 tetramer labeled with the PE-fluorophore. MAb:tetramer competition was assessed via flow-cytometry.

7.7 Flow Cytometry

For Jurkat T-cell activation assays, target and T cells from each condition were resuspended in PBS + 2% fetal bovine serum. Cells were stained with Live-Dead fluorescent dye, α-CD19 to gate targeT cells, α-Vγ9 to gate T cells and α-CD69 fluorophore-conjugated mAbs as a marker for T-cell activation. For Primary T-cell activation assays, target and T cells from each condition were stained with 1:1500 dilution of Live/dead Fixable Dead Cell Stain, 1:50 dilution of α-Vγ9, α-Vδ2 to gate T cells, and 1:50 dilution of α-CD25, α-CD107a and α-CD69 fluorophore-conjugated mAbs as markers for activation. For mAb and TCR-tetramer competition, cells were resuspended in PBS + 2% fetal bovine serum and stained with DAPI and fluorescently-labeled G115 TCR tetramers. Data were collected on either the Aurora or AttuneNxt.

7.8 X-ray crystallography

7.8.1 Sample preparation

De-glycosylated and purified BTN2A1 ectodomain C219S was mixed with purified Fab at a 1:1 ratio. Complexes were concentrated and purified over size-exclusion chromatography using the S200 column in HBS. Complexes were then concentrated to 6.9mg/mL and tested

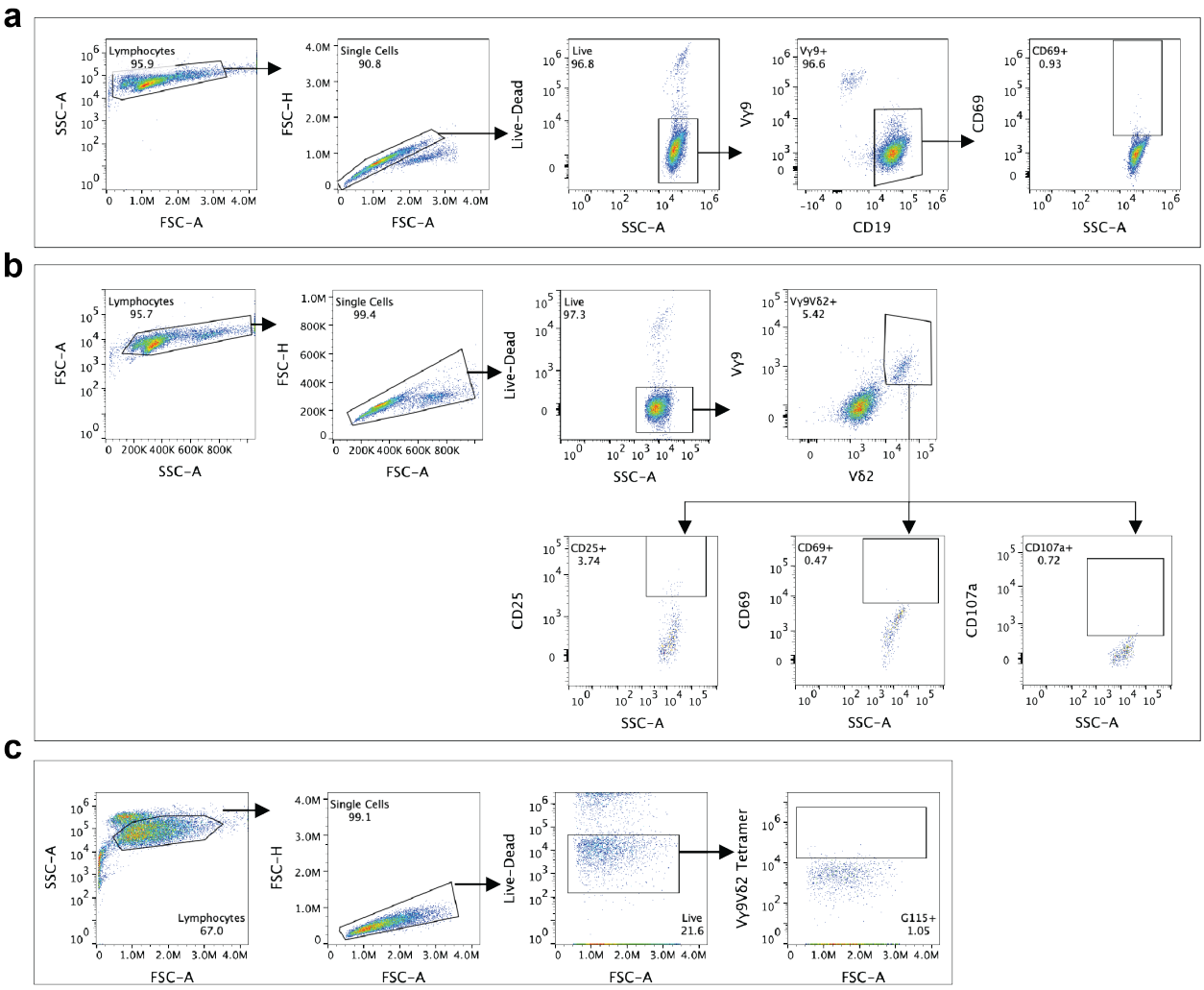

Figure 7.2: Gating strategies for flow cytometry

(A) Gating strategy for Jurkat T-cell activation assays. CD69 gate drawn to 1% positive staining by isotype controls. **(B)** Gating strategy for Primary $V\gamma9V\delta2$ T-cell activation assays. CD25, CD107a, and CD69 gates drawn to 1% positive staining by isotype controls (Mean from 3 replicates). **(C)**Gating strategy for α-BTN2A1 mAbs - $V\gamma9V\delta2$ TCR competition assays. $V\gamma9V\delta2$ TCR Tetramer positive gate drawn to 1% positive staining in – mAb condition.

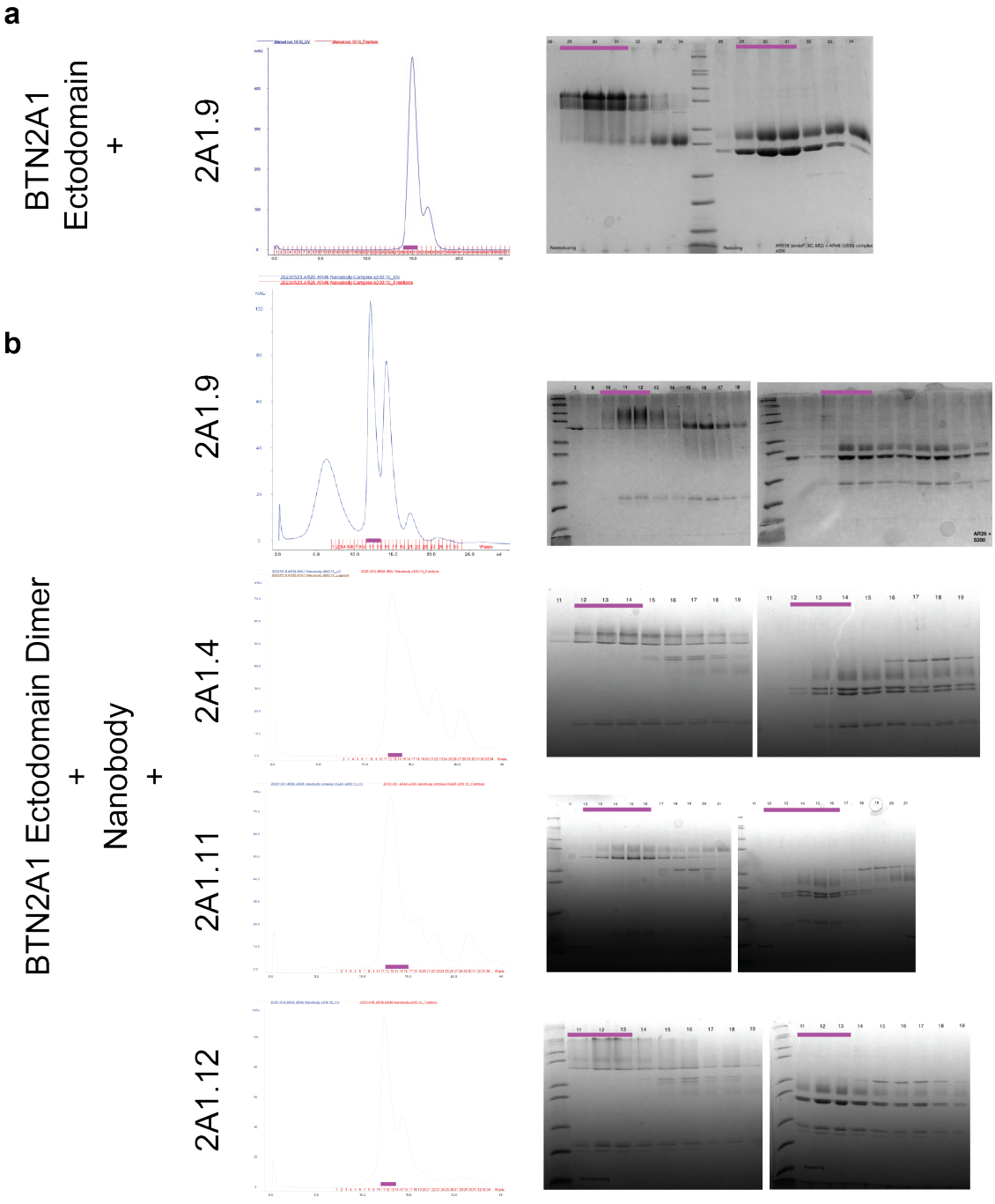

Figure 7.3: Complex expression and purification

(Continued on next page)

Figure 7.3: Complex expression and purification, continued)

(Continued from previous page) **(A)** Chromatography trace of 2A1.9 Fab - BTN2A1 ectodomain complex purified over the S200 Size Exclusion Chromatography (left) for X-ray crystallographic structure determination. SDS-PAGE gel showing Complex elution fractions from S200 purification (Fab: 48kDa, BTN2A1 ectodomain: 26kDa) (right). **(B)** Chromatography traces of Fab - BTN2A1 ectodomain dimer - nanobody complexes purified over the S200 Size Exclusion Chromatography (left) for Cryo-EM structure determination. Nonreducing (middle) and reducing (right) SDS-PAGE gels showing complex elution fractions from S200 purification (Fab: 48 kDa, BTN2A1 dimer: 51 kDa, Nanobody: 15 kDa). Fractions used for structural determination are indicated (purple bar).

for crystallization using the Morpheus I protein crystallization screen in 3-well sitting drop plates. Crystallization conditions from well G9 were optimized to 0.1 M Buffer System 3, pH 8.3 with 0.1 M Carboxylic Acids and 20% Precipitant mix 1. Optimized crystals were cryoprotected with 20% Ethylene Glycol in 0.1 M Buffer System 3, pH 8.3 with 0.1 M Carboxylic Acids and 25% Precipitant mix 1 and flash-frozen in Liquid Nitrogen.

7.8.2 Data collection and processing

X-ray datasets were collected at the Stanford SSRL beamline 14-1 on a Dectris Pilatus 6M at 100K. A complete dataset was collected at a wavelength of 1.1950E-10 m. XDS, truncate, pointless, freeR, and aimless were used for data reduction and scaling. An initial molecular replacement solution was obtained using PHASER through Phenix[54] with PDB ID code 8dfw[32]: Chain B and 4rrp[55]: Chains D,J with CDR loop atoms deleted (D:25-33, 49-61, 90-96. J:28-34, 50-58, 95-100). The initial model was improved using iterative rounds of manual building with Coot followed by refinement with Phenix[54]. A second round of phasing was performed using Chains C,D and J from the refined BTN2A1-Fab complex structure and followed by subsequent rounds of refinement.

7.9 Cryo-electron microscopy

7.9.1 Sample preparation

Deglycosylated and purified BTN2A1 ectodomain was mixed with purified Fab and Nanobody at a 1:1.2:1.44 ratio. Complexes were concentrated and purified over size-exclusion chromatography using the S200 column in HBS. Purified complexes were concentrated to~2.3mg/mL and diluted to 0.85 mg/mL in HBS containing CHAPSO detergent at 0.25 x CMC. Complexes were frozen on Quantifoil Au 200 grids using the FEI Vitrobot.

7.9.2 Data collection and processing

Data was collected on the Thermo Scientific Titan Krios G3i at the University of Chicago Advanced Electron Microscopy Core. Relion was used for motion correction, CTF finding (Max Res<6Å), particle-picking (laplacian, mask: 130-280), particle-extraction (Box: 420Å), 2D classification, 3D-classification (reference map: PDB ID: 8dfw) and 3D-refinement[56].

7.10 Data Analysis

7.10.1 General

Flow-Jo was utilized to analyze flow-cytometry data. All results from flow-cytometry, and affinity-determination experiments were plotted and statistically-analyzed in GraphPad Prism. Adobe Illustrator was used to design figures.

7.10.2 Analysis of protein complex structures

CCP4-Contact was used to determine van der Waals interactions with a distance cut-off of 4.001. PDB-ePISA[43] was used to find salt-bridge and hydrogen-bond interactions between Fab and BTN2A1.

7.10.3 Statistics

All statistical analyses were performed in Graphpad Prism. All data sets were representative of at least 3 replicates with means displayed as points and standard deviations (SD) displayed as error bars. Data from activation assays involving titration of a reagent were displayed on an XY graph and, in specific cases, analyzed using non-linear regression (variable-slope, 4 parameters). Data from specific concentrations within a titration were assessed for statistical significance using multiple t-tests with the Dunnett's method. Activation assays involving use of a reagent at a single concentration and the TCR competition insect-cell assay were analyzed using multiple t-tests with the Dunnett's method. Crystallography statistical analyses were carried out in Phenix.

REFERENCES

[1] L. Gay, S. Mezouar, C. Cano, P. Frohna, L. Madakamutil, J. L. Mège, and D. Olive. Role of v 9v 2 t lymphocytes in infectious diseases. *Frontiers in Immunology*, (1664-3224 (Electronic)), 2022. doi:10.3389/fimmu.2022.928441.

[2] Isabel Correa, Mark Bix, Nan Shih Liao, Maarten Zijlstra, Rudolf Jaenisch, and David Raulet. Most t cells develop normally in 2-microglobulin-deficient mice. *Proceedings of the National Academy of Sciences of the United States of America*, 89(2):653–657, 1992. doi:10.1073/pnas.89.2.653.

[3] Craig T. Morita, Evan M. Beckman, Jack F. Bukowski, Yoshimasa Tanaka, Hamid Band, Barry R. Bloom, David E. Golan, and Michael B. Brenner. Direct presentation of nonpeptide prenyl pyrophosphate antigens to human t cells. *Immunity*, 3(4): 495–507, 1995. doi:10.1016/1074-7613(95)90178-7.

[4] Sarina Ravens, Alina S. Fichtner, Maike Willers, Dennis Torkornoo, Sabine Pirr, Jennifer Schöning, Malte Deseke, Inga Sandrock, Anja Bubke, Anneke Wilharm, Daniel Dodoo, Beverly Egyir, Katie L. Flanagan, Lars Steinbrück, Paul Dickinson, Peter Ghazal, Bright Adu, Dorothee Viemann, and Immo Prinz. Microbial exposure drives polyclonal expansion of innate t cells immediately after birth. *Proceedings of the National Academy of Sciences of the United States of America*, 117(31):18649–18660, 2020. doi:10.1073/pnas.1922588117.

[5] Alina S. Fichtner, Anja Bubke, Francesca Rampoldi, Anneke Wilharm, Likai Tan, Lars Steinbrück, Christian Schultze-Florey, Constantin von Kaisenberg, Immo Prinz, Thomas Herrmann, and Sarina Ravens. Tcr repertoire analysis reveals phosphoantigen-induced polyclonal proliferation of v 9v 2 t cells in neonates and adults. *Journal of Leukocyte Biology*, 107(6):1023–1032, 2020. doi:10.1002/JLB.1MA0120-427RR.

[6] Maria Papadopoulou, Paola Tieppo, Naomi McGovern, Françoise Gosselin, Jerry K. Y. Chan, Glenn Goetgeluk, Nicolas Dauby, Alexandra Cogan, Catherine Donner, Florent Ginhoux, Bart Vandekerckhove, and David Vermijlen. Tcr sequencing reveals the distinct development of fetal and adult human v 9v 2 t cells. *The Journal of Immunology*, 203(6):1468–1479, 2019. doi:10.4049/jimmunol.1900592.

[7] Andrew Sandstrom, Cassie Marie Peigné, Alexandra Léger, James E. Crooks, Fabienne Konczak, Marie Claude Gesnel, Richard Breathnach, Marc Bonneville, Emmanuel Scotet, and Erin J. Adams. The intracellular b30.2 domain of butyrophilin 3a1 binds phosphoantigens to mediate activation of human v 9v 2t cells. *Immunity*, 40(4):490–500, 2014. doi:10.1016/j.immuni.2014.03.003.

[8] Khiem Nguyen, Jin Li, Robbins Puthenveetil, Xiaochen Lin, Michael M. Poe, Chia Hung Christine Hsiao, Olga Vinogradova, and Andrew J. Wiemer. The butyrophilin 3a1 intracellular domain undergoes a conformational change involving the juxtamembrane region. *FASEB Journal*, 31(11):4697–4706, 2017. doi:10.1096/fj.201601370RR.

[9] Cassie-Marie Peigné, Alexandra Léger, Marie-Claude Gesnel, Fabienne Konczak, Daniel Olive, Marc Bonneville, Richard Breathnach, and Emmanuel Scotet. The juxtamembrane domain of butyrophilin btn3a1 controls phosphoantigen-mediated activation of human v 9v 2 t cells. *The Journal of Immunology*, 198(11):4228–4234, 2017. doi:10.4049/jimmunol.1601910.

[10] M. M. Karunakaran, H. Subramanian, Y. Jin, F. Mohammed, B. Kimmel, C. Juraske, L. Starick, A. Nohren, N. Lander, C. R. Willcox, R. Singh, W. W. Schamel, V. O. Nikolaev, V. Kunzmann, A. J. Wiemer, B. E. Willcox, and T. Herrmann. A distinct topology of btn3a igv and b30.2 domains controlled by juxtamembrane regions favors optimal human gammadelta t cell phosphoantigen sensing. *Nat Commun*, 14(1): 7617, 2023. ISSN 2041-1723 (Electronic) 2041-1723 (Linking). doi:10.1038/s41467-023-41938-8. Karunakaran, Mohindar M. Subramanian, Hariharan. Jin, Yiming. Mohammed, Fiyaz. Kimmel, Brigitte. Juraske, Claudia. Starick, Lisa. Nohren, Anna. Lander, Nora. Willcox, Carrie R. Singh, Rohit. Schamel, Wolfgang W. Nikolaev, Viacheslav O. Kunzmann, Volker. Wiemer, Andrew J. Willcox, Benjamin E. Herrmann, Thomas.

[11] H. Wang, M. H. Nada, Y. Tanaka, S. Sakuraba, and C. T. Morita. Critical roles for coiled-coil dimers of butyrophilin 3a1 in the sensing of prenyl pyrophosphates by human vgamma2vdelta2 t cells. *J Immunol*, 203(3):607–626, 2019. ISSN 1550-6606 (Electronic) 0022-1767 (Print) 0022-1767 (Linking). doi:10.4049/jimmunol.1801252.

[12] Marc Rigau, Simone Ostrouska, Thomas S. Fulford, Darryl N. Johnson, Katherine Woods, Zheng Ruan, Hamish E. G. McWilliam, Christopher Hudson, Candani Tutuka, Adam K. Wheatley, Stephen J. Kent, Jose A. Villadangos, Bhupinder Pal, Christian Kurts, Jason Simmonds, Matthias Pelzing, Andrew D. Nash, Andrew Hammet, Anne M. Verhagen, Gino Vairo, Eugene Maraskovsky, Con Panousis, Nicholas A. Gherardin, Jonathan Cebon, Dale I. Godfrey, Andreas Behren, and Adam P. Uldrich. Butyrophilin 2a1 is essential for phosphoantigen reactivity by t cells. *Science*, pages eaay5516–eaay5516, 2020. doi:10.1126/science.aay5516.

[13] Mohindar M. Karunakaran, Carrie R. Willcox, Fiyaz Mohammed, Benjamin E. Willcox, and Thomas Herrmann. Butyrophilin-2a1 directly binds germline-encoded regions of the vg9vd2 tcr and is essential for phosphoantigen sensing. *Immunity*, 52, 2020. doi:10.1016/j.immuni.2020.02.014.

[14] Linjie Yuan, Xianqiang Ma, Yunyun Yang, Yingying Qu, Xin Li, Xiaoyu Zhu, Weiwei Ma, Jianxin Duan, Jing Xue, Haoyu Yang, Jian Wen Huang, Simin Yi, Mengting Zhang, Ningning Cai, Lin Zhang, Qingyang Ding, Kecheng Lai, Chang Liu, Lilan Zhang, Xinyi Liu, Yirong Yao, Shuqi Zhou, Xian Li, Panpan Shen, Qing Chang, Satish R. Malwal, Yuan He, Wenqi Li, Chunlai Chen, Chun Chi Chen, Eric Oldfield, Rey Ting Guo, and Yonghui Zhang. Phosphoantigens glue butyrophilin 3a1 and 2a1 to activate v 9v 2 t cells. *Nature*, 621(7980):840–848, 2023. doi:10.1038/s41586-023-06525-3.

[15] Chia Hung Christine Hsiao, Khiem Nguyen, Yiming Jin, Olga Vinogradova, and Andrew J. Wiemer. Ligand-induced interactions between butyrophilin 2a1 and 3a1 internal domains in the hmbpp receptor complex. *Cell Chemical Biology*, 29(6):985–995.e5, 2022. doi:10.1016/j.chembiol.2022.01.004.

[16] Carrie R. Willcox, Mahboob Salim, Charlotte R. Begley, Mohindar M. Karunakaran, Emily J. Easton, Carlotta von Klopotek, Katie A. Berwick, Thomas Herrmann, Fiyaz Mohammed, Mark Jeeves, and Benjamin E. Willcox. Phosphoantigen sensing combines tcr-dependent recognition of the btn3a igv domain and germline interaction with btn2a1. *Cell Reports*, 42(4), 2023. doi:10.1016/j.celrep.2023.112321.

[17] Hans Jürgen Gober, Magdalena Kistowska, Lena Angman, Paul Jenö, Lucia Mori, and Gennaro De Libero. Human t cell receptor cells recognize endogenous mevalonate metabolites in tumor cells. *Journal of Experimental Medicine*, 197(2):163–168, 2003. doi:10.1084/jem.20021500.

[18] Y. Liu and C. Zhang. The role of human gammadelta t cells in anti-tumor immunity and their potential for cancer immunotherapy. *Cells*, 9(5), 2020. ISSN 2073-4409 (Electronic) 2073-4409 (Linking). doi:10.3390/cells9051206. Liu, Yuxia Zhang, Cai eng Research Support, Non-U.S. Gov't Review Switzerland 2020/05/18 Cells. 2020 May 13;9(5):1206. doi: 10.3390/cells9051206.

[19] Patricia Constant, François Davodeau, Marie Alix Peyrat, Yannick Poquet, Germain Puzo, Marc Bonneville, and Jean Jacques Fournié. Stimulation of human t cells by nonpeptidic mycobacterial ligands. *Science*, 264(5156):267–270, 1994. doi:10.1126/science.8146660.

[20] Morten M. Nielsen, Deborah A. Witherden, and Wendy L. Havran. t cells in homeostasis and host defence of epithelial barrier tissues. 17:733–745, 2017/12// 2017. doi:10.1038/nri.2017.101.

[21] Aj Auid-Orcid Wiemer. Structure-activity relationships of butyrophilin 3 ligands. (1860-7187 (Electronic)).

[22] Klaus Peter Künkele, Daniela Wesch, Hans Heinrich Oberg, Martin Aichinger, Verena Supper, and Christoph Baumann. V 9v 2 t cells: Can we re-purpose a potent anti-infection mechanism for cancer therapy?, 2020/3// 2020.

[23] S. Chen, Z. Li, W. Huang, Y. Wang, and S. Fan. Prognostic and therapeutic significance of btn3a proteins in tumors. *J Cancer*, 12(15):4505–4512, 2021. ISSN 1837-9664 (Print) 1837-9664 (Electronic) 1837-9664 (Linking). doi:10.7150/jca.57831.

[24] C. David Pauza, Mei Ling Liou, Tyler Lahusen, Lingzhi Xiao, Rena G. Lapidus, Cristiana Cairo, and Haishan Li. Gamma delta t cell therapy for cancer: It is good to be local, 2018/6// 2018.

[25] Yoshimasa Tanaka, Yoko Tanaka, Barry R. Bloom, Craig T. Morita, Michael B. Brenner, and Edward Nieves. Natural and synthetic non-peptide antigens recognized by human t cells, 1995/5// 1995.

[26] Craig T. Morita, Hoi K. Lee, Hong Wang, Hongmin Li, Roy A. Mariuzza, and Yoshimasa Tanaka. Structural Features of Nonpeptide Prenyl Pyrophosphates That Determine Their Antigenicity for Human T Cells1. *The Journal of Immunology*, 167(1): 36–41, 07 2001. ISSN 0022-1767. doi:10.4049/jimmunol.167.1.36.

[27] Aparna Palakodeti, Andrew Sandstrom, Lakshmi Sundaresan, Christelle Harly, Steven Nedellec, Daniel Olive, Emmanuel Scotet, Marc Bonneville, and Erin J. Adams. The molecular basis for modulation of human v 9v 2 t cell responses by cd277/butyrophilin-3 (btn3a)-specific antibodies. *Journal of Biological Chemistry*, 287(39):32780–32790, 2012. ISSN 7738349816. doi:10.1074/jbc.M112.384354.

[28] Siyi Gu, Joseph R. Sachleben, Christopher T. Boughter, Wioletta I. Nawrocka, Marta T. Borowska, Jeffrey T. Tarrasch, Georgios Skiniotis, Benoît Roux, and Erin J. Adams. Phosphoantigen-induced conformational change of butyrophilin 3a1 (btn3a1) and its implication on v 9v 2 t cell activation. *Proceedings of the National Academy of Sciences of the United States of America*, 114(35):E7311–E7320, 2017. doi:10.1073/pnas.1707547114.

[29] Pierre Vantourout, Adam Laing, Martin J. Woodward, Iva Zlatareva, Luis Apolonia, Andrew W. Jones, Ambrosius P. Snijders, Michael H. Malim, and Adrian C. Hayday. Heteromeric interactions regulate butyrophilin (btn) and btn-like molecules governing t cell biology. *Proceedings of the National Academy of Sciences*, 115(5):1039–1044, 2018. doi:10.1073/pnas.1701237115.

[30] Carla E. Cano, Christine Pasero, Aude De Gassart, Clement Kerneur, Mélanie Gabriac, Marie Fullana, Emilie Granarolo, René Hoet, Emmanuel Scotet, Chirine Rafia, Thomas Hermman, Caroline Imbert, Laurent Gorvel, Norbert Vey, Antoine Briantais, Anne Charlotte le Floch, and Daniel Olive. Btn2a1, an immune checkpoint targeting v 9v 2 t cell cytotoxicity against malignant cells. *Cell Reports*, 36(2), 2021. doi:10.1016/j.celrep.2021.109359.

[31] Yunyun Yang, Liping Li, Linjie Yuan, Xiaoying Zhou, Jianxin Duan, Hongying Xiao, Ningning Cai, Shuai Han, Xianqiang Ma, Weidong Liu, Chun Chi Chen, Lingle Wang, Xin Li, Jiahuan Chen, Ning Kang, Jing Chen, Zhixun Shen, Satish R. Malwal, Wanli Liu, Yan Shi, Eric Oldfield, Rey Ting Guo, and Yonghui Zhang. A structural change in butyrophilin upon phosphoantigen binding underlies phosphoantigen-mediated v 9v 2 t cell activation. *Immunity*, 50(4):1043–1053.e5, 2019. doi:10.1016/j.immuni.2019.02.016.

[32] Thomas S. Fulford, Caroline Soliman, Rebecca G. Castle, Marc Rigau, Zheng Ruan, Olan Dolezal, Rebecca Seneviratna, Hamish G. Brown, Eric Hanssen, Andrew Hammet, Shihan Li, J. Redmond, Samuel, Amy Chung, Michael A. Gorman,

Michael W. Parker, Onisha Patel, Thomas S. Peat, Janet Newman, Andreas Behren, Nicholas A. Gherardin, Dale I. Godfrey, and Adam P. Uldrich. V 9v 2 t cells recognize butyrophilin 2a1 and 3a1 heteromers. *bioRxiv*, page 2023.08.30.555639, 2023. doi:10.1101/2023.08.30.555639.

[33] Caitlin D. Castro, Christopher T. Boughter, Augusta E. Broughton, Amrita Ramesh, and Erin J. Adams. Diversity in recognition and function of human t cells. *Immunological Reviews*, 298(1):134–152, 2020. doi:10.1111/imr.12930.

[34] M. S. Davey, C. R. Willcox, S. Hunter, S. A. Kasatskaya, E. B. M. Remmerswaal, M. Salim, F. Mohammed, F. J. Bemelman, D. M. Chudakov, Y. H. Oo, and B. E. Willcox. The human vdelta2(+) t-cell compartment comprises distinct innate-like vgamma9(+) and adaptive vgamma9(-) subsets. *Nat Commun*, 9(1):1760, 2018. ISSN 2041-1723 (Electronic) 2041-1723 (Linking). doi:10.1038/s41467-018-04076-0.

[35] M. Paduch, A. Koide, S. Uysal, S. S. Rizk, S. Koide, and A. A. Kossiakoff. Generating conformation-specific synthetic antibodies to trap proteins in selected functional states. *Methods*, 60(1):3–14, 2013. ISSN 1046-2023 (Print) 1046-2023. doi:10.1016/j.ymeth.2012.12.010.

[36] F. Miyagawa, Y. Tanaka, S. Yamashita, B. Mikami, K. Danno, M. Uehara, and N. Minato. Essential contribution of germline-encoded lysine residues in jgamma1.2 segment to the recognition of nonpeptide antigens by human gammadelta t cells. *J Immunol*, 167(12):6773–9, 2001. ISSN 0022-1767 (Print) 0022-1767 (Linking). doi:10.4049/jimmunol.167.12.6773.

[37] Hong Wang, Zhimei Fang, and Craig T. Morita. V 2v 2 t cell receptor recognition of prenyl pyrophosphates is dependent on all cdrs. *The Journal of Immunology*, 184(11): 6209–6222, 2010. doi:10.4049/jimmunol.1000231.

[38] F. Davodeau, M. A. Peyrat, M. M. Hallet, I. Houde, H. Vie, and M. Bonneville. Peripheral selection of antigen receptor junctional features in a major human gamma delta subset. *Eur J Immunol*, 23(4):804–8, 1993. ISSN 0014-2980 (Print) 0014-2980 (Linking). doi:10.1002/eji.1830230405. Davodeau, F Peyrat, M A Hallet, M M Houde, I Vie, H Bonneville, M eng Research Support, Non-U.S. Gov't Germany 1993/04/01 Eur J Immunol. 1993 Apr;23(4):804-8. doi: 10.1002/eji.1830230405.

[39] J. F. Bukowski, C. T. Morita, H. Band, and M. B. Brenner. Crucial role of tcr gamma chain junctional region in prenyl pyrophosphate antigen recognition by gamma delta t cells. *Journal of immunology (Baltimore, Md. : 1950)*, 161(1):286–93, 1998.

[40] Anna Vyborova, Dennis X. Beringer, Domenico Fasci, Froso Karaiskaki, Eline van Diest, Lovro Kramer, Aram de Haas, Jasper Sanders, Anke Janssen, Trudy Straetemans, Daniel Olive, Jeanette Leusen, Lola Boutin, Steven Nedellec, Samantha L. Schwartz, Michael J. Wester, Keith A. Lidke, Emmanuel Scotet, Diane S. Lidke, Albert J. R.

Heck, Zsolt Sebestyen, and Jürgen Kuball. 9 2t cell diversity and the receptor interface with tumor cells. *Journal of Clinical Investigation*, 130(9):4637–4651, 2020. doi:10.1172/JCI132489.

[41] C. M. Parker, V. Groh, H. Band, S. A. Porcelli, C. Morita, M. Fabbi, D. Glass, J. L. Strominger, and M. B. Brenner. Evidence for extrathymic changes in the t cell receptor gamma/delta repertoire. *J Exp Med*, 171(5):1597–612, 1990. ISSN 0022-1007 (Print) 1540-9538 (Electronic) 0022-1007 (Linking). doi:10.1084/jem.171.5.1597.

[42] F. A. Fellouse, K. Esaki, S. Birtalan, D. Raptis, V. J. Cancasci, A. Koide, P. Jhurani, M. Vasser, C. Wiesmann, A. A. Kossiakoff, S. Koide, and S. S. Sidhu. High-throughput generation of synthetic antibodies from highly functional minimalist phage-displayed libraries. *J Mol Biol*, 373(4):924–40, 2007. ISSN 0022-2836 (Print) 0022-2836. doi:10.1016/j.jmb.2007.08.005.

[43] E. Krissinel and K. Henrick. Inference of macromolecular assemblies from crystalline state. (0022-2836 (Print)).

[44] J. Auid-Orcid Agirre, M. Auid-Orcid Atanasova, H. Auid-Orcid Bagdonas, C. B. Ballard, A. Baslé, J. Auid-Orcid Beilsten-Edmands, Rj Auid-Orcid Borges, D. G. Brown, Jj Auid-Orcid Burgos-Mármol, J. M. Berrisford, Ps Auid-Orcid Bond, I. Auid-Orcid Caballero, L. Auid-Orcid Catapano, G. Auid-Orcid Chojnowski, A. G. Cook, Kd Auid-Orcid Cowtan, T. I. Croll, JÉ Debreczeni, N. E. Devenish, E. J. Dodson, T. R. Drevon, P. Emsley, G. Auid-Orcid Evans, Pr Auid-Orcid Evans, M. Fando, J. Foadi, L. Auid-Orcid Fuentes-Montero, Ef Auid-Orcid Garman, M. Gerstel, Rj Auid-Orcid Gildea, K. Hatti, Ml Auid-Orcid Hekkelman, P. Auid-Orcid Heuser, S. W. Hoh, Ma Auid-Orcid Hough, Ht Auid-Orcid Jenkins, E. Auid-Orcid Jiménez, Rp Auid-Orcid Joosten, Rm Auid-Orcid Keegan, N. Auid-Orcid Keep, Eb Auid-Orcid Krissinel, P. Auid-Orcid Kolenko, O. Kovalevskiy, Vs Auid-Orcid Lamzin, Dm Auid-Orcid Lawson, Aa Auid-Orcid Lebedev, Agw Auid-Orcid Leslie, B. Auid-Orcid Lohkamp, F. Auid-Orcid Long, M. Malý, A. J. McCoy, S. J. McNicholas, A. Auid-Orcid Medina, C. Auid-Orcid Millán, Jw Auid-Orcid Murray, Gn Auid-Orcid Murshudov, Ra Auid-Orcid Nicholls, M. E. M. Noble, R. Auid-Orcid Oeffner, N. S. Pannu, J. M. Parkhurst, N. Pearce, J. Auid-Orcid Pereira, A. Auid-Orcid Perrakis, Hr Auid-Orcid Powell, Rj Auid-Orcid Read, Dj Auid-Orcid Rigden, W. Auid-Orcid Rochira, M. Auid-Orcid Sammito, F. Auid-Orcid Sánchez Rodríguez, G. M. Sheldrick, K. L. Shelley, F. Simkovic, A. J. Simpkin, P. Auid-Orcid Skubak, E. Auid-Orcid Sobolev, Ra Auid-Orcid Steiner, K. Stevenson, I. Auid-Orcid Tews, Jmh Auid-Orcid Thomas, A. Auid-Orcid Thorn, J. T. Valls, V. Auid-Orcid Uski, I. Usón, A. Vagin, S. Auid-Orcid Velankar, M. Vollmar, H. Auid-Orcid Walden, D. Auid-Orcid X. Waterman, Ks Auid-Orcid Wilson, Md Auid-Orcid Winn, G. Winter, M. Auid-Orcid Wojdyr, and K. Auid-Orcid Yamashita. The ccp4 suite: integrative software for macromolecular crystallography. (2059-7983 (Electronic)).

[45] T. D. Goddard, C. C. Huang, E. C. Meng, E. F. Pettersen, G. S. Couch, J. H. Morris,

and Te Auid-Orcid Ferrin. Ucsf chimerax: Meeting modern challenges in visualization and analysis. (1469-896X (Electronic)).

[46] K. Matsui, J. J. Boniface, P. A. Reay, H. Schild, B. Fazekas de St Groth, and M. M. Davis. Low affinity interaction of peptide-mhc complexes with t cell receptors. *Science*, 254(5039):1788–91, 1991. ISSN 0036-8075 (Print) 0036-8075 (Linking). doi:10.1126/science.1763329.

[47] Christelle Harly, Yves Guillaume, Steven Nedellec, Cassie Marie Peigné, Hannu Mönkkönen, Jukka Mönkkönen, Jianqiang Li, Jürgen Kuball, Erin J. Adams, Sonia Netzer, Julie Déchanet-Merville, Alexandra Léger, Thomas Herrmann, Richard Breathnach, Daniel Olive, Marc Bonneville, and Emmanuel Scotet. Key implication of cd277/butyrophilin-3 (btn3a) in cellular stress sensing by a major human t-cell subset. *Blood*, 120(11):2269–2279, 2012. doi:10.1182/blood-2012-05-430470.

[48] Siyi Gu, Wioletta Nawrocka, and Erin J. Adams. Sensing of pyrophosphate metabolites by v 9v 2 t cells, 2015.

[49] F. Davodeau, M. A. Peyrat, M. M. Hallet, J. Gaschet, I. Houde, R. Vivien, H. Vie, and M. Bonneville. Close correlation between daudi and mycobacterial antigen recognition by human gamma delta t cells and expression of v9jpc1 gamma/v2djc delta-encoded t cell receptors. *J Immunol*, 151(3):1214–23, 1993. ISSN 0022-1767 (Print) 0022-1767 (Linking).

[50] Kyle K. Payne, Jessica A. Mine, Subir Biswas, Ricardo A. Chaurio, Alfredo Perales-Puchalt, Carmen M. Anadon, Tara Lee Costich, Carly M. Harro, Jennifer Walrath, Qianqian Ming, Evgenii Tcyganov, Andrea L. Buras, Kristen E. Rigolizzo, Gunjan Mandal, Jason Lajoie, Michael Ophir, Julia Tchou, Douglas Marchion, Vincent C. Luca, Piotr Bobrowicz, Brooke McLaughlin, Ugur Eskiocak, Michael Schmidt, Juan R. Cubillos-Ruiz, Paulo C. Rodriguez, Dmitry I. Gabrilovich, and Jose R. Conejo-Garcia. Btn3a1 governs antitumor responses by coordinating ab and gd t cells. *Science*, 369 (6506):942–949, 2020. doi:10.1126/science.aay2767.

[51] Emilien Billon, Brice Chanez, Philippe Rochigneux, Laurence Albiges, Cécile Vicier, Géraldine Pignot, Jochen Walz, Anne-Sophie Chretien, Gwenaelle Gravis, and Daniel Olive. Soluble btn2a1 is a potential prognosis biomarker in pre-treated advanced renal cell carcinoma. *Frontiers in Immunology*, 12, 2021. ISSN 1664-3224. doi:10.3389/fimmu.2021.670827. URL `https://www.frontiersin.org/articles/10.3389/fimmu.2021.670827`.

[52] J. Ereno-Orbea, T. Sicard, H. Cui, J. Carson, P. Hermans, and J. P. Julien. Structural basis of enhanced crystallizability induced by a molecular chaperone for antibody antigen-binding fragments. *J Mol Biol*, 430(3):322–336, 2018. ISSN 1089-8638 (Electronic) 0022-2836 (Linking). doi:10.1016/j.jmb.2017.12.010.

[53] Murad R. Mamedov, Shane Vedova, Jacob W. Freimer, Avinash Das Sahu, Amrita Ramesh, Maya M. Arce, Angelo D. Meringa, Mineto Ota, Peixin Amy Chen, Kristina Hanspers, Vinh Q. Nguyen, Kirsten A. Takeshima, Anne C. Rios, Jonathan K. Pritchard, Jürgen Kuball, Zsolt Sebestyen, Erin J. Adams, and Alexander Marson. Crispr screens decode cancer cell pathways that trigger t cell detection. *Nature*, 621 (7977):188–195, 2023. ISSN 1476-4687. doi:10.1038/s41586-023-06482-x.

[54] D. Liebschner, P. V. Afonine, M. L. Baker, G. Bunkóczi, V. B. Chen, T. I. Croll, B. Hintze, L. W. Hung, S. Jain, A. J. McCoy, N. W. Moriarty, R. D. Oeffner, B. K. Poon, M. G. Prisant, R. J. Read, J. S. Richardson, D. C. Richardson, M. D. Sammito, O. V. Sobolev, D. H. Stockwell, T. C. Terwilliger, A. G. Urzhumtsev, L. L. Videau, C. J. Williams, and P. D. Adams. Macromolecular structure determination using x-rays, neutrons and electrons: recent developments in phenix. *Acta crystallographica. Section D, Structural biology*, 75:861–877, 2019. doi:10.1107/S2059798319011471.

[55] A. Kuzin, S. Lew, J. Seetharaman, L. Mao, R. Xiao, P.T. Oconnell, M. Maglaqui, L. Bailey, J.K. Everett, T.B. Acton, G.T. Montelione, J.F. Hunt, and L. Tong. Crystal structure of the fab complexed with antigen asf1p, northeast structural genomics consortium (nesg) target pdr16. 2014. doi:https://doi.org/10.2210/pdb4RRP/pdb.

[56] Jasenko Zivanov, Joaquín Otón, Zunlong Ke, Andriko von Kügelgen, Euan Pyle, Kun Qu, Dustin Morado, Daniel Castaño-Díez, Giulia Zanetti, Tanmay A. M. Bharat, John A. G. Briggs, and Sjors H. W. Scheres. A bayesian approach to single-particle electron cryo-tomography in relion-4.0. *eLife*, 11:e83724, 2022. ISSN 2050-084X. doi:10.7554/eLife.83724.

[57] A. Y. Lai, A. Patel, F. Brewer, K. Evans, K. Johannes, L. E. Gonzalez, K. J. Yoo, G. Fromm, K. Wilson, T. H. Schreiber, and S. de Silva. Cutting edge: Bispecific gammadelta t cell engager containing heterodimeric btn2a1 and btn3a1 promotes targeted activation of vgamma9vdelta2(+) t cells in the presence of costimulation by cd28 or nkg2d. *J Immunol*, 209(8):1475–1480, 2022. ISSN 1550-6606 (Electronic) 0022-1767 (Print) 0022-1767 (Linking). doi:10.4049/jimmunol.2200185. Lai, Anne Y Patel, Arpita Brewer, Faraha Evans, Kinsley Johannes, Kellsey Gonzalez, Louis E Yoo, Kyung Jin Fromm, George Wilson, Keith Schreiber, Taylor H de Silva, Suresh eng Research Support, Non-U.S. Gov't 2022/09/13 J Immunol. 2022 Oct 15;209(8):1475-1480. doi: 10.4049/jimmunol.2200185. Epub 2022 Sep 12.

[58] Chloé Laplagne, Laetitia Ligat, Juliet Foote, Frederic Lopez, Jean Jacques Fournié, Camille Laurent, Salvatore Valitutti, and Mary Poupot. Self-activation of v 9v 2 t cells by exogenous phosphoantigens involves tcr and butyrophilins. *Cellular and Molecular Immunology*, 18(8):1861–1870, 2021. doi:10.1038/s41423-021-00720-w.

[59] Carrie R. Willcox, Pierre Vantourout, Mahboob Salim, Iva Zlatareva, Daisy Melandri, Leonor Zanardo, Roger George, Svend Kjaer, Mark Jeeves, Fiyaz Mohammed, Adrian C. Hayday, and Benjamin E. Willcox. Butyrophilin-like 3 directly binds a

human v 4+ t cell receptor using a modality distinct from clonally-restricted antigen. *Immunity*, 51(5):813–825.e4, 2019. doi:10.1016/j.immuni.2019.09.006.

[60] Michael M. Poe, Sherry S. Agabiti, Caroline Liu, Victoria Li, Kelly A. Teske, Chia Hung Christine Hsiao, and Andrew J. Wiemer. Probing the ligand-binding pocket of btn3a1. *Journal of Medicinal Chemistry*, 62(14):6814–6823, 2019. doi:10.1021/acs.jmedchem.9b00825.

[61] Mijeong Lee, Chanho Park, Jeongmin Woo, Jinho Kim, Inseong Kho, Do Hyun Nam, Woong Yang Park, Yeon Soo Kim, Doo Sik Kong, Hye Won Lee, and Tae Jin Kim. Preferential infiltration of unique v 9j 2-vΔ2 t cells into glioblastoma multiforme. *Frontiers in Immunology*, 10(MAR):555–555, 2019. doi:10.3389/fimmu.2019.00555.

[62] Carrie R. Willcox, Martin S. Davey, and Benjamin E. Willcox. Development and selection of the human v 9v 2+ t-cell repertoire, 2018/7// 2018.

[63] Elrashdy M. Redwan, Ahmed M. Al-Hejin, Hussein A. Almehdar, Abdelrahman M. Elsaway, and Vladimir N. Uversky. Prediction of disordered regions and their roles in the anti-pathogenic and immunomodulatory functions of butyrophilins. *Molecules*, 23 (2):1–29, 2018. doi:10.3390/molecules23020328.

[64] Timm Hoeres, Manfred Smetak, Dominik Pretscher, and Martin Wilhelm. Improving the efficiency of v 9v 2 t-cell immunotherapy in cancer, 2018/4// 2018.

[65] Martijn Van Rosmalen, Mike Krom, and Maarten Merkx. Tuning the flexibility of glycine-serine linkers to allow rational design of multidomain proteins. *Biochemistry*, 56(50):6565–6574, 2017. doi:10.1021/acs.biochem.7b00902.

[66] Yvonne Stark, Sophie Venet, and Annika Schmid. *Whole cell panning with phage display*, volume 1575, pages 67–91. Humana Press Inc., 2017. doi:10.1007/978-1-4939-6857-2_5.

[67] Rebekah R. Shippy, Xiaochen Lin, Sherry S. Agabiti, Jin Li, Brendan M. Zangari, Benjamin J. Foust, Michael M. Poe, Chia Hung Christine Hsiao, Olga Vinogradova, David F. Wiemer, and Andrew J. Wiemer. Phosphinophosphonates and their tris-pivaloyloxymethyl prodrugs reveal a negatively cooperative butyrophilin activation mechanism. *Journal of Medicinal Chemistry*, 60(6):2373–2382, 2017. doi:10.1021/acs.jmedchem.6b00965.

[68] Thomas M. Schmitt, David H. Aggen, Kumiko Ishida-Tsubota, Sebastian Ochsenreither, David M. Kranz, and Philip D. Greenberg. Generation of higher affinity t cell receptors by antigen-driven differentiation of progenitor t cells in vitro. *Nature Biotechnology*, 35(12):1188–1195, 2017. doi:10.1038/nbt.4004.

[69] Mahboob Salim, Timothy J. Knowles, Alfie T. Baker, Martin S. Davey, Mark Jeeves, Pooja Sridhar, John Wilkie, Carrie R. Willcox, Hachemi Kadri, Taher E. Taher,

Pierre Vantourout, Adrian Hayday, Youcef Mehellou, Fiyaz Mohammed, and Benjamin E. Willcox. Btn3a1 discriminates t cell phosphoantigens from nonantigenic small molecules via a conformational sensor in its b30.2 domain. *ACS Chemical Biology*, 12(10):2631–2643, 2017. doi:10.1021/acschembio.7b00694.

[70] Sarina Ravens, Christian Schultze-Florey, Solaiman Raha, Inga Sandrock, Melanie Drenker, Linda Oberdörfer, Annika Reinhardt, Inga Ravens, Maleen Beck, Robert Geffers, Constantin Von Kaisenberg, Michael Heuser, Felicitas Thol, Arnold Ganser, Reinhold Förster, Christian Koenecke, and Immo Prinz. Human t cells are quickly reconstituted after stem-cell transplantation and show adaptive clonal expansion in response to viral infection. *Nature Immunology*, 18(4):393–401, 2017. doi:10.1038/ni.3686.

[71] Morten M. Nielsen, Deborah A. Witherden, and Wendy L. Havran. t cells in homeostasis and host defence of epithelial barrier tissues, 2017/12// 2017.

[72] Zsolt Sebestyen, Wouter Scheper, Anna Vyborova, Siyi Gu, Zuzana Rychnavska, Marleen Schiffler, Astrid Cleven, Coraline Chéneau, Martje Van Noorden, Cassie-Marie Marie Peigné, Daniel Olive, Robert Jan Lebbink, Rimke Oostvogels, Tuna Mutis, Gerrit-Jan Jan Schuurhuis, Erin J. Adams, Emmanuel Scotet, and Jürgen Kuball. Rhob mediates phosphoantigen recognition by v 9v 2 t cell receptor. *Cell Reports*, 15 (9):1973–1985, 2016. doi:10.1016/j.celrep.2016.04.081.

[73] David A. Rhodes, Walter Reith, and John Trowsdale. Regulation of immunity by butyrophilins. *Annual Review of Immunology*, 34(1):151–172, 2016. doi:10.1146/annurev-immunol-041015-055435.

[74] Cristina Lebrero-Fernández, Ulf Alexander Wenzel, Paulina Akeus, Ying Wang, Hans Strid, Magnus Simrén, Bengt Gustavsson, Lars G. Börjesson, Susanna L. Cardell, Lena Öhman, Marianne Quiding-Järbrink, and Anna Bas-Forsberg. Altered expression of butyrophilin (btn) and btn-like (btnl) genes in intestinal inflammation and colon cancer. *Immunity, Inflammation and Disease*, 4(2):191–200, 2016. doi:10.1002/iid3.105.

[75] Audrey Benyamine, Aude Le Roy, Emilie Mamessier, Julie Gertner-Dardenne, Céline Castanier, Florence Orlanducci, Laurent Pouyet, Armelle Goubard, Yves Collette, Norbert Vey, Emmanuel Scotet, Remy Castellano, and Daniel Olive. Btn3a molecules considerably improve v 9v 2t cells-based immunotherapy in acute myeloid leukemia. *OncoImmunology*, 5(10), 2016. doi:10.1080/2162402X.2016.1146843.

[76] Sheena N. Smith, Daniel T. Harris, and David M. Kranz. T cell receptor engineering and analysis using the yeast display platform. *Methods in Molecular Biology*, 1319: 95–141, 2015. doi:10.1007/978-1-4939-2748-7_6.

[77] Sérgio T. Ribeiro, Julie C. Ribot, and Bruno Silva-Santos. Five layers of receptor signaling in t-cell differentiation and activation, 2015.

[78] D. A. Rhodes, H. C. Chen, A. J. Price, A. H. Keeble, M. S. Davey, L. C. James, M. Eberl, and J. Trowsdale. Activation of human gammadelta t cells by cytosolic interactions of btn3a1 with soluble phosphoantigens and the cytoskeletal adaptor periplakin. *J Immunol*, 194(5):2390–8, 2015. ISSN 1550-6606 (Electronic) 0022-1767 (Print) 0022-1767 (Linking). doi:10.4049/jimmunol.1401064. Epub 2015 Jan 30.

[79] David A. Rhodes, Hung-Chang Chen, Amanda J. Price, Anthony H. Keeble, Martin S. Davey, Leo C. James, Matthias Eberl, and John Trowsdale. Activation of human t cells by cytosolic interactions of btn3a1 with soluble phosphoantigens and the cytoskeletal adaptor periplakin. *The Journal of Immunology*, 194(5):2390–2398, 2015. doi:10.4049/jimmunol.1401064.

[80] Tanya Dimova, Margreet Brouwer, Françoise Gosselin, Joël Tassignon, Oberdan Leo, Catherine Donner, Arnaud Marchant, and David Vermijlen. Effector v 9v 2 t cells dominate the human fetal t-cell repertoire. *Proceedings of the National Academy of Sciences of the United States of America*, 112(6):E556–E565, 2015. doi:10.1073/pnas.1412058112.

[81] Gennaro De Libero, Sze Yi Lau, and Lucia Mori. Phosphoantigen presentation to tcr cells, a conundrum getting less gray zones, 2015.

[82] Felipe Riãno, Mohindar M. Karunakaran, Lisa Starick, Jianqiang Li, Claus J. Scholz, Volker Kunzmann, Daniel Olive, Sabine Amslinger, and Thomas Herrmann. V 9v 2 tcr-activation by phosphorylated antigens requires butyrophilin 3 a1 (btn3a1) and additional genes on human chromosome 6. *European Journal of Immunology*, 44(9): 2571–2576, 2014. doi:10.1002/eji.201444712.

[83] Virginie Lafont, Françoise Sanchez, Emilie Laprevotte, Henri Alexandre Michaud, Laurent Gros, Jean François Eliaou, and Nathalie Bonnefoy. Plasticity of t cells: Impact on the anti-tumor response, 2014.

[84] Joshua S. Klein, Siduo Jiang, Rachel P. Galimidi, Jennifer R. Keeffe, Pamela J. Bjorkman, and Lynne Regan. Design and characterization of structured protein linkers with differing flexibilities. In *Protein Engineering, Design and Selection*, volume 27, pages 325–330. Oxford University Press. doi:10.1093/protein/gzu043.

[85] Stefano Vavassori, Anil Kumar, Gan Siok Wan, Gundimeda S. Ramanjaneyulu, Marco Cavallari, Sary El Daker, Travis Beddoe, Alex Theodossis, Neal K. Williams, Emma Gostick, David A. Price, Dinish U. Soudamini, Kong Kien Voon, Malini Olivo, Jamie Rossjohn, Lucia Mori, and Gennaro De Libero. Butyrophilin 3a1 binds phosphorylated antigens and stimulates human t cells. *Nature Immunology*, 14(9):908–916, 2013. doi:10.1038/ni.2665.

[86] A. Morin, B. Eisenbraun, J. Key, P. C. Sanschagrin, M. A. Timony, M. Ottaviano, and P. Sliz. Cutting edge: Collaboration gets the most out of software. *eLife*, 2, 2013. doi:10.7554/eLife.01456.

[87] Akshay A. D'Cruz, Jeffrey J. Babon, Raymond S. Norton, Nicos A. Nicola, and Sandra E. Nicholson. Structure and function of the spry/b30.2 domain proteins involved in innate immunity. *Protein Science*, 22(1):1–10, 2013. doi:10.1002/pro.2185.

[88] Zheng W. Chen. Multifunctional immune responses of hmbpp-specific v 2v 2 t cells in m. tuberculosis and other infections, 2013/1// 2013.

[89] Fréderic Pont, Julien Familiades, Sébastien Déjean, Séverine Fruchon, Delphine Cendron, Mary Poupot, Rémy Poupot, Fatima L'Faqihi-Olive, Nais Prade, Bernard Ycart, and Jean-Jacques Fournié. The gene expression profile of phosphoantigen-specific human   t lymphocytes is a blend of t-cell and nk-cell signatures. *European Journal of Immunology*, 42(1):228–240, 2012. doi:10.1002/eji.201141870.

[90] Cordula Gründer, Suzanne Van Dorp, Samantha Hol, Esther Drent, Trudy Straetemans, Sabine Heijhuurs, Kirsten Scholten, Wouter Scheper, Zsolt Sebestyen, Anton Martens, Roland Strong, and Jürgen Kuball. 9 and 2cdr3 domains regulate functional avidity of t cells harboring 9 2tcrs. *Blood*, 120(26):5153–5162, 2012. doi:10.1182/blood-2012-05-432427.

[91] Ricardo Henriques, Caron Griffiths, E. Hesper Rego, and Musa M. Mhlanga. Palm and storm: Unlocking live-cell super-resolution. *Biopolymers*, 95(5):322–331, 2011. doi:10.1002/bip.21586.

[92] Yan Kong, Wei Cao, Xueyan Xi, Chi Ma, Lianxian Cui, and Wei He. The nkg2d ligand ulbp4 binds to tcr9/2 and induces cytotoxicity to tumor cells through both tcr and nkg2d. 2009. ISSN 2009;114:310317. doi:10.1182/blood-2008.

[93] Cristiana Cairo, Nadia Propp, Giovanni Auricchio, Cheryl L. Armstrong, Alash'le Abimiku, Giorgio Mancino, Vittorio Colizzi, William Blattner, and C. David Pauza. Altered cord blood t cell repertoire in nigeria: Possible impacts of environmental factors on neonatal immunity. *Molecular Immunology*, 45(11):3190–3197, 2008. doi:10.1016/j.molimm.2008.02.029.

[94] Yangbing Zhao, Alan D. Bennett, Zhili Zheng, Qiong J. Wang, Paul F. Robbins, Lawrence Y. L. Yu, Yi Li, Peter E. Molloy, Steven M. Dunn, Bent K. Jakobsen, Steven A. Rosenberg, and Richard A. Morgan. High-affinity tcrs generated by phage display provide cd4 + t cells with the ability to recognize and kill tumor cell lines. *The Journal of Immunology*, 179(9):5845–5854, 2007. doi:10.4049/jimmunol.179.9.5845.

[95] Georg Malcherek, Luzia Mayr, Pedro Roda-Navarro, David Rhodes, Nigel Miller, and John Trowsdale. The b7 homolog butyrophilin btn2a1 is a novel ligand for dc-sign. *The Journal of Immunology*, 179(6):3804–3811, 2007. doi:10.4049/jimmunol.179.6.3804.

[96] Joshua S. Klein and Pamela J. Bjorkman. J.s. klein thesis - flexible linker mabs against hiv. 2004, 2004.

[97] A. E. Green, A. Lissina, S. L. Hutchinson, R. E. Hewitt, B. Temple, D. James, J. M. Boulter, D. A. Price, and A. K. Sewell. Recognition of nonpeptide antigens by human v 9v 2 t cells requires contact with cells of human origin. *Clinical and Experimental Immunology*, 136(3):472–482, 2004. doi:10.1111/j.1365-2249.2004.02472.x.

[98] Benoit Favier, Eric Espinosa, Julie Tabiasco, Cédric Dos Santos, Marc Bonneville, Salvatore Valitutti, and Jean-Jacques Fournié. Uncoupling between immunological synapse formation and functional outcome in human t lymphocytes. *The Journal of Immunology*, 171(10):5027–5033, 2003. doi:10.4049/jimmunol.171.10.5027.

[99] Zheng W. Chen and Norman L. Letvin. V 2v 2+ t cells and anti-microbial immune responses, 2003.

[100] Yun Shen, Dejiang Zhou, Liyou Qiu, Xioamin Lai, Meredith Simon, Ling Shen, Zhongchen Kou, Qifan Wang, Liming Jiang, Jim Estep, Robert Hunt, Michelle Clagett, Prabhat K. Sehgal, Yunyaun Li, Xuejun Zeng, Craig T. Morita, Michael B. Brenner, Norman L. Letvin, and Zheng W. Chen. Adaptive immune response of v 2v 2 t cells during mycobacterial infections, 2002/3// 2002.

[101] Timothy J. Allison, Christine C. Winter, Jean Jacques Fournié, Marc Bonneville, and David N. Garboczi. Structure of a human t-cell antigen receptor. *Nature*, 411(6839): 820–824, 2001. doi:10.1038/35081115.

[102] Helen M. Berman, John Westbrook, Zukang Feng, Gary Gilliland, T. N. Bhat, Helge Weissig, Ilya N. Shindyalov, and Philip E. Bourne. The protein data bank. *Nucleic Acids Research*, 28(1):235–242, 2000. ISSN 0305-1048. doi:10.1093/nar/28.1.235.

[103] F. Poccia, L. Battistini, B. Cipriani, G. Mancino, F. Martini, M. L. Gougeon, and V. Colizzi. Phosphoantigen-reactive vgamma9vdelta2 t lymphocytes suppress in vitro human immunodeficiency virus type 1 replication by cell-released antiviral factors including cc chemokines. *J Infect Dis*, 180(3):858–61, 1999. ISSN 0022-1899 (Print) 0022-1899 (Linking). doi:10.1086/314925.

[104] Brenner F. Jack Bukowski, Craig T. Morita, and Hamid Band. Chain junctional region in crucial role of tcr. Report, 1998.

[105] F. Jouen-Beades, E. Paris, C. Dieulois, J. F. Lemeland, V. Barre-Dezelus, S. Marret, G. Humbert, J. Leroy, and F. Tron. In vivo and in vitro activation and expansion of gammadelta t cells during listeria monocytogenes infection in humans. *Infect Immun*, 65(10):4267–72, 1997. ISSN 0019-9567 (Print) 1098-5522 (Electronic) 0019-9567 (Linking). doi:10.1128/iai.65.10.4267-4272.1997.

[106] Jean Jacques Fournié and Marc Bonneville. Stimulation of t cells by phosphoantigens. *Research in Immunology*, 147(5):338–347, 1996. doi:10.1016/0923-2494(96)89648-9.

[107] F. Lang, M. A. Peyrat, P. Constant, F. Davodeau, J. David-Ameline, Y. Poquet, H. Vié, J. J. Fournié, and M. Bonneville. Early activation of human v gamma 9v delta

2 t cell broad cytotoxicity and tnf production by nonpeptidic mycobacterial ligands. *Journal of immunology (Baltimore, Md. : 1950)*, 154(11):5986–59894, 1995.

[108] Martin R. Bürk, Lucia Mori, and Gennaro de Libero. Human v 9-v 2 cells are stimulated in a crossreactive fashion by a variety of phosphorylated metabolites. *European Journal of Immunology*, 25(7):2052–2058, 1995. doi:10.1002/eji.1830250737.

[109] M. K. Perera, R. Carter, R. Goonewardene, and K. N. Mendis. Transient increase in circulating gamma/delta t cells during plasmodium vivax malarial paroxysms. *J Exp Med*, 179(1):311–5, 1994. ISSN 0022-1007 (Print) 1540-9538 (Electronic) 0022-1007 (Linking). doi:10.1084/jem.179.1.311.

[110] Anke Bender, Brigitte Heckl-östreicher, and Dieter Kabelitz. Clonal specificity of human y8 t cells : Vy9 + t-cell clones frequently recognize plasmodium. pages 12–18, 1993.

[111] T. Sumida, T. Maeda, H. Takahashi, S. Yoshida, F. Yonaha, A. Sakamoto, H. Tomioka, T. Koike, and S. Yoshida. Predominant expansion of v gamma 9/v delta 2 t cells in a tularemia patient. *Infect Immun*, 60(6):2554–8, 1992. ISSN 0019-9567 (Print) 1098-5522 (Electronic) 0019-9567 (Linking). doi:10.1128/iai.60.6.2554-2558.1992.

[112] S. Raziuddin, A. W. Telmasani, M. el-Hag el Awad, O. al Amari, and M. al Janadi. Gamma delta t cells and the immune response in visceral leishmaniasis. *Eur J Immunol*, 22(5):1143–8, 1992. ISSN 0014-2980 (Print) 0014-2980 (Linking). doi:10.1002/eji.1830220506.

[113] Eric M. Janis, Stefan H. E. Kaufmann, Ronald H. Schwartz, and Drew M. Pardoll. Activation of t cells in the primary immune response to mycobacterium tuberculosis. *Science*, 244(4905):713–716, 1989. doi:10.1126/science.2524098.

[114] Jannie Borst, Annemieke Wicherink, Jacques J. M. Van Dongen, Evert De Vries, W. Marieke Comans-Bitter, Fred Wassenaar, and Peter Van Den Elsen. Non-random expression of t cell receptor and variable gene segments in functional t lymphocyte clones from human peripheral blood. *European Journal of Immunology*, 19(9):1559–1568, 1989. doi:10.1002/eji.1830190907.

[115] Anna Vyborova, Dennis X. Beringer, Domenico Fasci, Froso Karaiskaki, Eline van Diest, Lovro Kramer, Aram de Haas, Jasper Sanders, Anke Janssen, Trudy Straetemans, Daniel Olive, Jeanette Leusen, Lola Boutin, Steven Nedellec, Samantha L. Schwartz, Michael J. Wester, Keith A. Lidke, Emmanuel Scotet, Diane S. Lidke, Albert J. R. Heck, Zsolt Sebestyen, and Jürgen Kuball. Diversity of 9 2t cells and the molecular interface of 9 2tcr with tumor cells.